5-2007

WALL AND GROUND MOVEMENTS IN A BRACED EXCAVATION IN CLAYS AND SERVICEABILITY RELIABILITY OF ADJACENT BUILDINGS

Cheng liang Hsiao
Clemson University, evan.chsiao@gmail.com

WALL AND GROUND MOVEMENTS IN A BRACED EXCAVATION IN CLAYS AND SERVICEABILITY RELIABILITY OF ADJACENT BUILDINGS

A Dissertation
Presented to
the Graduate School of
Clemson University

In Partial Fulfillment
of the Requirements for the Degree
Doctor of Philosophy
Civil Engineering

---

by
Cheng Liang Hsiao
May 2007

Accepted by:
Dr. Hsein Juang, Committee Chair
Dr. David Prevatt
Dr. Ronald Andrus
D. Serji Amirkhanian

ABSTRACT

The goal of this dissertation research is to establish an improved procedure for evaluating the excavation-induced ground settlement and building serviceability. This research covers several closely related topics. Firstly, a simplified small strain soil model developed by Hsieh et al. (2003), called the Modified Pseudo Plasticity (MPP) model, is evaluated for its capability and performance in the prediction of the excavation-induced ground deformation behavior using Finite Element Method (FEM). Secondly, for the development of the envisioned empirical models for estimating the excavation-induced wall and ground responses, a database of excavation case histories are compiled. To complement the database of excavation case histories, artificial data is also generated using FEM solutions, in which the well-calibrated MPP soil model was implemented. Thirdly, based on the established database a simplified semi-empirical model is developed for predicting the maximum wall deflection, the maximum surface settlement and the surface settlement profile caused by excavations in soft to medium clays. Further, a reliability-based approach is presented to assess the serviceability reliability of adjacent buildings based on the developed semi-empirical model. Finally, a procedure is proposed to make use of the filed observation data to update the settlement prediction at subsequent stages of excavation, and the serviceability reliability of the adjacent building is then updated accordingly.

DEDICATION

I dedicate this work to my parents. This dissertation exists because of their love and support.

ACKNOWLEDGEMENTS

I would like to thank my advisor, Dr. C. Hsein Juang, for all of his untiring guidance and support during the course of my doctoral program at Clemson University. I am grateful to other committee members: Drs. Ronald Andrus, Serji Amirkhanian, and David Prevatt. They were all supportive and actively helped in the completion of the dissertation.

I am grateful to Matt Schuster, Gordon Kung, Raul Flores, Sunny Fang, David Li, and Yuting Su for engaging discussion and for their friendship.

I am grateful to Lorraine Cheng. She has supported me without fail in this special period. The success of this work belongs to her as much as anyone else.

Finally, I would like to thank my family for their enduring support and encouragement through my education

TABLE OF CONTENTS

Table of Contents (Continued)

Table of Contents (Continued) Page

LIST OF TABLES

List of Tables (Continued)

Table Page

LIST OF FIGURES

List of Figures (Continued)

List of Figures (Continued)

Figure Page

List of Figures (Continued)

Figure Page

CHAPTER I

INTRODUCTION

Background – Purpose of the Research

Braced excavation is commonly involved in the construction for basements of high-rise buildings, stations of underground transportation systems, and underground parking spaces. Construction of a braced excavation system inevitably induces lateral movement and settlement of the ground which can have detrimental effects on adjacent buildings. Figure 1.1 shows the typical wall deflection and ground movement caused by excavation in soft to medium clays. As illustrated, the adjacent building may be damaged due to the excessive differential settlement caused by soil movement induced by the wall deflection. This potential problem is amplified in the case of deep excavation in the congested urban area where existing structures are constructed adjacent to the excavation. Therefore, the goal of this study is to establish a systematic and reliable approach for evaluating the excavation-induced ground deformation and building serviceability.

The design of braced excavations in clays is a complicated soil-structure interaction problem. Increasingly, engineers rely on the finite element method (FEM) and finite difference method to analyze these soil-structure interaction problems. It is generally acknowledged that wall deflection is relatively easier to predict than the ground movement using FEM with the conventional soil

constitutive model such as the Modified Cam-clay (MCC) model (e.g., Atkinson 1993; Whittle and Hashash 1994). In other words, with the conventional soil constitutive model, the FEM prediction of the associated ground movement is often not as accurate as the prediction of the wall deflection. Previous studies (Simpson 1993; Whittle et al. 1993; Hight and Higgins 1995; Stallebrass and Taylor 1997; Kung 2003) have shown that the accuracy of surface settlement predictions by FEM can be significantly improved if the soil behavior at small strain levels can be properly modeled. Although the accuracy of the excavation-induced ground movement prediction may be improved by employing a small-strain constitutive model, many of these models are relatively complex, which often requires a lengthy and time-consuming computation process. Thus, it may be difficult for engineers to employ FEM with complicated constitutive models in a routine analysis of braced excavations. A simple soil model capable of simulating the small-strain behaviors of soils would be of great interest to practitioners. To this end, a part of this dissertation study is to evaluate the capacity of one simplified small strain soil model developed by Hsieh et al. (2003), called the Modified Pseudo Plasticity (MPP) model, in modeling excavation-induced deformation behavior.

Although the excavation-induced ground movement could be analyzed properly through various FEM solutions with small-strain soil models or simple soil models capable of simulating the small-strain behaviors of soils, in general, FEM solutions are still too time-consuming and require much effort and considerable engineering judgment. As a result, empirical and semi-empirical

methods (Peck 1969; Bowles 1988; Clough and O'Rourke 1990; Ou et al. 1993; Hsieh and Ou 1998) are often used for estimating the ground surface settlement induced by an excavation. All these empirical methods are developed based on the field observations of excavation case histories. However, there is high scatter in the predicted ground movements using these methods. Thus, another part of this dissertation study is to establish the improved procedures for estimating ground movements.

Finally but not the least importantly, another focus of this dissertation study is to develop a framework for performing a reliability-based evaluation of excavation-induced ground movements. The parameter uncertainties and uncertainties of the developed empirical models will be examined in this study, and this allows probabilistic evaluation of excavation-induced ground movement for building evaluation.

By and large, the end product of this dissertation study is to develop a reliability-based approach to evaluate the excavation-induced ground deformation and building serviceability. Various elements of this dissertation study are illustrated as shown in Figure 1.2.

Objectives and Scope of the Research

The scope of this dissertation research is aimed at establishing deterministic and probabilistic procedures to evaluate the excavation-induced ground movement for building serviceability evaluation. The specific objectives of the research are to:

1. Validate the capacity and accuracy of a simplified small-strain soil model (MPP soil model) in the FEM solution of the wall and ground deformation behaviors in an excavation.
2. Establish a database for developing the intended empirical models. The database consists of collected case histories and those generated from FEM solutions with a validated MPP soil model.
3. Develop empirical models to evaluate the excavation-induced responses (wall deflection and ground surface settlement) through least square regression analyses.
4. Develop a reliability-based framework to perform a probabilistic evaluation of the excavation-induced wall and ground responses.

Significance of the Research

It is generally difficult to predict with certainty building damage potential caused by an adjacent deep excavation. As a result of this difficulty, engineers often face the problem of over-design or under-design and associated disputes and lawsuits. Accordingly, prevention of adjacent building damage is recognized as one of the most important tasks in a deep braced excavation in urban area. Thus, any improvement to the existing methods for evaluating the excavation-induced building damage is a contribution to the field of civil engineering.

Furthermore, in recent years, there has been growing recognition that the probabilistic approach to geotechnical design can offer much insight and benefit to complement the traditional deterministic approach. One important aspect of

the probabilistic approach to geotechnical design in the context of the excavation field is the development of a robust procedure with which the uncertainty of an empirical model for the prediction of the excavation-induced ground movement can be estimated. The proposed empirical models allow the consideration of the model uncertainties so that they can provide a platform to perform a probabilistic evaluation of the excavation-induced ground movements.

The Structure of the Dissertation

This dissertation consists of six chapters. In the first chapter, the current paper, an introduction is presented that sets the stage for the entire dissertation. The purpose and the scope of the research and the outline of the dissertation are presented. The second through fifth chapters present major contents of three articles that deal with different aspects of the dissertation work. Chapter II presents a major part of a paper on "Evaluation of a Simplified Small-Strain Soil Model for Analysis of Excavation-Induced Movements." A simplified small strain soil model developed by Hsieh et al. (2003), called the Modified Pseudo Plasticity (MPP) model, is evaluated for its capability and performance in the FEM predictions of the excavation-induced wall deflection and ground movements. Chapter III presents excerpts of a paper on "A Simplified Model for Wall Deflection and Ground Surface Settlement Caused by Braced Excavation in Clays." Compilation of thirty-three case histories is presented in this chapter. Also presented in this chapter is generation of hypothetical cases that can complement the collected case histories for the development of the envisioned empirical models for predicting the ground movement. Chapter IV presents these

empirical models for predicting the excavation-induced ground movement in soft to medium clays. These models are developed based on the established database and verified using additional case histories which are not used in the development of the model. Chapter V presents a major part of a paper on "Reliability Analysis of Excavation-induced Ground Settlement and Building Serviceability Problem." A framework to perform the probabilistic evaluation of the excavation-induced ground response based on the models presented in Chapter IV is developed. Finally, in Chapter VI, the last chapter, the summary and conclusions of this dissertation research are presented.

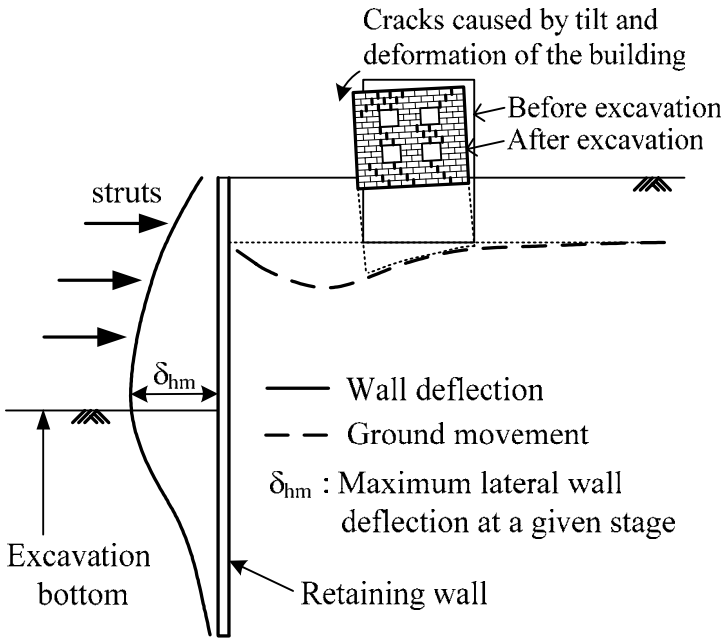

Figure 1.1 Effects caused by excavation in clays: wall deflection, ground movement and building response

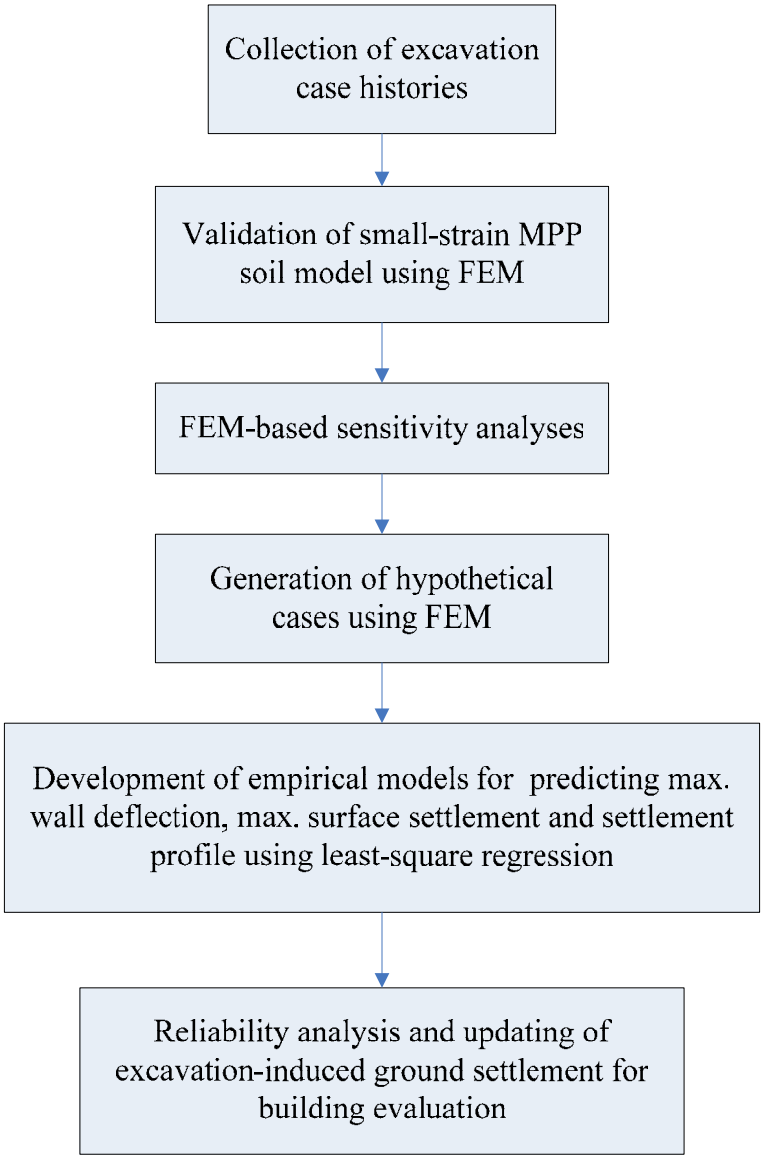

Figure 1.2 Flowchart showing various elements of this dissertation study

CHAPTER II

EVALUATION OF A SIMPLIFIED SMALL-STRAIN SOIL MODEL FOR ANALYSIS OF EXCAVATION-INDUCED MOVEMENTS*

Introduction

Braced excavation in clays is a complicated soil-structure interaction problem and can cause lateral wall deflection and ground movement (including lateral movement and surface settlement), which may result in damage to adjacent buildings and utilities. It is generally acknowledged (e.g., Atkinson 1993; Whittle and Hashash 1994) that wall deflection is relatively easier to predict than the ground movement using finite element method (FEM) with the conventional soil constitutive model such as the Modified Cam-clay (MCC) model. In other words, with the conventional soil constitutive model, the FEM prediction of the ground movement is often not as accurate as the prediction of the wall deflection. To overcome this deficiency, various FEM solutions with small-strain soil models have been proposed (Jardine et al. 1986; Burland 1989; Simpson 1993; Stallebrass and Taylor 1997; Kung 2003). Results from previous studies generally showed that the stress-strain characteristics of soils at small strains have the predominant influence on the accuracy of ground movement predictions using FEM.

In this study, a simplified small strain soil model developed by Hsieh et al. (2003), called the Modified Pseudo Plasticity (MPP) model, is evaluated for its

capability and performance in the FEM predictions of two well-documented excavation case histories. The results presented later show that the excavation-induced movements, including wall deflection, ground surface settlement and lateral soil deformation, can be accurately predicted using this simplified small strain soil model.

The MPP Soil Model

The MPP soil model is originally developed from Hsieh et al. (2003) based on well-known hyperbolic model (Duncan and Chang 1970). The MPP model improves upon the hyperbolic model in three aspects: (1) the anisotropic undrained shear strength can be accounted for to differentiate the states of primary loading and unloading-reloading; (2) the stress-strain equation of soil is modified to account for soil behaviors at small strain, and (3) the tangential Young's modulus is determined based on the unloading-reloading stiffness.

A total of six soil parameters, E_i / s_{uc}, s_{uc} / σ'_v, R_f, K_s, a, and b, are required to define the MPP model. In addition, Poisson's ratio is also required in the FEM analysis. The parameter E_i / s_{uc} can be determined from the small-strain compression triaxial tests at a strain approximately equal to or smaller than 10^{-5}. The parameters s_{uc} / σ'_v and R_f can be determined from the same triaxial compression tests. The parameter K_s can be determined with *additional* triaxial

---

*A similar form of this chapter has been accepted for publication by Canadian Geotechnical Journal at the time of writing; Kung, G.T.C., Hsiao, E.C.L., and Juang, C.H., "Evaluation of a Simplified Small-Strain Soil Model for Analysis of Excavation-Induced Movements."

extension tests. The parameters *a* and *b* can be determined from the multiple unloading/reloading triaxial tests conducted with strains from 10^{-5} to 10^{-2}. The reader is referred to Hsieh et al. (2003) and Kung (2003) for additional detail.

Assessment of the MPP soil model through case studies

The MPP model is incorporated into the computer code AFENA (Carter and Balaam 1990; Zienkiewicz 1979) by Hsieh et al. (2003). In this study, the assessment of the MPP soil model is conducted by comparing the FEM predictions of the excavation-induced wall and ground movements with the field observations in the two excavation case histories, TNEC case and Lurie Center Case. A summary of these cases is listed in Table 2.1 and the detailed construction sequences are listed in Table 2.2.

Case 1: TNEC Case

Field observations in Case 1, the Taipei National Enterprise Center (TNEC) case, were reported by Ou et al. (1998). As shown in Figure 2.1, the shape of the TNEC site was slightly irregular. The width was 43 m, while the lengths of the southern and northern edges were 106 m and 61 m, respectively. A diaphragm wall, which was 0.9 m thick and 35 m deep, was used as the earth-retaining structure. The foundation of the TNEC case was constructed using the Top-down construction method, in which the wall was supported by 150 mm thick solid concrete floor slabs. It is noted that with the Top-down method, slabs (or floors) are used as support in lieu of struts and anchors; they are cast from the

top of the excavation and proceeding downward to the bottom of the excavation. The entire excavation was carried out in seven stages of excavation, while the final excavation depth was 19.7 m.

Instrumentation plan

The plan view of instrumentation along the main observation section is also shown in Figure 2.1. Figure 2.1 shows that the excavation-induced wall deflection and ground movement were observed through five inclinometers (WI is installed in the wall; SI-1 to SI-4 are installed in the soil), three extensometers and a number of settlement points along the main observation section. Three pairs of inclinometer casings, SI-1, SI-2 and SI-3, and rod-type multipoint extensometers were installed to measure the vertical and horizontal deformation of soil simultaneously. According to Ou et al. (1996), the excavation-induced deformation along the main observation section assumed to be in a plane-strain condition. The reader is referred to Ou et al. (1998) for additional detail.

Stratigraphy

The TNEC site case is located in the Taipei Basin (in Taiwan) which is generally formed by a thick alluvium formation (the Sungshan Formation) lying above the Chingmei gravel Formation. The Sungshan Formation is approximately 40 to 50 m thick, and it has six alternating silty sand (SM) and silty clay (CL) layers and mainly consists of low-plasticity and slightly over-consolidated soft to

medium clay. Typical soil properties of the Sungshan Formation have been documented by many studies (e.g., Huang et al. 1987).

In this case, the soft to medium clay are located at depths from 8 m to 33 m (see part of Figure 2.2 for the soil profile) and they have the predominant effect in the excavation-induced deformation behavior. Ou et al. (2000) performed the unconsolidated undrained (UU) tests and field vane shear tests for this clay layer; their results showed that the average ratio of s_u / σ'_v was about 0.36 from the UU tests and 0.32 from the vane shear tests. The Chingmei gravel Formation can be found at the depth of 46 m. The depth of ground water table is around 2 m.

FEM Analysis with the MPP model

In order to study the capability and performance of the MPP model in the FEM predictions in excavation-induced ground movements, various aspects of the FEM analysis as applied to the TNEC case, including determination of element types, soil and structural parameters, initial conditions, and modeling of soil and structure, are described in the following sub-sections.

(1) Element types

The 8-noded rectangular isoparametric quadrilateral elements (Q8) were used to model soil and diaphragm wall elements. Bar elements were used to model struts, which were either steel members or concrete slabs, subjected to axial force.

(2) Modeling of soil and structure

The diaphragm wall was assumed to behave as a linear-elastic material, for which both Young's modulus and Poisson's ratio were assumed constant. The clayey soil and sandy soil were assumed to behave as elastic-plastic materials as described by the MPP Model and hyperbolic model, respectively. The undrained analysis for the clayey layers and drained analysis for the sandy layers were employed in the FEM analyses of the TNEC case.

(3) Initial conditions

The effective horizontal stress is equal to the effective vertical stress multiplied by the coefficient of the at-rest lateral earth pressure (K_0) at initial conditions. In the TNEC case, K_0 was determined from the triaxial tests using the undisturbed Taipei clay (Kung 2003). In the analysis of the TNEC case, the pore water pressure, which was slightly lower than the hydrostatic pressure, was determined from the measurement of the in-situ pore water pressure using piezometers. The total stresses are equal to the sum of effective stress and pore water pressure.

(4) Determination of soil parameters

The MPP model for clay layers and hyperbolic model for sand layers are employed in the analysis. The determination of parameters for hyperbolic model is referred to the original definitions (Duncan and Chang 1970) and is not repeated here. As mentioned previously, six soil parameters, E_i / s_u, s_u / σ'_v, R_f, a, b and K_s, are required to define the MPP model. The values of E_i / s_u, s_u / σ'_v and K_s were directly determined by the small-strain triaxial tests on the undisturbed Taipei clay sampled from the TNEC case and performed by Kung

(2003). Test results showed that E_i / s_u fell in the range from 1600 to 2500 and s_u / σ_v' varied from 0.30 to 0.35. According to Hsieh (1999) and Kung (2003), K_s for the Taipei clay is approximately equal to 0.75. For the term R_f, the value of $R_f = 0.9$ is considered adequate to simulate the stress-strain characteristics in the analysis. Finally, Heish et al. (2003) indicates that $a = 0.0001$ and $b = 1.4$ adequately represented the degradation behavior of Taipei clay based on the results of the multiple unloading/reloading triaxial tests. The values of the six soil parameters used in the analysis are listed in Table 2.3.

(5) Determination of structural parameters

The nominal Young's modulus of diaphragm wall, E_c, can be calculated from the suggestion by ACI code (1995):

$$E_c = 4700\sqrt{f_c'} \tag{2.1}$$

where f_c' is the compressive strength of concrete (MPa).

Typically for FEM analysis of braced excavation, the nominal E_c is reduced to account for the effect of the underwater construction of the diaphragm wall. Thus, in this study, 80% of nominal E_c is taken to conduct the FEM analysis. In the TNEC case, f_c' is equal to 27.44 MPa. The stiffness of struts or floor slabs, *k*, is determined by:

$$k = \frac{EA}{LS} \tag{2.2}$$

where E is Young's modulus of steel or concrete; A is the cross-section area; L is the length; S is the horizontal span. The stiffness of struts, floor slabs, and anchors used in the analysis are shown in Table 2.2.

(6) Analysis results

Figure 2.3 shows the comparison of the wall deflection between field observations and FEM predictions. The cantilever-type wall deflection at first and second stages can be accurately estimated. After the construction of concrete floor slabs, the deep-inward movements of wall deflection were induced at subsequent stages. The calculated maximum wall deflections are very close to the observations at stages 3 to 7, while the locations where the maximum wall deflection occurred can be accurately estimated except stages 6 and 7, where the estimated position is slightly deeper than the observations. The calculated maximum wall deflection is 109 mm, which is practically identical to the measured wall deflection.

Figure 2.4 shows the comparison of ground surface settlement between field observations and FEM predictions. The observations reveal that the concave shape of surface settlement was induced mainly at distances of 0 to 30 m away from the wall. The maximum surface settlement after the completion of the final excavation stage (stage 7, excavation depth = 19.7 m) is around 74 mm and the location where the maximum surface settlement occurred is 13 m away from the wall. The results show that the trend of the settlement profile is fairly accurately estimated. The predictions of the surface settlement at the range of 0 to 25 m away from the wall compare well to the observations, but the predictions of the

surface settlement at the range of 25 to 40 m away from the wall are slightly larger than the observations. Generally, predictions of the maximum surface settlement at each stage are considered satisfactory except that at stages 5, 6, and 7, the maximum surface settlement is slightly underestimated.

Figure 2.5 shows the comparison of the horizontal soil deformation between field observations and FEM predictions. The results show that the computed maximum horizontal soil deformation and profiles along the SI-1 and SI-2 sections are generally close to the observations, although the difference is observed for the location where the maximum horizontal soil deformation occurred at the final two stages. However, the soil deformation along the SI-3 and SI-4 sections are accurately predicted at depths smaller than 10 m and over-predicted at depths larger than 10 m. Moreover, compared with predictions of the vertical settlement shown in Figure 2.4, both the vertical and horizontal soil deformation were overestimated by the MPP model in the distance range of 25 to 40 m.

In view of the difficulty of obtaining satisfactory predictions of all three responses (wall deflection, surface settlement, and lateral soil deformation) *simultaneously* with a finite element analysis, the results obtained in this study using the MPP soil model are considered satisfactory. The results also strengthen and expand the findings of a previous study (Hsieh et al. 2003), which focused only on the wall deflection and ground surface settlement.

Case 2: Lurie Center case

The observations of the Lurie center located on the Chicago campus of Northwestern University were documented by Finno and Roboski (2005). A plan view of the foundation, approximately 80 m × 68 m in size, is shown in Figure 2.6. The four-stage excavation is supported by a hot-rolled PZ-27 sheet pile wall on all sides. The average final excavation depth is 12.8 m.

Two levels of tied-back ground anchors are installed on the east wall due to the presence of the basement of the Prentice Pavilon as shown in Figure 2.6. Three levels of tied-back anchors provided lateral support on the other three walls. Both the first and second level anchors are founded in the beach sand. The anchors were installed at a horizontal spacing of 2.74 m on the first level and 1.83 m on the second and third levels. Design ground anchor loads were 623, 534, and 623 kN for the first, second, and third levels, respectively. All anchors were locked off to a prestress of 100% of the design load. The angles of tied-back installation are 20°, 10°, and 30° for the first, second, and third levels, respectively. The reader is referred to Finno and Roboski (2005) for additional detail.

Instrumentation plan

The plan view of instrumentation is also shown in Figure 2.6. To monitor the ground response to excavation activities, 150 surface survey points, 18 embedded settlement points, and 30 utility points were installed on three surrounding streets prior to wall installation. In addition to optical survey data,

seven inclinometers were installed behind the wall at distances of 1 to 2.4 m from the sheet pile wall. Inclinometer LR-4 was installed 6.1m from the wall. It should be noted that unlike the TNEC case, the inclinometers were not installed in the wall, and thus, the lateral soil deformation measured from inclinometers behind the wall (but very close to the wall) are used to examine the FEM results, as presented later.

Stratigraphy

The stratigraphy at the site is shown in Figure 2.2. Beneath the top layer of medium dense to dense rubble fill lies a loose to medium dense beach sand. The granular soils overlie a sequence of glacial clays of increasing shear strength with depth. Undrained shear strengths measured by the vane shear tests are 29 to 43 kPa for the soft to medium clay and 105 kPa for the stiff clay, respectively. The ground water level was located at a depth of about 3 m.

FEM Analysis with the MPP model

The soil and structure parameters used in the FEM analysis in this dissertation study were determined based on Finno and Roboski (2005), Holman (2005), and Finno and Chung (1992). Note that the sheet-pile wall was simulated by the solid element with the constant bending and axial stiffness, and the equivalent thickness and modulus of wall were determined based on the methodology presented by Day and Potts (1993). Similar to the equivalent strut stiffness used in the analysis of the TNEC case, the equivalent stiffness of anchors

calculated by the horizontal spacing and the nominal stiffness is used in the FEM analysis. Given different arrangement of anchors and the locations of inclinometers and settlement points (Finno and Roboski 2005), the FEM analyses were conducted at the cross-section perpendicular to the North and South walls. Note that the approximate plane strain zone on the North and South walls is identified in Figure 2.9 based on the observations by Finno and Roboski (2005).

For the soft clay layer, the average Young's modulus $E_i / s_u = 1300$ determined from the bender element tests performed by Holman (2005) in the Lurie case and undrained shear strength $s_u / \sigma'_v = 0.25$ determined from Finno and Roboski (2005) were employed. For the soft clay in the Lurie case, parameters *a* and *b* were assumed to be equal to those in the TNEC case as the properties of two clays are similar. For the stiff clay layer, the parameters E_i / s_u, *a*, and *b* were determined based on the sensitivity studies.

Figure 2.7 compares FEM predictions of the lateral soil deformation in this study with field observations of the inclinometers LR-3 and LR-8, which are adjacent to the wall. The observed lateral soil deformation at first stage already exhibits the trend of deep-inward movement, which is significantly different with the TNEC case examined in this study. This may be due to the fact that the strength and stiffness of the soft clay at the depth of 8 to 15m are much smaller than those of the sand layer and stiff clay layer. The soil deformation at first and second stages can be simulated accurately by the FEM with the MPP model. The obvious increase of the soil deformation observed from Stage 2 to Stage 3 might have resulted from the excavation of the entire sand layer, which would cause a

rapid reduction in the resistance stiffness of the soil in the excavation zone. The FEM prediction at Stage 3 also simulates this behavior accurately. Overall, the performance of the FEM with the MPP model in the prediction of the maximum lateral soil deformation and its location at each stage is deemed satisfactory.

Figure 2.8 compares the predicted and observed surface settlement. Settlements from all settlement points located in the plane strain zone as shown in Figure 2.6 are collected. At Stage 2, the observed settlements are much larger than the predicted values (Figure 2.8b), and at Stages 3 and 4, the predicted settlements are slightly less than the observed values. The averaged profile of surface settlement along the two cross-sections intersecting LR-3 and LR-8 sections, determined based on the contour of settlement presented by Finno and Roboski (2005), is also shown in Figure 2.8d. While the maximum settlement is somewhat underestimated at Stage 4, the predicted trend of settlement profile and the location where the maximum surface settlement occurred are quite consistent with the observations.

Summary

Soil-structure interaction such as the wall and ground responses in an excavation may be significantly affected by the stress-strain behavior of soils at small strain. To accurately estimate the wall and ground movements in a braced excavation, the small-strain behavior of soils should be incorporated in the FEM analysis. Whereas many elasto-plastic soil models capable of simulating the small-strain behavior of soils are available (Whittle 1990; Jardine 1991; Simpson

1993; Stallebrass and Taylor 1997), these models tend to be complicated and require input parameters that may be *relatively* difficult to determine, and as such, they may have limited practicability in the geotechnical applications. In this study, the Modified Pseudo-Plasticity (MPP) model is evaluated with two well-documented excavation case histories that involved different construction methods (the Top-down method and Anchor method) and with different soil deposits. The MPP model can account for high initial stiffness and nonlinear behavior of soils at small strain and requires only six input parameters. Satisfactory results were obtained in the FEM predictions of the wall deflection, ground surface settlement, and lateral soil deformation using the MPP soil model.

Conclusion

The MPP model improves upon the well-known hyperbolic model (Duncan and Chang 1970) in three aspects: (1) the anisotropic undrained shear strength can be accounted for to differentiate the states of primary loading and unloading-reloading; (2) the stress-strain equation of soil is modified to account for soil behaviors at small strain, and (3) the tangential Young's modulus is determined based on the unloading-reloading stiffness. The simulation of stress-strain curves of clay from representative triaxial tests showed that the MPP model can predict the stress-strain behavior of clay at small strains when the measured high initial stiffness is directly employed.

The results of FEM analyses of the two case histories showed that the predicted wall deflection profile generally agreed well with the observations. The

predictions of the maximum wall deflection and its location are generally satisfactory. For ground surface settlement, the predicted settlement profile generally resembles the observed profile. The trend of the measured concave settlement adjacent to the wall can be correctly predicted by the MPP model. The maximum surface settlement can also be fairly accurately predicted. For lateral soil deformation behind the wall at relatively shorter distance, the predictions of the maximum lateral soil deformation agreed well with the observations. However, at greater distance from the wall, the predicted deformation profile exhibited deep inward movement, which did not agree well with the observed cantilever movement behavior.

Based on the presented results obtained from the analysis of two excavation case histories, the MPP model is considered an effective soil model for FEM analysis of the wall and ground movements in a braced excavation. Further validation of this model with additional quality case histories is desirable.

Table 2.1 Summary of case histories in validating MPP soil model

Case	Location	L (m)	B (m)	Construction method	H_e (m)	H (m)	H_w (m)	t (m)	EI ($kN/m^2/m$)	δ_{hm} (mm)	δ_{vm} (mm)	Reference
TNEC	Taipei	60 to 105	43	Top-down (Diaphragm)	19.7	3.28	35.0	0.9	1494450	106.4	78.0	Ou et al. (1998)
Lurie	Chicago	80	64	Anchor (Sheet piles)	11.8	3.65	18.3	(0.6)*	(71820)*	66.3	48.8	Finno and Roboski (2005)

()* denotes the equivalent values of t and EI in the parentheses were determined by (Day and Potts 1993).

Table 2.2 Propping arrangements for the excavation case histories and stiffness of struts, floor slab and anchors used in FEM analyses

Stage No.	TNEC case			Lurie case		
	H_e (m)	H_p (m)	K (kN/m/m)	H_e (m)	H_p (m)	k (kN/m/m)
1	2.8	N/A	N/A	1.8	N/A	N/A
2	4.9	2.0 (s)	8240	5.7	1.2 (a)	20906
3	8.6	3.5 & 0 (f)	125568	9.1	4.5 (a)	31303
4	11.8	7.1 (f)	125568	11.8	8.5 (a)	38132
5	15.2	10.3 (f)	125568	N/A	N/A	N/A
6	17.3	13.7 (f)	125568	N/A	N/A	N/A
7	19.7	16.5 (s)	24035	N/A	N/A	N/A

Note: H_e is the excavation depth; H_p is the depth where the strut is installed; (a), (s), and (f) denote anchor, steel strut and floor slab, respectively, and k denotes the corresponding stiffness.

Table 2.3 Soil parameters used in FEM analyses

(a) Parameters of clayey layers (MPP model)

Case history	Depth (m)	γ_t (kN/m^3)	K_o	$\frac{E_i}{s_u}$	$\frac{s_{uc}}{\sigma'_v}$	R_f	a	b	ν	K_s
TNEC	0-5.6	18.3	1.0	2100	0.32	0.9	0.0001	1.4	0.499	0.75
	8-33	18.9	0.51	2100	0.32	0.9	0.0001	1.4	0.499	0.75
	35-37.5	18.2	0.51	2100	0.34	0.9	0.0001	1.4	0.499	0.75
Lurie	8.5-15.9	18.9	0.5	1300	0.25	0.9	0.0001	1.4	0.499	0.75
	15.9-25	18.9	0.85	2500	0.6	0.9	0.00001	1.2	0.499	0.75

(b) Parameters of sandy layers (Duncan-Chang model)

Case history	Depth (m)	γ_t (kN/m^3)	K_o	c' (kPa)	ϕ' ($^\circ$)	R_f	$K = K_{ur}$	n	ν
TNEC	5.6-8	18.9	0.49	0	31	0.9	750	0.5	0.3
	33-35	19.6	0.49	0	31	0.9	2500	0.5	0.3
	37.5-46	19.6	0.47	0	32	0.9	2500	0.5	0.3
Lurie	0-3.5	18.9	1.0	0	33	0.9	1000	0.5	0.3
	3.5-8.5	19.6	0.46	0	33	0.9	1500	0.5	0.3

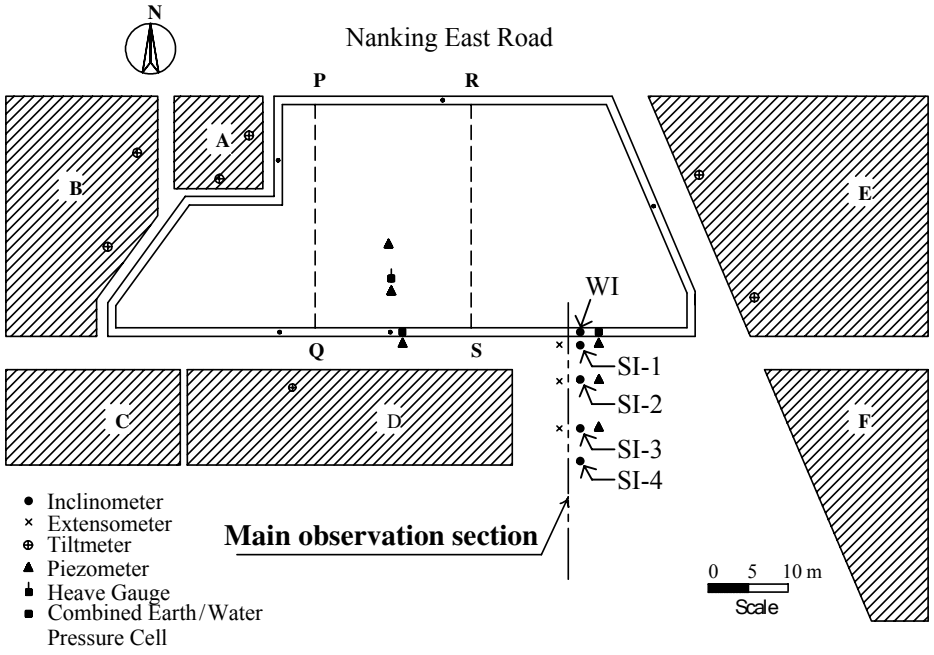

Figure 2.1 Plan view of the TNEC case and the instrumentation plan (Modified from Ou et al., 1998)

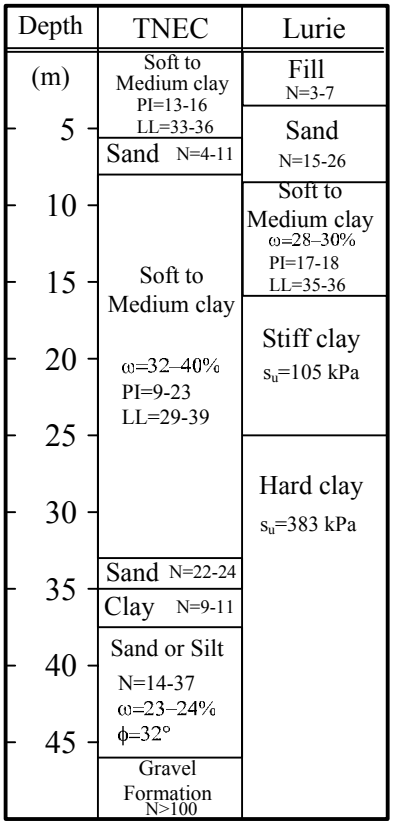

Figure 2.2 Stratigraphy of each of the two excavation case histories (Modified from Ou et al. 1998, and Finno and Roboski 2005)

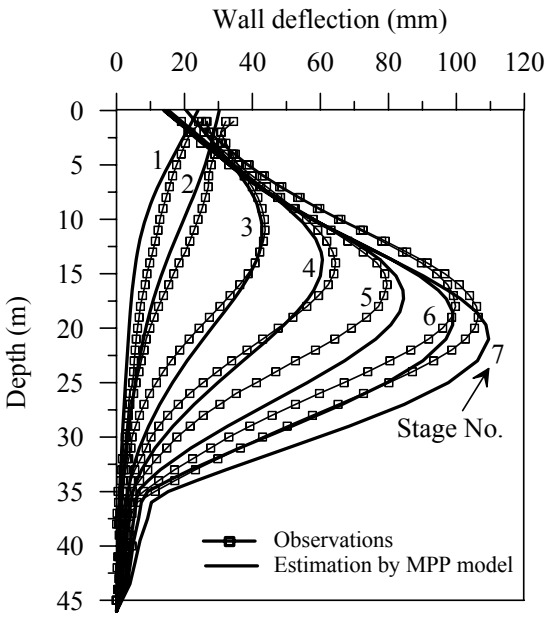

Figure 2.3 Comparison of the wall deflection in the TNEC case

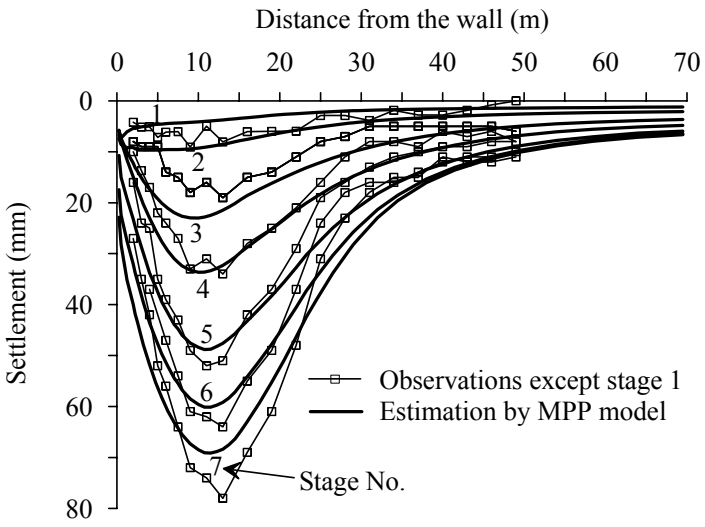

Figure 2.4 Comparison of the surface settlement in the TNEC case

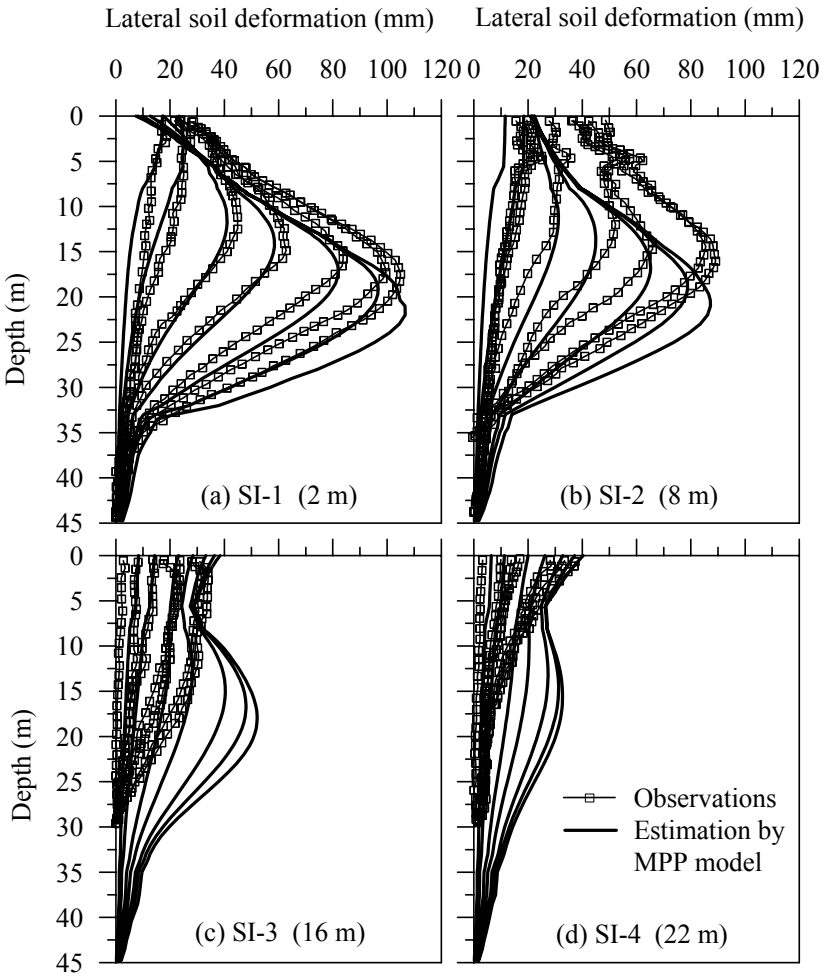

Figure 2.5 Comparison of the soil deformation in the TNEC case

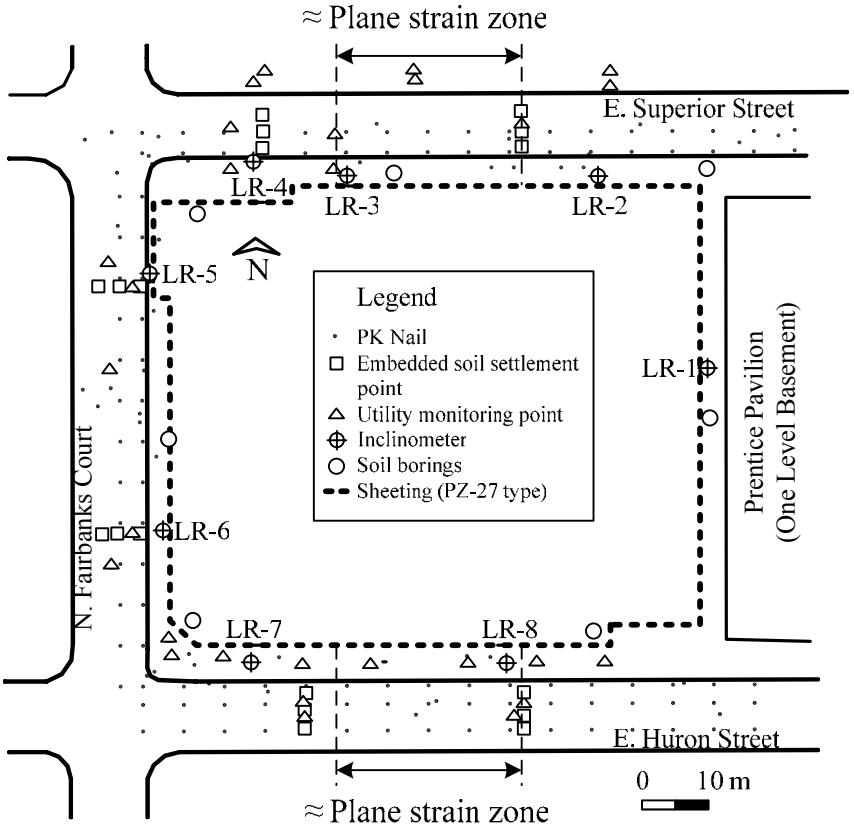

Figure 2.6 Plan view of the Lurie center case and the instrumentation plan (Modified from Finno and Roboski, 2005)

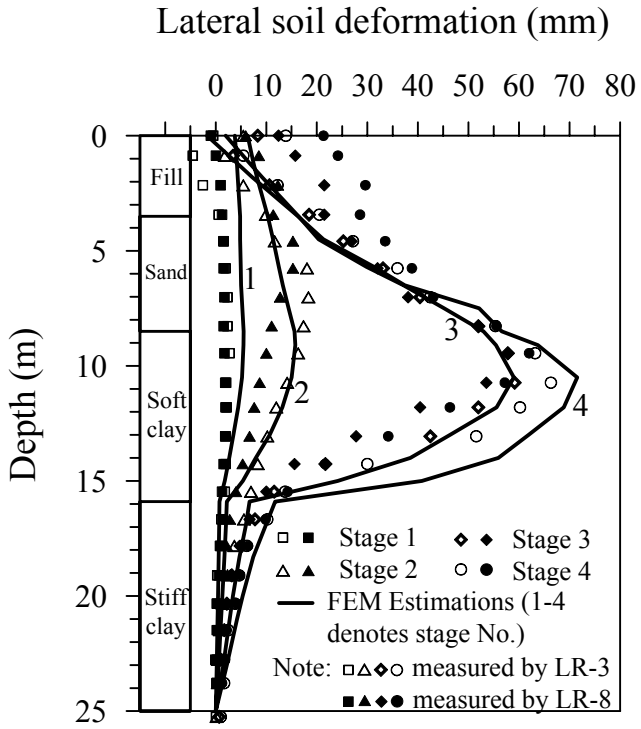

Figure 2.7 Comparison of the measured and predicted lateral soil deformation in the Lurie center case

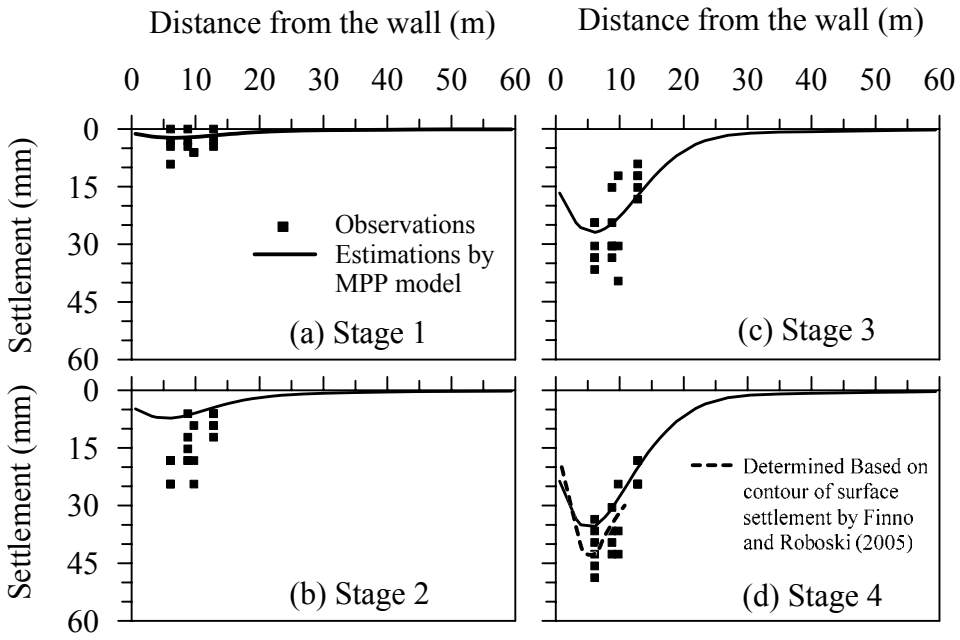

Figure 2.8 Comparison of the surface settlement in the Lurie center case

CHAPTER III

COLLECTION OF EXCAVATION CASE HISTORIES AND GENERATION OF ARTIFICIAL DATA OF WALL DEFLECTION AND GROUND SETTLEMENT*

Introduction

Over the past two decades, the number of well-documented deep excavation with field measurements at each stage of excavation has increased significantly. However, experience from these cases has not been systematically extracted into knowledge that can be put into use in future deep excavation projects. One of the tasks of this dissertation study is to collect the well-documented deep excavation cases and explore means of learning and extracting knowledge from them. It is noted that the total number of collected case histories had been less than ideal for the purpose of developing empirical models for estimating the wall deflection and ground surface settlement. Thus, in this study, secondary data were generated from numerical experimentation using FEM solutions with the aforementioned MPP soil model.

Thirty-three deep-excavation case histories are collected in this dissertation study. Prior to the compilation of deep-excavation case histories and generation of artificial data from numerical experimentation, it is necessary to recognize the influential factors in terms of excavation-induced wall deflection

*A major part of this chapter was taken from an article that is in press at the time of writing; Kung, G.T.C., Juang, C.H., Hsiao, E.C.L., and Hashash, Y.M.A., "A simplified model for wall deflection and ground surface settlement caused by braced excavation in clays," *Journal of Geotechnical and Geoenvironmental Engineering*, Vol. 133, No. 6, June 2007.

and ground settlement. This can be done through literature review of existing methods for the estimation of wall deflection and ground surface settlement, and through sensitivity study using FEM solutions. Thus, a brief review of the existing methods for the estimation of wall deflection and ground settlement is presented, followed by the compilation of the collected case histories, and parametric study using FEM

The influential factors found are then included in the FEM numerical experimentation for generating artificial data used for development of the intended models that is presented in Chapter IV.

Existing Empirical Methods for Wall Deflection and Ground Surface Settlement

Several empirical and semi-empirical methods are available for estimating the excavation-induced maximum wall deflection (Mana and Clough 1981; Wong and Broms 1989; Clough and O'Rourke 1990; Hashash and Whittle 1996; Addenbrooke et al. 2000) and the surface settlement profile (Peck 1969; Mana and Clough 1981; Clough and O'Rourke 1990; Ou et al. 1993; Hashash and Whittle 1996; Hsieh and Ou 1998). Deformation behavior of a braced excavation may be affected by factors such as the excavation width and depth, wall stiffness, strut spacing, strut stiffness and preloading on the strut, depth to the underlying hard stratum, soil stiffness and strength distribution, dewatering operation, adjacent surcharge, soil consolidation and creep, and workmanship. It is, however, not practical to incorporate all these factors in a simplified model for

excavation-induced wall and ground deformations, and the existing methods generally reflect this reality.

Analysis of excavation-induced wall and ground movements generally consists of the following steps:

(1) Estimate the maximum lateral wall deflection δ_{hm},

(2) Estimate the deformation ratio R ($=\delta_{vm}/\delta_{hm}$),

(3) Calculate the maximum surface settlement δ_{vm}, and

(4) Estimate the surface settlement profile.

For estimating δ_{hm}, Mana and Clough (1981) studied a number of excavation case histories and recognized the strong correlation between δ_{hm} and the potential for basal heave, in terms of factor of safety defined by Terzaghi (1943). Therefore, Mana anc Clough (1981) used case history data to develop an empirical chart for predicting the maximum wall deflection in soft to medium clays by means of factor of safety against the basal heave. Wong and Broms (1989) proposed a simple procedure to estimate the lateral deflection of strutted or anchored sheet-pile walls. The procedure was developed based on an assumption that the walls are flexible and the lateral deflections are governed by plastic yielding of the soil below the bottom of excavation. The excavation width, excavation depth and secant or tangent moduli of the soil are included in the analysis. Clough and O'Rourke (1990) proposed a semi-empirical chart (see Figure 3.1) for estimating δ_{hm} for soft to medium clays, which can simultaneously consider the factor of safety against basal heave and the system stiffness

($EI/\gamma_w h_{avg}^4$; where EI is the wall stiffness, γ_w is the unit weight of water, and h_{avg} is the average support spacing). This chart is perhaps the most widely used method by practicing engineers for preliminary estimation of the maximum lateral wall deflection.

The first practical approach for estimating excavation-induced settlement for in-situ wall systems was proposed by Peck (1969). The design chart by Peck (1969) was based mostly on data compiled for settlements of the ground adjacent to temporary braced sheet-pile and soldier pile walls with lower system stiffness. With the use of newer design and construction technologies (e.g., use of stiff diaphragm wall), it would be more appropriate to use charts that are developed for stiffer walls. Clough and O'Rourke (1990) found that the maximum surface settlement caused by an excavation is mostly less than 0.5% H (where H is the excavation depth). They also developed soil type-related settlement envelopes for estimating the profiles of settlement adjacent to an excavation (see Figure 3.2). With knowledge of the maximum surface settlement, the dimensionless diagrams in Figure 3.2 may be used to estimate the surface settlement profile.

Hsieh and Ou (1998) proposed a procedure for estimating the excavation-induced surface settlement profiles. These profiles are divided into two parts, the primary influence zone and the secondary influence zone, and can be determined with the prerequisite that δ_{vm} is already known. They further suggested that δ_{vm} could be estimated from the relationship between δ_{hm} and δ_{vm}, which can be expressed as:

$$\delta_{vm} = R\delta_{hm} \tag{3.1}$$

where R is the deformation ratio. Based on excavation case history data, the deformation ratio generally falls in the range of 0.5 to 1.0 for soft to medium clays.

Collection of Excavation Case Histories

In this dissertation study, thirty-three (33) case histories of braced excavations in soft to medium clays are obtained from Taipei, Singapore, Oslo, Tokyo, and Chicago. These case histories include cases for the construction of the building basements, the underground subway stations and cut-and-cover tunnels for mass transit systems, and they are used for developing or validating the intended model in Chapter IV. The case histories collected were constructed by the Top-down method or Bottom-up method or Semi-top-down method. It is noted that with the Top-down method, slabs (or floors) are used as support in lieu of struts and anchors; they are cast from the top of the excavation and proceeding downward to the bottom of the excavation. With the Bottom-up method, where the retaining wall is supported by struts and anchors during the excavation, slabs are cast after the excavation from the bottom of excavation and proceeding upward to the top of the excavation. Table 3.1 provides a summary of these excavation case histories, including the construction method, excavation stages, excavation width, final depth of excavation, wall length, wall thickness, flexural stiffness of wall material (EI), the ratio of maximum lateral wall deflection (δ_{hm}) over final depth of excavation (H_{ef}), and the depth of "hard" stratum. Note that the term, "hard" stratum is relative to soft to medium clay examined in this paper;

the hard stratum can be the bedrock, gravel formation, very dense sand or hard clay layer.

For these case histories, the excavation width ranges from 11.0 to 70 m; the final depth of excavation is in the range of 7.8 to 28.8 m; the wall length is in the range of 16 to 51 m; the wall thickness is in the range of 0.4 to 1.2 m. The wall thickness in Cases 32 and 33 is not available because a sheet-pile wall is used. The data base comprising the 33 case histories collected in this study is considered adequate to represent the engineering behavior of braced excavations in soft to medium clays. In addition, the depths of excavation and the depths where the struts or concrete floor slabs were installed or constructed at all stages in these case histories are shown in Tables 3.2 and 3.3, respectively.

The wall deflections at various stages of excavation observed in Cases 1 through 28 are shown in Figure 3.3; for Cases 29 and 30, the wall deflection observations are available only at the last stage of excavation and thus not shown in this figure. For most case histories, the cantilever type of wall deflection behavior can be observed at first and/or second stages, at which time the strut had not been installed or the stiffness of the installed strut was not high enough. The diaphragm wall then displayed the deep inward movements at subsequent stages. Figure 3.4 displays the maximum wall deflections at given excavation stages with the corresponding depths of excavation. Most data points fall into the region bounded by the line of $\delta_{hm} = 0.2\%H_e$ and the line of $\delta_{hm} = 0.6\%H_e$, which is similar to those presented by Ou et al. (1993). It is noted that the mean trend line, $\delta_{hm} = 0.3\%H_e$, is also shown in Figure 3.4. Figure 3.5 shows the relationship

between normalized maximum lateral wall deflection and factor of safety against basal heave, defined by Terzaghi (1943), for all case histories at stages 3 to 7. The limits suggested by Mana and Clough (1981) are also shown in this figure. The collected case histories generally fall into the region bounded by the two limits suggested by Mana and Clough (1981). The data points from the case histories examined are seen to be closer to the lower limit, which could be explained by the fact that Mana and Clough's limits were established mostly with case histories of excavations constructed with low-stiffness sheet-pile walls or soldier pile walls, whereas the high-stiffness diaphragm walls were used in the case histories (cases 1 to 30) examined herein.

Factors Affecting Maximum Wall Deflection and Deformation Ratio

Factors that might affect maximum wall deflection and deformation ratio (and thus the maximum surface settlement) are examined based on the findings reported in the literature and a series of sensitivity analyses conducted in this study.

Factors affecting wall deflection

Four factors, including excavation width, excavation depth, shear strength, and system stiffness, were generally employed in the existing empirical methods. According to the previous studies (Burland 1989; Atkinson 1993; Whittle et al. 1993; Hight and Higgins 1995), the stiffness of soil at small strain levels also has a significant influence on the excavation-induced deformation. Moreover, the

presence of a hard stratum could affect the size of the yielding zone (e.g., see Wong and Broms 1989) and its effect on the maximum wall deflection should be investigated. According to Wong and Broms (1989), the displacement of soil beneath and around the bottom of excavation could be restrained by the presence of the hard stratum. They pointed out that the wall deflection tends to increase with the increase of the ratio *T/B* (where *T* is the depth to the hard stratum measured from the *current* excavation level and *B* is the excavation width). When the ratio of T/B is large enough (i.e., the hard stratum is at a great depth relative to the excavation width), however, the wall deflection is no longer affected by this ratio.

Hashash and Whittle (1996) pointed out that the wall length has a minimal effect on the pre-failure deformations for excavations in deep layers of clay where there is no constraint on toe movement, although it is believed to have a significant influence on the location of failure mechanism within the soil. Therefore, the wall length is not included as a factor for predicting wall deflection. Thus, six factors are considered essential for predicting the wall deflection in this dissertation study; they are excavation depth (H_e), system stiffness ($EI/\gamma_w h_{avg}^4$), excavation width (*B*), ratio of the average shear strength over the vertical effective stress (s_u/σ_v'), ratio of the average initial Young's modulus over the vertical effective stress (E_i/σ_v'), and ratio of the depth to hard stratum measured from the current excavation level over the excavation width (T/B). Use of these six factors is considered adequate for the sole purpose of predicting the maximum

wall deflection induced in a braced excavation, as is evidenced by the performance of the developed model presented later in Chapter IV.

Factors affecting deformation ratio

The deformation ratio *R* which is the ratio of maximum surface settlement and maximum wall deflection may be affected by many factors such as the geometry of excavation (e.g., the excavation width), the wall system (the wall thickness, the wall length, and the strut stiffness) and the ground conditions (soil properties). To ascertain the effect of these factors on the deformation ratio, Case 7 was selected for conducting a series of sensitivity study to examine the possible effect of the geometry of excavation, the excavation width, wall thickness, wall length, and floor (strut) stiffness. The sensitivity study includes a variation in the *excavation width* (20 m, 40 m, 60 m, 80 m, or 100m), in the *wall thickness* (0.6 m, 0.9 m, 1.2 m, or 1.5 m), in the *wall length* (35 m or 40 m), and in the *strut stiffness* (12.5%, 25%, 50%, or 100% of the nominal strut stiffness). The results of this sensitivity study showed that all four parameters have little effect on the deformation ratio *R*.

The next series of sensitivity study is to investigate the effect of ground conditions or soil parameters on the deformation ratio. In particular, two parameters, the shear strength and Young's modulus, were selected for the sensitivity study of this case history. The results showed that the deformation ratio *R* is significantly affected by these two soil parameters. In addition, the preliminary FEM analyses also found that the thickness of clay layer relative to

the wall length, in terms of *normalized thickness* ($\sum H_{clay} / H_{wall}$, see Figure 3.6), could also affect the deformation ratio *R*. Although this dissertation study deals primarily with soft to medium clay, it was decided to include this factor in the numerical experimentation so that the results may be extended from "pure clay" to "clay-dominant" site.

The effect of T / B and excavation depth on the deformation ratio is also examined by the FEM analyses and the results show that the deformation ratio *R* is not significantly affected by these two factors; no significant correlations between the deformation ratio *R* and these two factors can be observed in the sensitivity study. Therefore, the two factors are not included in the intended model for the deformation ratio.

Thus, the deformation ratio is believed to be strongly influenced by three parameters, the shear strength, Young's modulus, and the clay layer thickness relative to wall length. These three parameters are expressed hereinafter as normalized parameters, namely, the normalized clay layer thickness with respect to the wall length ($\sum H_{clay} / H_{wall}$), the normalized shear strength with respect to the vertical effective stress (s_u / σ'_v), and the normalized Young's modulus with respect to the vertical effective stress (E_i / σ'_v).

Generation of Artificial Data of Wall and Ground Responses

The factors that are believed to influence the maximum wall deflection and deformation ratio in a braced excavation in soft to medium clays described previously are included in the FEM numerical experimentation for generating

artificial data for development of the intended model. Data for developing the intended model are generated based on various scenarios of excavation (see Figure 3.7). For the analysis of these hypothetical cases, the strut is assumed to be installed 1 m above the current excavation level for each stage of excavation. Dewatering is not considered in the analyses. For the hypothetical cases shown in Figures 3.7(a), 3.7(b) and 3.7(c), the numbers of excavation stages are assumed to be four, five, and seven, respectively, while the wall length is varied to maintain approximately the same ratio of the final depth of excavation over the wall length so as to maintain approximately the same safety level against basal failure. The following ranges of parameters are incorporated in the FEM numerical experimentation to account for the parameters identified in the previous section:

1. Excavation width, B = 10 m, 20 m, 40 m, 60 m, 80m, or 100 m,
2. Wall thickness t is assumed as 0.6 m, 0.8 m, 1.0 m, 1.2m, or 1.4 m, which yields a wide range of system stiffness $EI/\gamma_w h_{avg}^4$,
3. s_u/σ'_v = 0.25, 0.29, 0.32, 0.36, or 0.40,
4. E_i/σ'_v = 1500, 1750, 2035, 2400, or 3000 times of s_u/σ'_v ,
5. The depth of hard stratum is assumed as 1 m, 5 m, 10 m, 20 m, 30 m, 40 m, or 50 m below the toe of the diaphragm wall for each reference excavation, which yields a wide range of T/B , and
6. $\sum H_{clay}/H_{wall}$ = 0.6, 0.7, 0.8, 0.9, or 1.0.

Table 3.4 shows a summary of these input variables and their ranges that are incorporated in the FEM numerical experimentation for generation of artificial data of wall and ground responses.

Summary

Thirty-three (33) case histories of braced excavations in soft to medium clays, obtained from Taipei, Singapore, Oslo, Tokyo, and Chicago. Clearly, the total number of collected case histories had been less than ideal for the purpose of developing empirical models for estimating the wall deflection and ground surface settlement. Thus, in this dissertation study, secondary data were artificially generated from numerical experimentation using FEM solutions with the well-validated MPP soil model.

Literature review and parametric study using FEM first show that six factors are considered essential for predicting the wall deflection ; they are excavation depth (H_e), system stiffness ($EI/\gamma_w h_{avg}^4$), excavation width (B), ratio of the average shear strength over the vertical effective stress (s_u/σ_v'), ratio of the average initial Young's modulus over the vertical effective stress (E_i/σ_v'), and ratio of the depth to hard stratum measured from the current excavation level over the excavation width (T/B). Literature review and parametric study using FEM also indicate that the deformation ratio is believed to be strongly influenced by three parameters; they are ratio of the average shear strength over the vertical effective stress (s_u/σ_v'), ratio of the average initial Young's modulus over the vertical effective stress (E_i/σ_v'), and the normalized clay layer thickness with respect to the wall length ($\sum H_{clay}/H_{wall}$). These influential factors are then included in the FEM numerical experimentation for generating hypothetical cases

so that a large number of artificial data of wall deflection and ground settlement can be used for development of the intended models in Chapter IV.

Table 3.1 Summary of excavation case histories

Case No.	Case name	Construction method	Excavation stages	Excavation width (m)	Final excavation depth (m)	Wall length (m)	Wall thickness (m)	EI (MN-m^2/m)	δ_{hm}/H_{ef} (%)	Depth of hard stratum (m)	References
1	Formosa	BU	7	33.4	18.5	31.0	0.8	918	0.33	31.0	Ou et al. (1993)
2	Post Office	BU	4	29.3	10.0	18.0	0.6	447	0.22	42.0	Kung et al. (2007c)
3	Hsinkuang	BU	6	33.4	16.0	27.0	0.7	709	0.52	55.0	Kung et al. (2007c)
4	Sinyi	BU	5	49.3	12.3	21.5	0.6	447	0.37	46.0	Kung et al. (2007a)
5	Taiwan Sugar	BU	5	35.0	13.2	28.0	0.8	1059	0.44	45.0	Kung et al. (2007a)
6	Tai Kai	BU	5	54.1	12.6	22.0	0.6	447	0.48	48.0	Kung et al. (2007a)
7	TNEC	TD	7	41.2	19.7	35.0	0.9	1507	0.54	46.0	Ou et al. (1998)
8	Taipei Gas	BU	7	35.5	18.1	40.0	1.0	2067	0.42	46.0	Kung et al. (2007c)
9	Tzuchyang	TD	4	36.4	13.6	28.0	0.7	709	0.39	50.0	Kung et al. (2007c)
10	Capital	BU	5	24.6	12.3	23.0	0.6	447	0.48	40.5	Kung et al. (2007c)
11	Far-Eastern	TD	6	70.0	20.0	32.5	0.7	709	0.62	42.0	Hsieh and Ou (1998)
12	Electronics	BU	5	36.0	13.7	28.5	0.7	709	0.35	36.0	Kung et al. (2007a)
13	Baisern	BU	5	41.2	12.3	25.0	0.6	447	0.32	37.0	Kung et al. (2007c)
14	Tzuching	TD	4	31.2	13.9	28.0	0.7	709	0.40	54.4	Ou et al. (1993)
15	MRT-1	BU	6	16.0	16.8	30.0	0.8	1059	0.18	45.0	Kung et al. (2007c)
16	MRT-2	BU	6	19.0	16.4	30.0	0.8	1059	0.25	52.0	Kung et al. (2007c)
17	MRT-3	Semi-TD	4	21.0	12.4	36.5	1.0	2067	0.18	47.9	Kung et al. (2007c)
18	MRT-4	Semi-TD	6	20.0	16.2	33.0	1.0	2067	0.30	45.0	Kung et al. (2007c)
19	Subway-1	BU	5	12.3	14.5	26.0	0.8	1059	0.24	46.0	Kung et al. (2007a)
20	Subway-2	BU	6	15.0	19.4	30.0	1.1	2751	0.31	45.1	Kung et al. (2007a)
21	Subway-3	BU	6	15.0	19.4	30.0	1.1	2751	0.32	50.0	Kung et al. (2007a)
22	Subway-4	Semi-TD	6	20.0	16.2	33.0	1.0	2067	0.29	50.0	Kung et al. (2007c)
23	Subway-5	BU	6	18.4	15.5	31.0	1.2	3572	0.23	45.8	Kung et al. (2007c)
24	Subway-6	BU	5	17.6	12.7	27.0	1.2	3572	0.23	45.8	Kung et al. (2007c)
25	Subway-7	BU	7	17.6	19.9	27.0	1.2	3572	0.26	45.8	Kung et al. (2007a)
26	Subway-8	BU	11	25.7	28.8	51.0	1.2	3572	0.24	50.0	Kung et al. (2007c)
27	Subway-9	BU	10	20.0	26.4	49.0	1.2	3572	0.21	50.0	Kung et al. (2007c)
28	Subway-10	BU	8	17.2	21.7	39.0	1.2	3572	0.19	50.0	Kung et al. (2007c)
29	Syed Alwi	BU	3	28.0	7.8	20.0	0.6	447	0.62	16.0	Lim et al. (2003)
30	Lavender	BU	7	24.0	15.7	28.0	1.0	2067	0.20	20.5	Lim et al. (2003)
31	Tokyo subway	BU	6	30.0	17.0	32.0	0.4	280	1.03	37.0	Miyoshi (1977)
32	HDR-4	BU	4	12.2	12.2	19.2	N/A	161	1.40	19.2	Finno and Harahap (1991)
33	Norway subway	BU	5	11.0	11.0	16.0	N/A	74	2.01	16.0	NGI (1962)

Note: 1. BU is the Bottom-up construction method; TD is Top-down construction method; Semi-TD is Semi-top-down construction method.
2. The diaphragm wall with reinforcing cages was used in Case Nos. 1 through 30. The diaphragm wall with reinforcing I-beam was used in Case No. 31. The sheet pile wall was used in Case Nos. 32 and 33.

Table 3.2 Depths of excavation at various stages in the excavation case histories examined

Case No.	Depths of excavation at various stages (m)										
	Stage 1	Stage 2	Stage 3	Stage 4	Stage 5	Stage 6	Stage 7	Stage 8	Stage 9	Stage 10	Stage 11
1	1.60	4.30	6.90	10.15	13.20	16.20	18.45	-	-	-	-
2	2.50	5.50	7.30	10.00	-	-	-	-	-	-	-
3	2.50	5.30	8.55	11.35	14.05	16.00	-	-	-	-	-
4	2.00	3.95	6.90	9.82	12.25	-	-	-	-	-	-
5	1.10	3.70	7.25	10.75	13.15	-	-	-	-	-	-
6	2.00	4.00	7.00	9.60	12.60	-	-	-	-	-	-
7	2.80	4.90	8.60	11.80	15.20	17.30	19.70	-	-	-	-
8	1.80	4.10	7.30	10.80	12.70	14.20	18.10	-	-	-	-
9	5.20	8.40	11.40	13.60	-	-	-	-	-	-	-
10	1.80	3.90	7.00	10.00	12.30	-	-	-	-	-	-
11	4.95	8.55	12.40	15.40	16.90	20.00	-	-	-	-	-
12	2.20	5.70	8.70	11.70	14.50	16.80	-	-	-	-	-
13	5.20	8.40	11.40	13.60	-	-	-	-	-	-	-
14	1.80	3.90	7.00	10.00	12.30	-	-	-	-	-	-
15	4.95	8.55	12.40	15.40	16.90	20.00	-	-	-	-	-
16	2.20	5.70	8.70	11.70	14.50	16.80	-	-	-	-	-
17	2.80	5.00	9.60	12.40	-	-	-	-	-	-	-
18	2.10	3.65	6.60	9.20	11.70	13.70	16.20	-	-	-	-
19	2.50	4.50	8.50	12.50	14.50	-	-	-	-	-	-
20	-	1.50	2.70	6.00	8.60	11.10	13.30	-	-	-	-
21	2.10	3.65	6.60	9.20	11.70	13.70	16.20	-	-	-	-
22	2.53	4.73	5.73	8.63	11.83	15.83	-	-	-	-	-
23	2.10	3.65	6.60	9.20	11.70	13.70	16.20	-	-	-	-
24	2.50	4.50	8.50	12.50	14.50	-	-	-	-	-	-
25	2.40	5.86	9.06	11.56	14.16	17.66	19.86	-	-	-	-
26	3.20	5.20	8.20	11.00	14.00	16.70	20.00	22.50	25.00	27.00	28.80
27	2.40	5.86	9.06	11.56	14.16	17.66	19.86	-	-	-	-
28	3.20	5.20	8.20	11.00	14.00	16.70	20.00	22.50	25.00	27.00	28.80
29	2.50	6.00	7.80	-	-	-	-	-	-	-	-
30	1.50	5.00	7.50	10.50	12.50	14.50	15.70	-	-	-	-
31	4.00	7.00	9.00	12.00	15.00	17.00	-	-	-	-	-
32	4.70	7.90	11.30	12.20	-	-	-	-	-	-	-
33	5.00	6.00	8.00	10.00	11.00	-	-	-	-	-	-

Table 3.3 Depths where strut or concrete floor slab was installed at various stages in the excavation case histories examined

Case No.	Depths where strut or concrete floor slab was installed at various stages (m)									
	Stage 2	Stage 3	Stage 4	Stage 5	Stage 6	Stage 7	Stage 8	Stage 9	Stage 10	Stage 11
1	1.00	3.70	6.20	9.50	12.50	15.50	-	-	-	-
2	1.00	2.50	6.20	-	-	-	-	-	-	-
3	1.50	4.30	7.55	10.35	13.05	-	-	-	-	-
4	1.38	3.33	6.30	9.23	-	-	-	-	-	-
5	0.55	3.05	6.55	10.05	-	-	-	-	-	-
6	1.13	3.05	6.18	9.28	-	-	-	-	-	-
7	2.00	3.5 & 0	7.10	10.30	13.70	16.50	-	-	-	-
8	1.00	3.30	6.50	10.00	11.90	13.40	-	-	-	-
9	3.60	6.90	10.00	-	-	-	-	-	-	-
10	1.30	3.50	6.50	9.50	-	-	-	-	-	-
11	3.45	7.05	10.90	13.90	16.40	-	-	-	-	-
12	1.50	5.00	8.00	11.00	13.80	-	-	-	-	-
13	3.60	6.90	10.00	-	-	-	-	-	-	-
14	1.30	3.50	6.50	9.50	-	-	-	-	-	-
15	3.45	7.05	10.90	13.90	16.40	-	-	-	-	-
16	1.50	5.00	8.00	11.00	13.80	-	-	-	-	-
17	2.22	4.40	9.00	-	-	-	-	-	-	-
18	1.50	2.70	6.00	8.60	11.10	13.30	-	-	-	-
19	3.65	6.60	9.20	11.70	13.70	16.20	-	-	-	-
20	4.73	5.73	8.63	11.83	15.83	-	-	-	-	-
21	1.50	2.70	6.00	8.60	11.10	13.30	-	-	-	-
22	2.22	4.40	9.00	-	-	-	-	-	-	-
23	1.50	2.70	6.00	8.60	11.10	13.30	-	-	-	-
24	5.00	9.60	12.40	-	-	-	-	-	-	-
25	1.90	5.36	8.56	11.06	13.66	17.16	-	-	-	-
26	2.50	4.50	7.50	10.30	13.30	16.00	13.30	21.80	24.30	26.30
27	1.90	5.36	8.56	11.06	13.66	17.16	-	-	-	-
28	2.50	4.50	7.50	10.30	13.30	16.00	13.30	21.80	24.30	26.30
29	2.00	5.50	-	-	-	-	-	-	-	-
30	1.00	4.50	7.00	10.00	12.00	14.00	-	-	-	-
31	0.00	2.50	6.50	9.00	12.50	15.25	-	-	-	-
32	2.10	4.70 & 5.80	9.10	-	-	-	-	-	-	-
33	2.50	4.00	6.00	8.00	9.50	-	-	-	-	-

Table 3.4 A summary of input variables and their ranges in the numerical experiments

Variable	Ranges of parameters used in the Model	
	Model A for prediction of δ_{hm}	Model B for prediction of R
H_e	2 - 20 (m)	Not needed
$\ln(EI/\gamma_w h_{avg}^4)$	5.94 – 8.48	Not needed
B	10 - 100 (m)	Not needed
s_u/σ'_v	0.25 - 0.40	0.25 - 0.40
E_i/σ'_v	1500 - 3000 times of s_u/σ'_v	1500 - 3000 times of s_u/σ'_v
T/B	0.1 – 4.2 (m)	Not needed
$\sum H_{clay}/H_{wall}$	Not needed	0.6 - 1.0

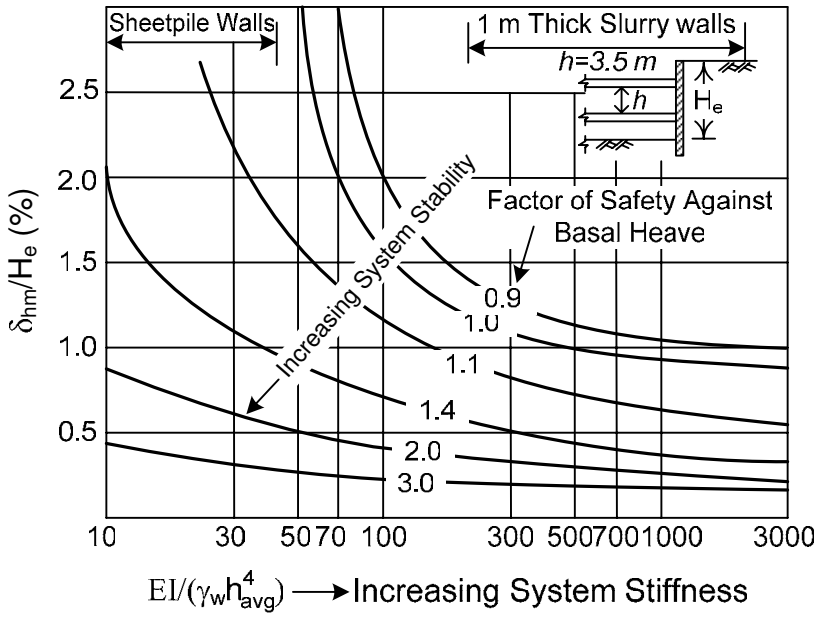

Figure 3.1 Design curves for maximum lateral wall movement for excavations in soft to medium clays
(Reprinted from Clough and O'Rourke, 1990)

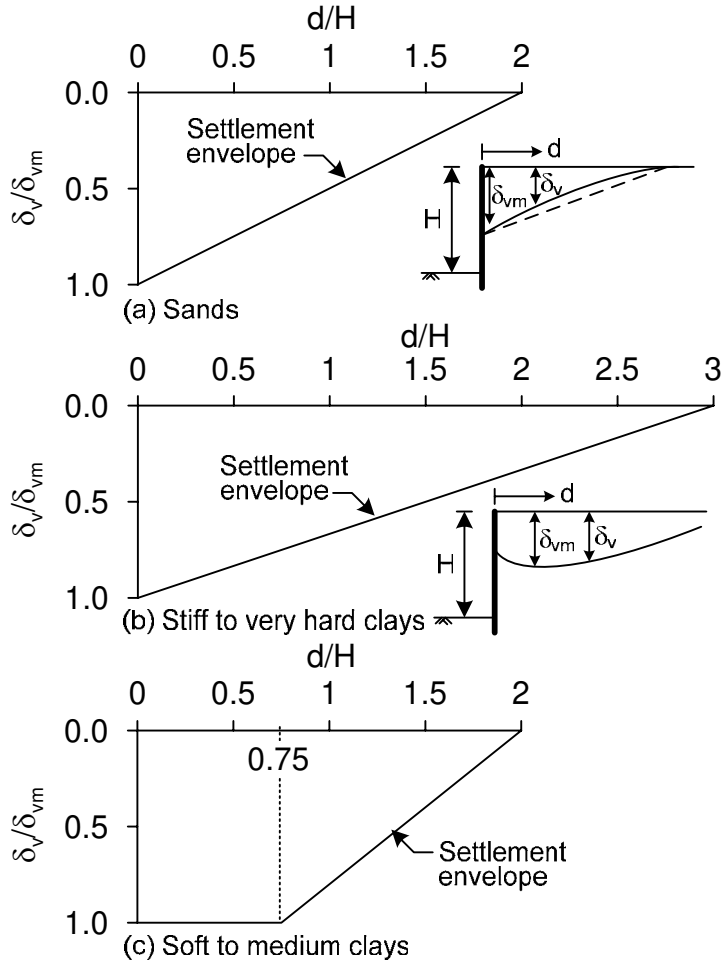

Figure 3.2 Design charts for estimating the profile of surface settlement adjacent to excavation in different soil types (Reprinted from Clough and O'Rourke, 1990)

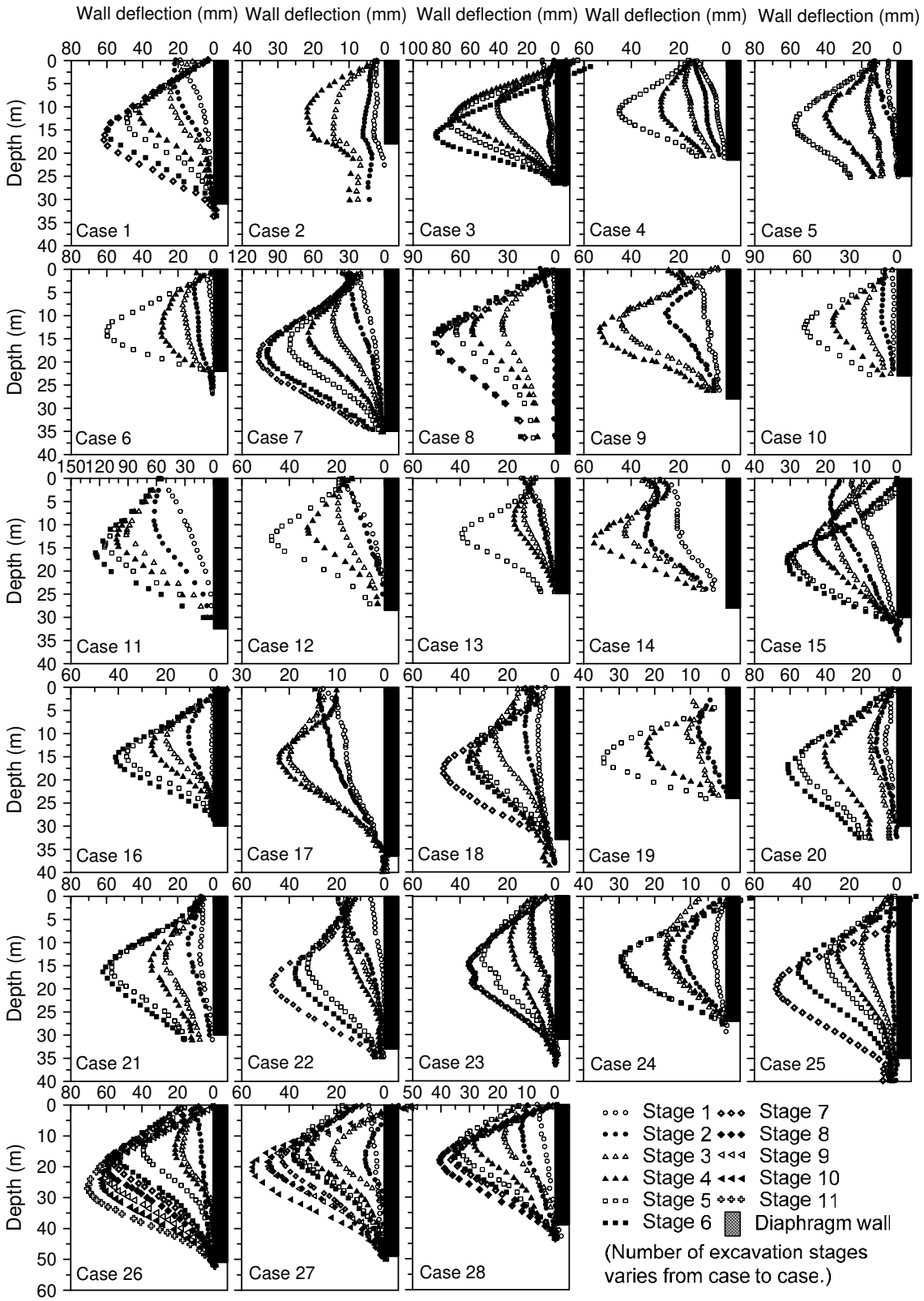

Figure 3.3 Wall deflections observed in excavation case histories

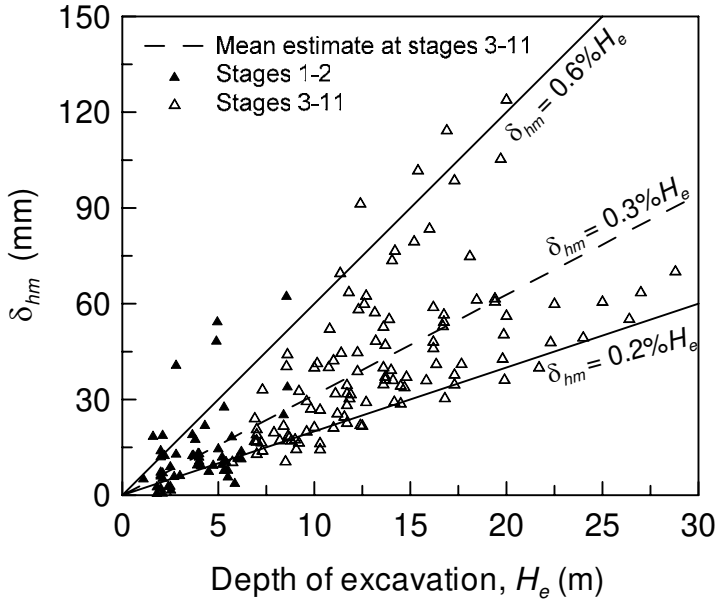

Figure 3.4 Maximum wall deflection versus excavation depth – field data (Cases 1 to 30)

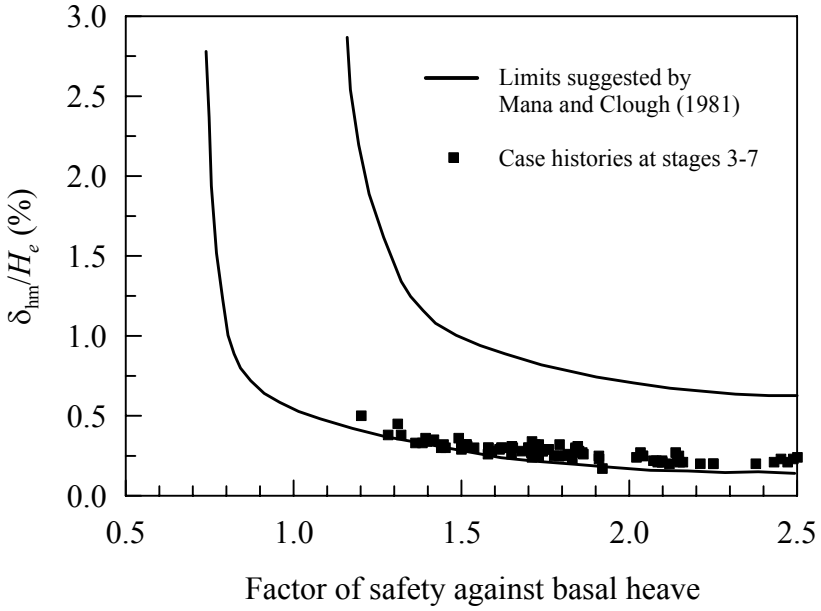

Figure 3.5 Relationship between factor of safety against basal heave and normalized maximum lateral wall deflection

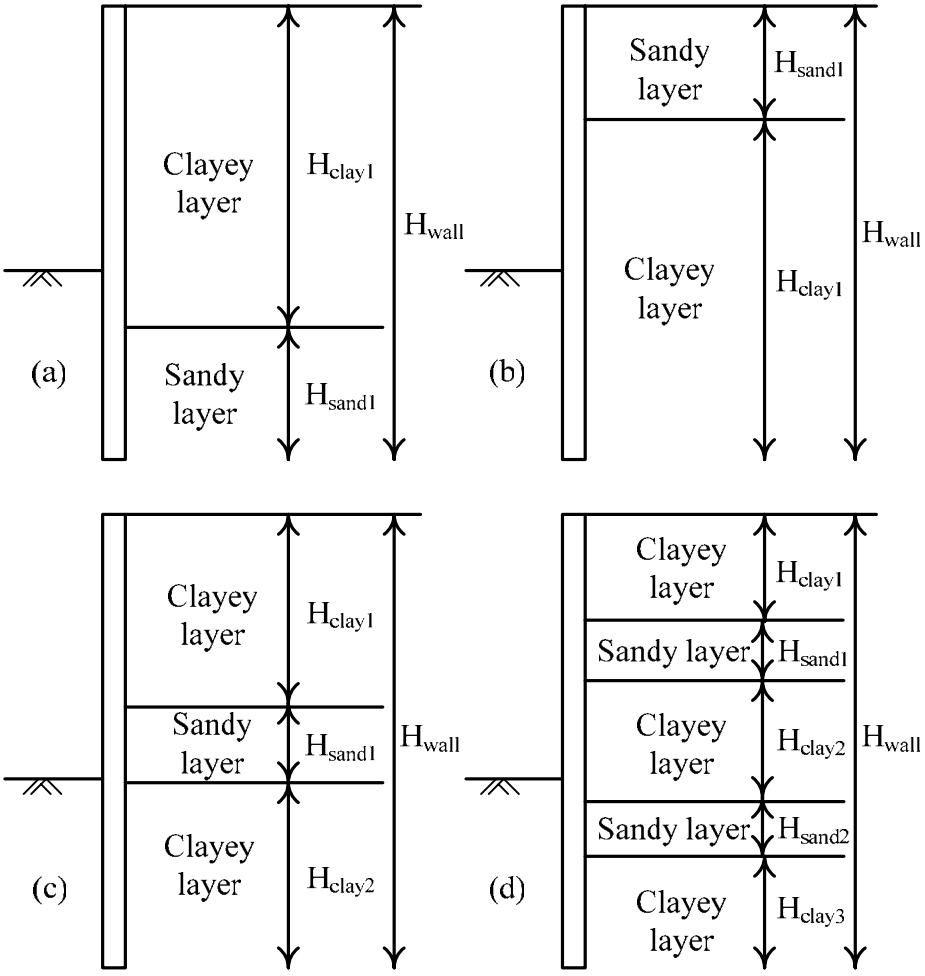

Note: 1. $\Sigma H_{clay} = H_{clay1}+H_{clay2}+...$
2. For a pure clay site, $\Sigma H_{clay} / H_{wall} = 1$

Fig. 3.6 Determination of normalized clay layer thickness ($\sum H_{clay} / H_{wall}$) for a clay dominant site

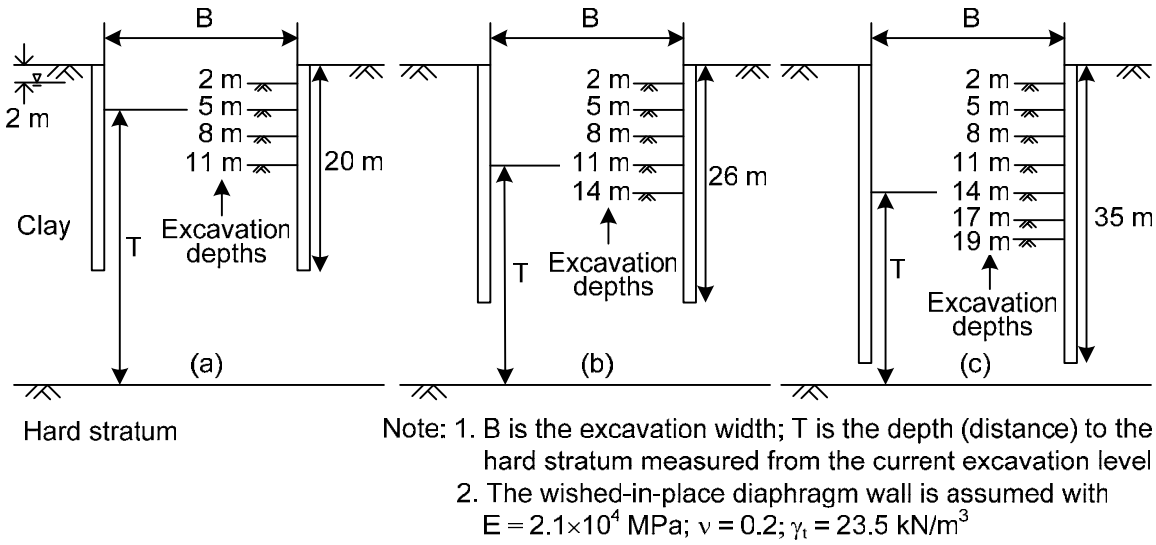

Figure 3.7 Reference hypothetical cases for generating artificial data

CHAPTER IV

SIMPLIFIED MODELS FOR WALL DEFLECTION AND GROUND SURFACE SETTLEMENT CAUSED BY BRACED EXCAVATION IN CLAYS*

Introduction

Buildings adjacent to an excavation may be damaged when the differential settlement induced by the excavation is greater than the allowable differential settlement of the buildings. The estimation of ground surface settlement profile around an excavation thus becomes an essential task of building protection. Finite element method (FEM) is often employed to model complex soil-structure interaction problems such as braced excavations. Although the deflection of the braced wall can generally be predicted well using a routine FEM analysis, the prediction of surface settlement is usually not as accurate (Whittle and Hashash 1994; Hsieh and Ou 1998). As stated in Chapter 2, previous studies have shown that the accuracy of surface settlement predictions by FEM can be significantly improved if the soil behavior at small strain levels can be properly modeled. However, it is generally difficult to model correctly the soil behavior at small strain levels for two reasons: 1) the behavior of soils behind the wall in a braced excavation is often difficult to characterize, and 2) the measurement of soil parameters at small strain (10^{-5} to 10^{-3}) requires a specialized triaxial apparatus

*A major part of this chapter was taken from an article that is in press at the time of writing; Kung, G.T.C., Juang, C.H., Hsiao, E.C.L., and Hashash, Y.M.A., "A simplified model for wall deflection and ground surface settlement caused by braced excavation in clays," *Journal of Geotechnical and Geoenvironmental Engineering*, Vol. 133, No. 6, June 2007.

with high-resolution instruments, which is generally not readily available to practitioners.

As stated in Chapter 3, empirical and semi-empirical methods (Peck 1969; Bowles 1988; Clough and O'Rourke 1990; Ou et al. 1993; Hsieh and Ou 1998) are often used for estimating the ground surface settlement induced by an excavation. Nevertheless these methods have incomplete linkage between wall deflections and surface settlement and do not quantify uncertainty in the estimates of deformations. Thus, improved procedures for estimating the ground surface settlement are needed.

The work done by Hsiao et al. (2006) and Kung et al. (2007a) show artificial neural network approach yields satisfactory results in predicting excavation-induced wall deflection. However, the least-square-regression based approach are used for developing the desired empirical models in this dissertation study as a result of the fact that using empirical models developed through least regression was preferred to reduce the complexity of the intended reliability-based framework for building damage assessment. The proposed model is verified using case histories not used in the development of the model. This dissertation study shows that the developed model can accurately predict maximum wall deflection and ground surface settlement caused by braced excavations in soft to medium clays.

Development of the Least-square Regression Models

The focus of this chapter is to develop a semi-empirical model, which consists of three component models for predicting wall deflection, deformation ratio, and ground surface settlement profile caused by a braced excavation in soft to medium clays. It should be noted that development of a component model of deformation ratio as a means for predicting the maximum ground surface settlement is chosen for two reasons: 1) ground surface settlement is difficult to predict directly from basic parameters, and 2) the concept of deformation ratio is well understood and the published results in the literature can be used as a guide.

The desired empirical models are developed upon the artificial data of selected hypothetical cases which are generated in Chapter 3 and verified using collected case histories not used in the development of the model. Further, model uncertainty (bias) of each component model and the whole model is also studied. Various elements in the development for the proposed models are shown in Figure 4.1.

Model A for Predicting Maximum Wall Deflection

The first component of the intended model, Model A, for predicting the maximum wall deflection caused by a braced excavation is developed in two steps. First, a regression-based equation is developed with five input variables (H_e, $EI/\gamma_w h_{avg}^4$, B, s_u/σ'_v, and E_i/σ'_v); the effect of hard stratum is purposefully excluded at this point. Thus, only the hypothetical cases that have a "deep" hard stratum (i.e., hard stratum is present at the depth of 50 m below the toe of wall)

are used to develop the equation. Then, the effect of the hard stratum, in terms of the variable T/B, is expressed as a "reduction factor" that is applied to the estimated maximum wall deflection.

The hypothetical cases in the first step are used to (a) investigate the relationship between each of the five variables and the maximum wall deflection at a given excavation depth, and (b) to provide data for the multiple-variable regression analysis. Before performing regression analysis, each of the five input variables is transformed so that approximately a linear trend between the maximum wall deflection and each of these variables is achieved. The form of the transformation function is established through numerous trial-and-error analyses with an objective of maintaining a uniform and simple functional form across all input variables. The following functional form is adopted for transformation:

$$X = t(x) = a_1 x^2 + a_2 x + a_3 \tag{4.1}$$

where x is each of the input variables (H_e, $\ln(EI/\gamma_w h_{avg}^4)$, $B/2$, s_u/σ'_v, or E_i/σ'_v); X is the transformed variable. The coefficients, a_1, a_2, and a_3, for each variable are obtained through error minimization using the artificial data generated from FEM analyses and are shown in Table 4.1. The appropriateness of these linear transformations is reflected in the coefficients of determination (R^2) that are in the range of 0.95 to 0.98. Possible drawback of using a polynomial transformation function such as Eq. 4.1 is that it is not a monotonic function, and as such, it may not be suitable for cases that fall outside of the intended data

ranges. Thus, the applicable ranges for input variables should be noted: (1) $0 \le H_e \le 30\,\text{m}$; (2) $0 \le EI/\gamma_w h_{avg}^4$; (3) $0 \le B \le 100\,\text{m}$; (4) $0.2 \le s_u/\sigma_v' \le 0.4$; and (5) $200 \le E_i/\sigma_v' \le 1200$.

A total of 144 representative hypothetical cases are then used to establish the regression equation for estimating the maximum wall deflection (δ_{hm}). The developed regression equation is expressed as:

$$\delta_{hm}(mm) = b_0 + b_1X_1 + b_2X_2 + b_3X_3 + b_4X_4 + b_5X_5 + b_6X_1X_2 + b_7X_1X_3 + b_8X_1X_5 \qquad (4.2)$$

where $X_1 = t(H_e)$, $X_2 = t(\ln(EI/\gamma_w h_{avg}^4))$, $X_3 = t(B/2)$, $X_4 = t(s_u/\sigma_v')$, and $X_5 = t(E_i/\sigma_v')$.

The coefficients for Eq. 4.2 determined through the least-square regression are as follows: $b_0 = -13.41973$, $b_1 = -0.49351$, $b_2 = -0.09872$, $b_3 = 0.06025$, $b_4 = 0.23766$, $b_5 = -0.15406$, $b_6 = 0.00093$, $b_7 = 0.00285$, and $b_8 = 0.00198$.

Figure 4.2 shows wall deflection values computed using Eq. 4.2 versus measured values from 30 real cases (Cases 1 to 30) and FEM analyses for the 144 hypothetical cases. Eqs. 4.1 and 4.2 are shown to be an effective model for estimating the excavation-induced maximum wall deflection in soft to medium clays given high *coefficient of determination* (R^2) and low *coefficient of variation* (COV). However, Eq. 4.2 does not account for possible effect of the presence of hard stratum. To this end, additional hypothetical cases with various scenarios of depths to the hard stratum are used to investigate this effect.

Figure 4.3 shows the results of the numerical experimentation where the effect of the presence of the hard stratum is investigated. The deflection reduction factor, *K*, presented in this figure is defined as:

$$K = \delta_{hm,m} / \delta_{hm} \tag{4.3}$$

where δ_{hm} is the maximum wall deflection assuming very deep hard stratum, and $\delta_{hm,m}$ is the modified maximum wall deflection that accounts for the presence of the hard stratum.

It should be noted that for a specific hypothetical case (a "fixed" *B* along with other parameters), the parameter *T* is allowed to vary, and the FEM results show that the computed maximum wall deflection increases initially with the increase of T/B ratio and then gradually converges to a constant at larger T/B. Thus, at smaller T/B ratios ($T/B < 0.4$), the presence of the hard stratum has an important influence on the magnitude of the maximum wall deflection, and at $T/B > 0.4$, the influence of the hard stratum is negligible. A simplified equation to account for the presence of the hard stratum is proposed below:

$$K = 1.5(T/B) + 0.4 \quad \text{for} \quad T/B \le 0.4$$

$$K = 1 \quad \text{for} \quad T/B > 0.4 \tag{4.4}$$

Thus, the maximum wall deflection may be determined from Eqs. 4.1 and 4.2. The result should then be modified with the reduction factor obtained from Eqs. 4.3 and 4.4 to account for the effect of the hard stratum.

A review of the 30 excavation case histories (cases 1 to 30) used to validate Eqs. 4.3 and 4.4 reveals that only four cases require modification (with $T/B \leq 0.4$). Specifically, the maximum wall deflection at the final stage of excavation in Cases 1, 29, and 30, respectively, and those at the last three stages of excavation in Case 11 require modification. The modified maximum wall deflections ($\delta_{hm,m}$) in these cases are more accurate than those without modification, when they are compared to the observed wall deflections, as reflected in Table 4.2.

In summary, six parameters (H_e, $\ln(EI/\gamma_w h_{avg}^4)$, $B/2$, s_u/σ_v', E_i/σ_v', and T/B) are considered essential for estimating the maximum wall deflection in a braced excavation in soft to medium clay. The first five parameters are included in Eqs. 4.1 and 4.2 for estimating the maximum wall deflection for situations where a hard stratum is deep. For situations where the effect of the hard stratum may be significant, the calculated maximum wall deflection is further modified with a reduction factor (Eqs. 4.3 and 4.4) into the modified maximum wall deflections ($\delta_{hm,m}$). Finally, Eqs. 4.1 through 4.4 are *collectively* termed Model A.

Model B for Predicting the Deformation Ratio

Development and assessment of the second component of the intended model, Model B, for predicting the deformation ratio *R* are presented in this

section. With the generated data described previously, attempts are made to develop an empirical equation that relates R to the three variables ($\sum H_{clay} / H_{wall}$, s_u/σ'_v, and $E_i/1000\sigma'_v$) through regression analyses. The regression equation takes the following form:

$$R = c_0 + c_1 Y_1 + c_2 Y_2 + c_3 Y_3 + c_4 Y_1 Y_2 + c_5 Y_1 Y_3 + c_6 Y_2 Y_3 + c_7 Y_3^3 + c_8 Y_1 Y_2 Y_3 \quad (4.5)$$

where $Y_1 = \sum H_{clay} / H_{wall}$, $Y_2 = s_u/\sigma'_v$, $Y_3 = E_i/1000\sigma'_v$, and the coefficients for Eq. 4.7 determined through the least-square regression are as follows: $c_0 = 4.55622$, $c_1 = -3.40151$, $c_2 = -7.37697$, $c_3 = -4.99407$, $c_4 = 7.14106$, $c_5 = 4.60055$, $c_6 = 8.74863$, $c_7 = 0.38092$, and $c_8 = -10.58958$.

Figure 4.4 shows the performance of Model B in reproducing the results of FEM solutions. The accuracy and precision of Model B for computing the deformation ratio is reflected by high R^2 (0.92) and low COV (0.11) shown in Figure 4.4. In addition, almost all data points are within ±15% of the 1-1 line where the predicted deformation ratio values are equal to those determined by FEM analyses.

Nine case histories (Cases 1, 6, 7, 11, 16, 18, 31, 32, and 33) listed in Table 3.1, in which both wall deflection and ground surface settlement measurements are available, are used to further validate Model B. The ranges of values of the three variables in these nine cases are shown in Table 4.3. The values of two variables, $\sum H_{clay} / H_{wall}$ and s_u/σ'_v, are derived from the published

literature and E_i/σ'_v is estimated from the studies in which the initial stiffness of clay has been measured by the small-strain triaxial test or by other tests capable of measuring shear wave velocity (such as cross-hole tests and bender element tests).

Kung (2003) developed a set of triaxial testing apparatus and carried out the small-strain triaxial tests and bender element tests on the Taipei silty clay sampled from the locations adjacent to the site of Case 7. His results showed that at the strain level of 10^{-5}, the normalized Young's modulus (E_i/σ'_v) of the Taipei silty clay ranged from 550 to 750. Based on this result, the E_i/σ'_v values for Cases 1, 6, 11, 16 and 18, which are located in the Taipei Basin, are assumed to vary from 550 to 750. For Case 32, the value of E_i/σ'_v varies in the range of 250 to 350 determined based on the measurements of small-strain triaxial tests and bender element tests of samples taken from the Chicago clay by Holman (2005). For Cases 31 and 33, no relevant testing results are available to determine the E_i/σ'_v of clay. They are estimated by comparing the shear strength of these two cases with that of Case 32, as listed in Table 4.4.

Figure 4.5 shows the performance of Model B, in which the predicted deformation ratio is compared with the observed deformation ratio for each of the nine cases. Six of the nine cases (data points) are within ±15% of the 1:1 line; the other three data points are near the ±15% zone. The result shows that the deformation ratio *R* is accurately predicted by Model B.

In summary, Model A (Eqs. 4.1, 4.2, 4.3, and 4.4) may be used to estimate the maximum wall deflection δ_{hm} (or $\delta_{hm,m}$ if the hard stratum is present) and Model B (Eq. 4.5) may be used to estimate the deformation ratio *R*. The

maximum surface settlement δ_{vm} can be then determined from Eq. 3.1 ($\delta_{vm} = R\delta_{hm}$).

Model C for Predicting the Surface Settlement Profile

Based on the findings presented by Clough and O'Rourke (1990) and Hsieh and Ou (1998), the concave-type settlement profile is generally observed for braced excavations in soft to medium clays. Figure 4.6 shows the surface settlement observed from the nine cases as well as the trends established in the previous studies and the present study.

The concept of the primary and secondary influence zones within the settlement profile (Hsieh and Ou 1998) is employed to examine the settlement profile in the nine cases (Cases 1, 6, 7, 11, 16, 18, 31, 32, and 33). Figure 4.6 shows three zones of Hsieh and Ou's settlement profile: zone 1 $(0 \le d / H_e \le 0.5)$, zone 2 $(0.5 \le d / H_e \le 2)$, and zone 3 $(2 \le d / H_e \le 4)$. Overall, their suggestion to divide the settlement profile into three zones is supported by the data presented. In the present study, linear regression analyses of the observed data are performed for each of the three zones, and in zone 1, the Hsieh and Ou's profile does not follow the trend established by regression. In fact, a negative R^2 value is obtained for the Hsieh and Ou's profile based on the observed data in zone 1. The result may be understandable since the Hsieh and Ou's profile in zone 1 was intended to be conservative and placed below the trend line established by linear regression (not shown in Figure 4.6).

In the present study, the pioneering work by Hsieh and Ou (1998) is modified so that a consistent accuracy and precision (in terms of R^2 and COV) between zones is maintained. The trends established by regression are used as a basis for such modification. With the proposed profile, the R^2 and COV of the predictions based on the data in zone 1 are 0.80 and 0.20, respectively, and R^2 and COV in zone 2 are 0.86 and 0.22, respectively. The proposed settlement profile, denoted herein as the Model C, may be expressed as:

$$\delta_v / \delta_{vm} = \left(1.6 \times d / H_e + 0.2\right) \qquad \text{for } 0 \le d/H_e \le 0.5 \tag{4.6a}$$

$$\delta_v / \delta_{vm} = \left(-0.6 \times d / H_e + 1.3\right) \qquad \text{for } 0.5 \le d/H_e \le 2.0 \tag{4.6b}$$

$$\delta_v / \delta_{vm} = \left(-0.05 d / H_e + 0.2\right) \qquad \text{for } 2.0 \le d/H_e \le 4.0 \tag{4.6c}$$

where d is the distance from the wall; H_e is the excavation depth; δ_v is the vertical settlement at the distance d; δ_{vm} is the maximum vertical settlement.

Model Bias of the Proposed Model

The proposed model consists of three component models, Model A (Eqs. 4.1 through 4.4) for the estimation of the maximum wall deflection, Model B (Eq. 4.5) for estimation the deformation ratio (and thus the maximum ground surface settlement through Eq. 3.1), and Model C (Eq 4.6) for the estimation of the surface settlement profile. The entire model is referred to herein as the KJHH model (Kung et al. 2007c).

For practical applications, it should be of interest to estimate model uncertainty or *model bias* of the developed KJHH model. The model bias is often expressed as a bias factor (*BF*):

$$BF = \frac{\text{observed value (or "true" value)}}{\text{estimated value}} \tag{4.7}$$

The bias factor *BF* is often assumed to follow normal or lognormal distribution (Phoon and Kulhawy 2005; Juang et al. 2006). The closer the mean of *BF* is to 1.0, the more *accurate* a model is, and the smaller the variation of *BF* is, the more *precise* a model is.

Following the definition of bias factor in Eq. 4.9, the model bias of Model A (Eqs. 4.1 through 4.4) is expressed in terms of a bias factor BF_A:

$$BF_A = \frac{\text{observed } \delta_{hm} \text{ from field measurement}}{\text{estimated } \delta_{hm,m} \text{ by Model A}} \tag{4.8}$$

As listed in Table 3.1, the maximum wall deflection observations are available for all 33 cases examined in this paper. Model A can be used to predict $\delta_{hm,m}$ for each of these cases, and thus, the values of BF_A for all 33 cases can be determined. Figure 4.7 shows the distribution of these BF_A values, which follows approximately a normal distribution. The mean and standard deviation of the calculated BF_A values are: $\mu_{BF_A} = 1.0$ and $\sigma_{BF_A} = 0.25$. It should be noted that almost identical results are obtained if both real cases and artificial data (shown in

Figure 4.2) are used in the calculation of the bias factor BF_A. This suggests that the sample size of 33 case histories used in the model bias assessment is adequate, and the obtained statistics ($\mu_{BF_A} = 1.0,$ and $\sigma_{BF_A} = 0.25$) may be considered as a best estimate.

Similarly, the model bias of Model B (Eq. 4.5) is expressed in terms of bias factor BF_B:

$$BF_B = \frac{\text{observed } R \text{ from field measurement}}{\text{estimated } R \text{ by Model B}} \tag{4.9}$$

As noted previously, the observed maximum ground surface settlement is available only in nine of the 33 cases. This follows that the bias factor BF_B for each of the nine cases can be determined, and the mean and standard deviation of the calculated BF_B values are determined to be: $\mu_{BF_B} = 1.05$ and $\sigma_{FB_B} = 0.21$. It should be noted that the statistics of the bias factor obtained here are based on very limited data (9 cases), and the obtained statistics ($\mu_{BF_B} = 1.05$ and $\sigma_{BF_B} = 0.21$) may not be the best estimate because of the sample size. Additional case histories that have both observed data of the wall deflection and the ground surface settlement are needed for the improved estimate of the statistics of the model bias factor. In the absence of additional case histories, 100 artificial data that were generated through FEM solutions (Figure 4.4) may be used to supplement the nine cases. Repeating the above analysis using both case histories and artificial data, the mean and standard deviation of the model bias factor BF_B are determined

to be: $\mu_{BF_B} = 1.0$ and $\sigma_{BF_B} = 0.13$. Figure 4.8 shows the distribution of these BF_B values, which follows approximately a normal distribution.

The maximum ground surface settlement δ_{vm} can be obtained by multiplying $\delta_{hm,m}$ with R, as indicated in Eq. 3.1. Thus, the bias factor BF_{vm} for the calculated maximum ground surface settlement based on Eq. 3.1 can be determined theoretically from the bias factors BF_A and BF_B without additional data. The mean of the bias factor BF_{vm}, denoted as $\mu_{BF_{vm}}$, is determined to be:

$$\mu_{BF_{vm}} = \mu_{BF_A} \cdot \mu_{BF_B} = (1.0)\,(1.0) = 1.0.$$

The standard deviation of the bias factor BF_{vm}, denoted as $\sigma_{BF_{vm}}$, may be determined using the first-order Taylor series approximation (Ang and Tang 2006; Harr 1987):

$$\sigma_{BF_{vm}} = \sqrt{\mu_{BF_A}^2 \sigma_{BF_A}^2 + \mu_{BF_B}^2 \sigma_{BF_B}^2 + 2\mu_{BF_A}\mu_{BF_B}\rho\sigma_{BF_A}\sigma_{BF_B}}$$

$$= \sqrt{(1.0)^2(0.25)^2 + (1.0)^2(0.13)^2 + 2(1.0)(1.0)(0.6)(0.25)(0.13)}$$

$$= 0.34$$

It should be noted that in the above calculation, the correlation coefficient ρ between $\delta_{hm,m}$ and R, or between the two bias factors, BF_A and BF_B, is estimated based on the cases examined in this paper. By applying both Models A and B to the database of 33 cases, the values of $\delta_{hm,m}$ and R can be obtained, and the correlation coefficient ρ can then be estimated based on these data, and the result shows that $\rho \approx 0.6$. Additional data may be needed to confirm this result but it is

deemed accurate enough for the purpose of estimating the COV of the bias factor BF_{vm}. Finally, the coefficient of variation (COV) of the bias factor BF_{vm} is calculated as: COV = 0.34/1.0 = 0.34 (or 34%).

The ground surface settlement δ_v at any distance away from the wall (expressed as a ratio, d/H_e) can be obtained by multiplying δ_{vm} with the normalized settlement ratio (δ_v/δ_{vm}) obtained from Model C. An investigation of the correlation between δ_{vm} and δ_v based on the well-documented Cases 1 and 7 reveals that there is a strong correlation between the two, which is expected as δ_v is related to δ_{vm} through Eq. 4.6. Thus, the coefficient of variation of δ_v may be taken as the COV of the calculated δ_{vm}, which is 0.34.

The model bias factor of the settlement profile (Model C; Eq. 4.6), denoted as BF_C, is the bias factor of the calculated δ_v. It is of interest to estimate this bias from actual field data such as those shown in Figure 4.6. In a manner similar to the analyses presented previously, BF_C may be defined as follows:

$$BF_C = \frac{\text{observed } (\delta_v/\delta_{vm}) \text{ from field measurement}}{\text{estimated } (\delta_v/\delta_{vm}) \text{ by Model C}} \tag{4.10}$$

Using the data shown in Figure 4.6, the mean of this model bias is determined to be: $\mu_{BF_C} = 1.0$, and the standard deviation is determined to be: $\sigma_{BF_C} = 0.35$, which results in a coefficient of variation of 0.35. Figure 4.9 shows the distribution of these BF_C values, which follows approximately a normal distribution. Thus, the result estimated from field data agree very well with that obtained through

theoretical calculation that was based on the model bias factors, BF_A and BF_B, as presented previously.

Summary of the Developed Model

The developed KJHH model may be used to estimate the maximum wall deflection, the deformation ratio, the maximum ground surface settlement, and the surface settlement profile. The KJHH model is applicable to braced excavations in soft to medium clays, and a step-by-step procedure to implement this model is presented below:

(1) Obtain values for seven variables, H_e, $\ln(EI/\gamma_w h_{avg}^4)$, $B/2$, s_u/σ'_v, E_i/σ'_v, T/B, and $\sum H_{clay}/H_{wall}$. The values of s_u/σ'_v and E_i/σ'_v should be obtained from the tests on the clay within the depth range of wall length. The small strain triaxial tests, bender element tests, or in-situ seismic tests are recommended to measure E_i/σ'_v.

(2) Transform first five variables using Eq. 4.1 and the coefficients in Table 4.1.

(3) Calculate the maximum wall deflection (δ_{hm}) using Eq. 4.2.

(4) Adjust the calculated maximum wall deflection ($\delta_{hm,m}$) with the reduction factor K to account for possible effect of hard stratum (Eqs. 4.3 and 4.4).

(5) Determine the deformation ratio R using Eq. 4.5.

(6) Calculate δ_{vm} based on $\delta_{hm,m}$ and the deformation ratio R (Eq. 3.1).

(7) Construct the surface settlement profile using Eq. 4.6.

(8) The variation of the computed $\delta_{hm,m}$, R, δ_{vm}, and ground surface settlement profile, in terms of standard deviation, can be estimated based on the assessed model biases.

Assessment of the Developed Model

Figures 4.10(a) and 4.10(b) compare the predicted and observed maximum wall deflection using cases histories where observed values from *various* stages of excavation are available. The intent is to show the performance of the model A at various stages of excavation, not just at the final stage. Here, the comparison is made between the predicted and observed values from *various* stages of excavation in Cases 1 to 28. The results shown in Figure 4.10 indicate that in general, the wall deflections for all case histories examined can be satisfactorily predicted by the Clough and O'Rourke method and the developed model A, although the latter was shown to be more accurate overall.

Figure 4.11 also compares the predicted and observed maximum wall deflections at various stages of excavation, but the results from all case histories are shown. In Figure 4.11(a), the predictions are made with the Clough and O'Rourke method, denoted as C&O method hereinafter, and in Figure 4.11(b), the predictions are made with the proposed model. The proposed model is shown to be closer to observed behavior; it has improved upon the important contributions of C&O method.

Figure 4.12 compares the predicted and observed maximum surface settlement using two high quality case histories where observed values from

various stages of excavation are available. The intent is to show the performance of the developed model at various stages of excavation, not just at the final stage. Here, the comparison is made between the predicted and observed values from *various* stages of excavation in Cases 1 and 7. The performance of the developed model in predicting the maximum wall deflection and maximum surface settlement is considered satisfactory, as all data points are either within or near ±15% of the 1-1 line.

Figure 4.13 compares the proposed model and C&O method for their accuracy in predicting the maximum surface settlement of nine cases (Cases 1, 6, 7, 11, 16, 18, 31, 32, and 33) listed in Table 4.3. For the proposed model, the prediction of the maximum surface settlement is straightforward (by means of a "dedicated" equation for the deformation ratio R), as described previously. Since no specific equation for deformation ratio R is available in the C&O method, the maximum surface settlement is predicted with the "mean" and the upper bound of the range of R values suggested in Clough and O'Rourke (1990). In the C&O method, the mean R value is equal to 0.75 and the upper bound is R = 1.0. The observed values are compared with the predicted values made with the proposed model and the C&O method. Linear regression trend lines are established for the three sets of predictions (the proposed model, the C&O method with R = 0.75, and the C&O method with R = 1.0). The results are shown in Figure 4.13 along with the 1-1 line. The regression trend line of the predicted versus observed maximum surface settlement obtained by the proposed model is very close to the

1-1 line, which indicates, again, the proposed model has improved upon the predictions given by the C&O method.

Finally, four of the nine case histories (Cases 1, 7, 11, and 31) previously employed in the validation are further examined using the KJHH model. A summary of the calculations for the maximum wall deflection and the deformation ratio is presented in Table 4.4. The predicted surface settlement profiles for these case histories at the final excavation stage along with field observations are shown in Figure 4.14. In addition to the mean prediction, the variation of the prediction, in terms of the mean ± 1 standard deviation is also shown in Figure 4.14. The *accuracy* and *precision* of the prediction of the surface settlement profile using the proposed model is fully assessed.

Summary and Conclusions

Use of empirical models developed through least square regression was preferred so as to reduce the complexity of the intended reliability-based framework for building damage assessment. To this end, the KJHH model was developed for the estimation of the maximum wall deflection, the maximum surface settlement, and the surface settlement profile in an excavation in soft to medium clays. The proposed KJHH model is developed based on a database of 33 case histories and the results of a large number of well-calibrated FEM analyses. The satisfactory performance of the proposed model is demonstrated and the model bias is assessed. The following conclusions are reached:

1. The effect of the presence of hard stratum on the excavation-induced maximum wall deflection is investigated through an extensive series of FEM experimentation. The effect is expressed as a reduction factor *K* that is related to the ratio of the depth to hard stratum, measured from the current excavation level, over the excavation width (T/B). At smaller T/B ratios (*T/B* < 0.4), the presence of the hard stratum is seen to have a great influence on the magnitude of the calculated maximum wall deflection, and at *T/B* > 0.4 and beyond, the influence of the hard stratum is negligible. For the cases with *T/B* < 0.4, the modified maximum wall deflections ($\delta_{hm,m}$), rather than δ_{hm}, should be reported.
2. Six factors, H_e, *B/2*, $EI/\gamma_w h_{avg}^4$, s_u/σ_v', E_i/σ_v', and T/B are considered essential for predicting the excavation-induced maximum wall deflection. These factors are the required variables in Model A, the first component of the proposed KJHH model. Two steps are needed for estimation of the maximum wall deflection using Model A. First, the first five factors are used to estimate δ_{hm} using Eqs. 4.1 and 4.2, and then the estimated δ_{hm} is modified into $\delta_{hm,m}$ considering the effect of hard stratum (Eqs. 4.3 and 4.4). Model A (Eqs. 4.1 through 4.4) is validated with 30 excavation case histories, and the results show that $\delta_{hm,m}$ (or δ_{hm} if the hard stratum is not present) can be accurately predicted using this model.
3. The deformation ratio *R* in a braced excavation in clay-dominant sites is found to be influenced by three normalized parameters,

$\sum H_{clay} / H_{wall}$, s_u / σ'_v, and $E_i / 1000\sigma'_v$. These three normalized parameters are the required input variables of Model B, the second component of the KJHH model. Satisfactory performance of Model B for predicting the deformation ratio R is evidenced by high R^2 and low COV obtained in the regression analysis. Validation of Model B using quality case histories is performed and satisfactory results are also obtained.

4. The proposed KJHH model is able to predict reasonably well the maximum wall deflection, the maximum ground surface settlement, and the ground surface settlement profile caused by braced excavations in soft to medium clays. It has improved upon the important contributions of earlier investigators.
5. The model bias of the developed KJHH model is assessed at the component level as well as the entire model as a whole. The KJHH model is judged to be accurate (with all mean bias factors approximately equal to 1.0), and the precision of the model is quite high for this type of soil-structure interaction problem, as the variation of the model prediction is generally small (COVs of 25%, 13%, and 35% for predictions of the maximum wall deflection, the deformation ratio, and the ground surface settlement, respectively).
6. The proposed KJHH model assumes normal workmanship and no basal failure in the braced excavation. Possible uncertainty caused by the soil variability at the excavation site and construction-related issues such as dewatering activity and over excavation prior to support installation, are not explicitly addressed in this paper. Engineering judgment is required and must be carefully

exercised to adjust the model bias of the KJHH model, as necessary, to account for these factors. They are, however, beyond the scope of this dissertation study.

7. Although it has been shown to be effective in estimating the excavation-induced maximum wall deflection, maximum surface settlement and surface settlement profile, the KJHH model should be regarded as the "first-order" approximation and more advanced numerical solutions should be pursued as appropriate.

Table 4.1 Coefficients for linear transformation of five variables

Variables x	Applicable range	Coefficients of Equation 2		
		a_1	a_2	a_3
H_e (m)	0 – 30	-0.4	24	-50
$\ln(EI/\gamma_w h_{avg}^4)$	≥ 0	11.5	-295	2000
$B/2$ (m)	$0 \le B \le 100$	-0.04	4	90
s_u/σ'_v	0.2 – 0.4	3225	-2882	730
E_i/σ'_v	200 – 1200	0.00041	-1	500

Table 4.2 Predicted maximum wall deflection with and without reduction factor versus the measured maximum wall deflection (Cases 1, 11, 29, and 30)

Case No.	Excavation depth (m)	Observed δ_{hm} (mm)	δ_{hm} (mm) predicted by Eq. 4.2	T / B	Reduction factor K	$\delta_{hm,m}$ (mm) modified by Eqs. 4.3 & 4.4
1	18.45 (7)*	61.7	84.6	0.376	0.96	81.2
11	15.40 (3)*	102.2	117.1	0.380	0.97	113.5
	16.90 (4)*	114.7	123.2	0.359	0.94	115.8
	20.00 (5)*	124.4	135.1	0.314	0.87	117.5
29	7.80 (3)*	48.0	68.9	0.293	0.84	55.3
30	15.70 (7)*	31.0	55.2	0.200	0.70	38.6

*Note: the number in parentheses denotes the excavation stage.

Table 4.3 Values of the input variables used to calculate the deformation ratio

Case	$\sum H_{clay} / H_{wall}$	Ranges of values from measurements		Values used	
		s_u/σ'_v	E_i/σ'_v	s_u/σ'_v	E_i/σ'_v
1	0.87	0.30-0.32	550-750[a]	0.31	650
6	0.75	0.30-0.32	550-750[a]	0.31	650
7	0.87	0.30-0.32	550-750[a]	0.31	650
11	0.88	0.30-0.32	550-750[a]	0.31	650
16	0.62	0.30-0.32	550-750[a]	0.31	650
18	1.00	0.30-0.32	550-750[a]	0.31	650
31	0.93	0.20-0.25	250-350[c]	0.22	300
32	0.79	0.19-0.25	250-350[b]	0.22	300
33	0.87	0.22-0.25	250-350[c]	0.23	300

Note: [a] Measured by Kung (2003).
[b] Measured by Holman (2005).
[c] Estimated based on shear strength.

Table 4.4 Data of four case histories used for validating the KJHH model

Case	H_{ef} (m)	$EI/\gamma_w h_{avg}^4$ at final stage	B (m)	s_u/σ'_v	E_i/σ'_v	$\frac{\sum H_{clay}}{H_{wall}}$	Observed		Predicted	
							δ_{hm} (mm)	R	δ_{hm} (mm)	R
1	18.45	1320	33.4	0.31	650	0.87	62.8	0.68	81.7[b]	0.60
7	19.70	1294	41.2	0.31	650	0.87	106.4	0.70	98.0	0.60
11	20.00	711	70.0	0.31	650	0.88	135.0	0.62	132.9	0.60
31	17.00	500[a]	30.0	0.23	300[a]	0.93	175.7	0.86	187.4	0.97

Note: [a] Denoting that the value is an estimate.
[b] Denoting that the value is further modified using Eqs. 4.3 and 4.4.

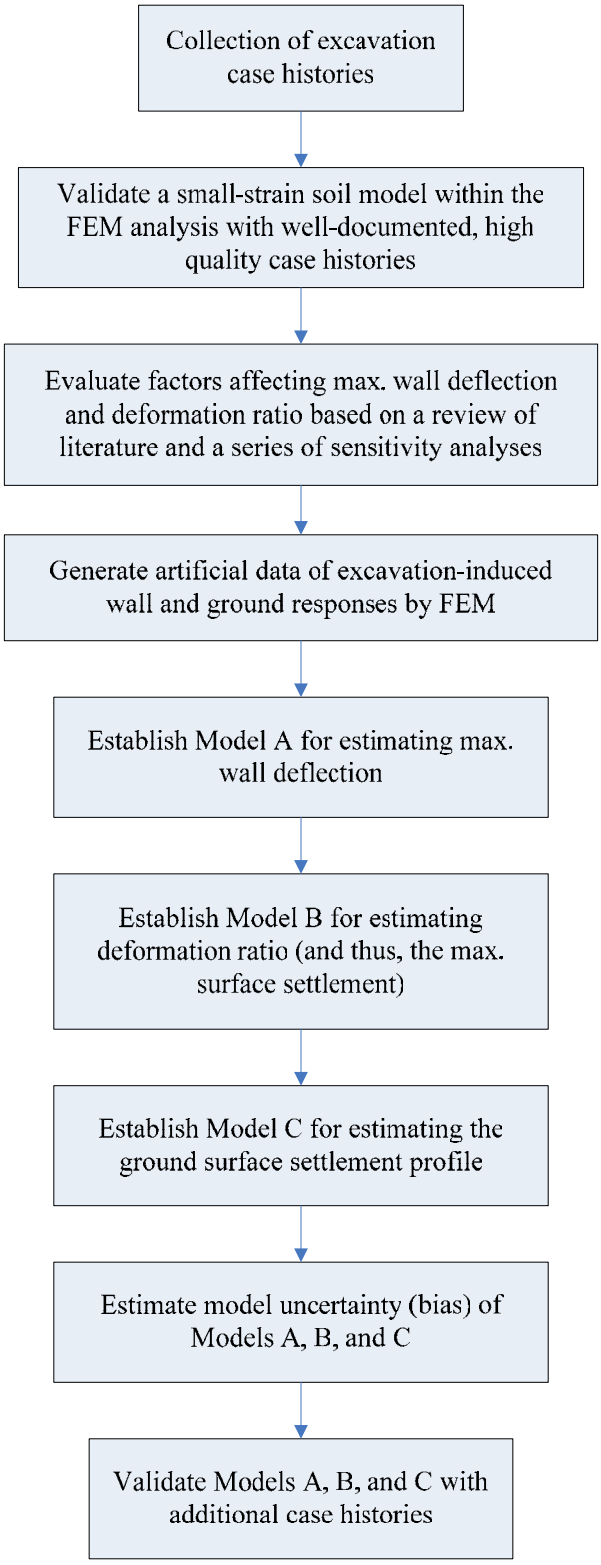

Figure 4.1 Flowchart showing various steps in the development of the intended models

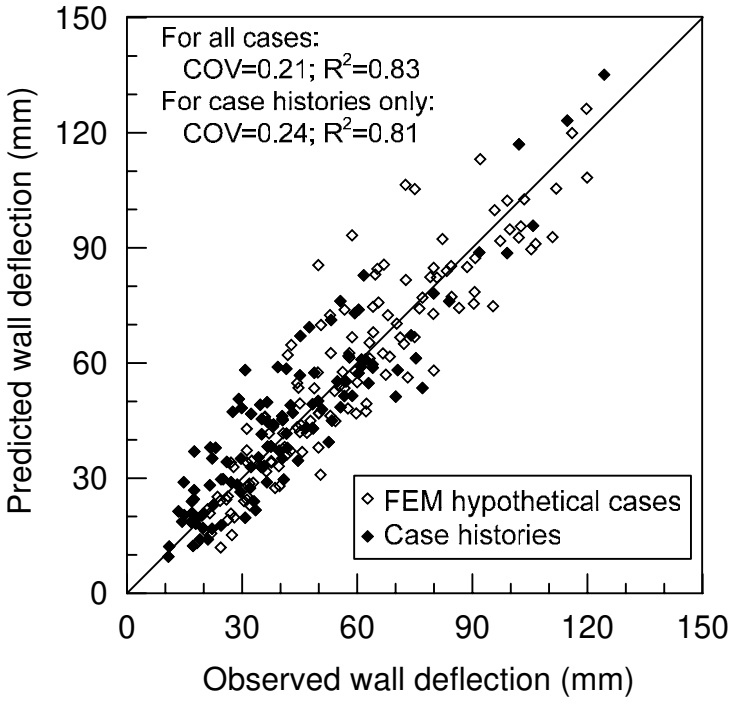

Figure 4.2 Performance of Eqs. 4.1 and 4.2 at various stages of excavation

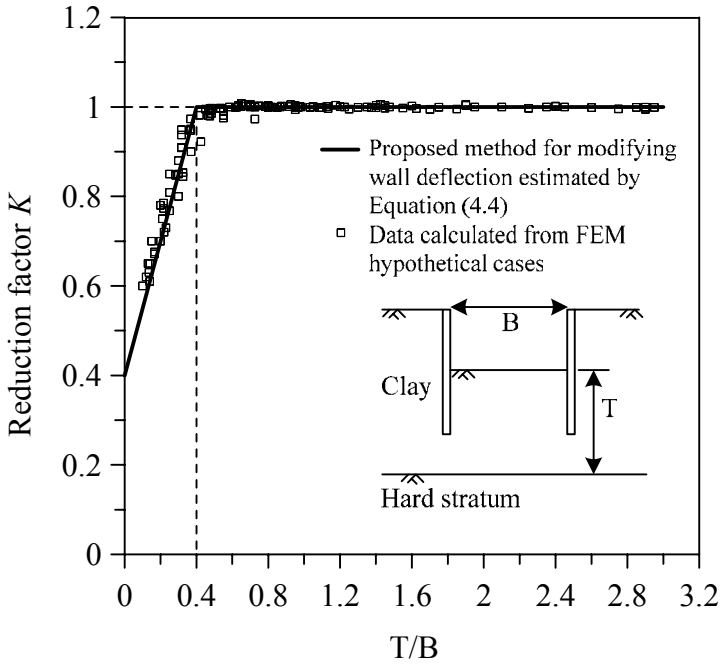

Figure 4.3 Effect of the hard stratum on the computed wall deflection

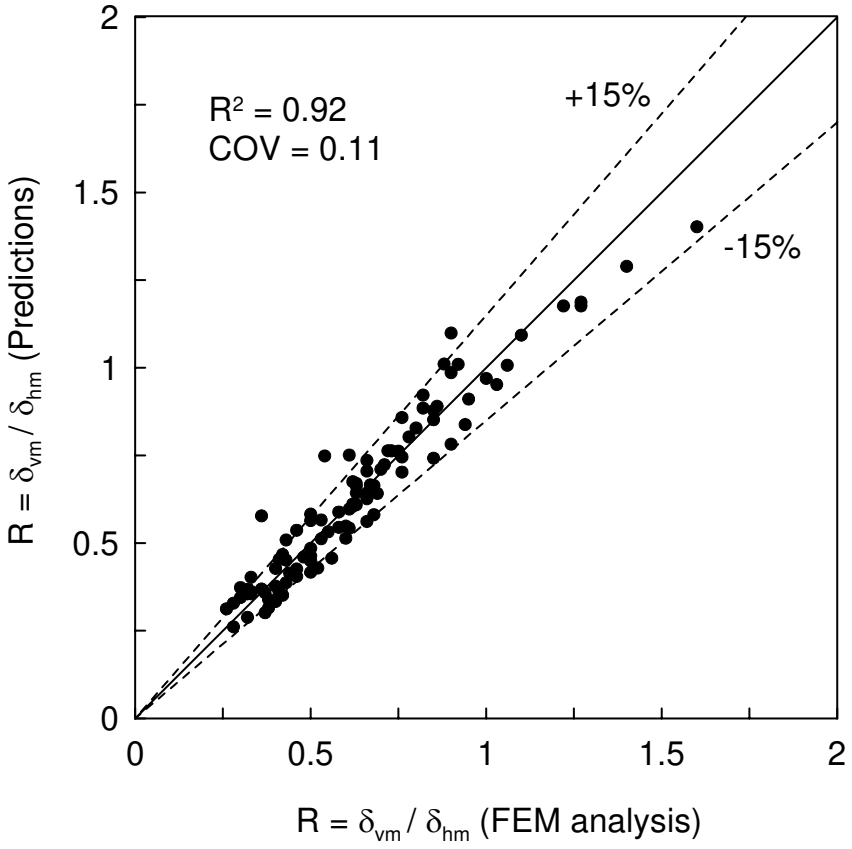

Figure 4.4 Performance of Eq. 4.5 in various types of grounds based on FEM solutions of hypothetical cases

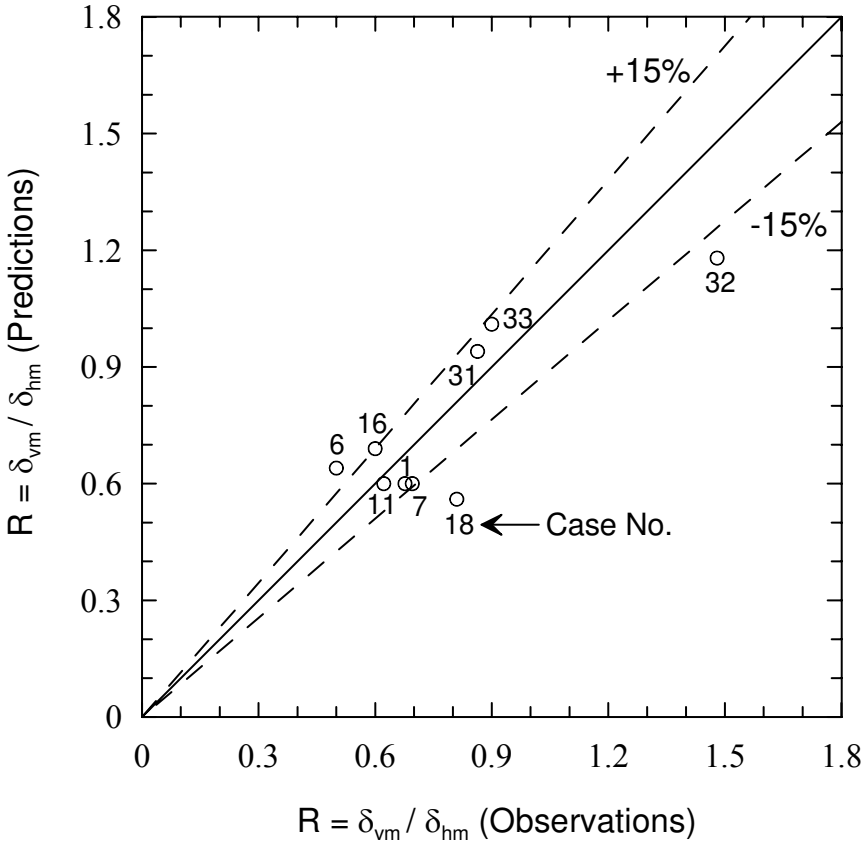

Figure 4.5 Predictions of $R = \delta_{vm}/\delta_{hm}$ in the nine excavation cases using Eq. 4.5

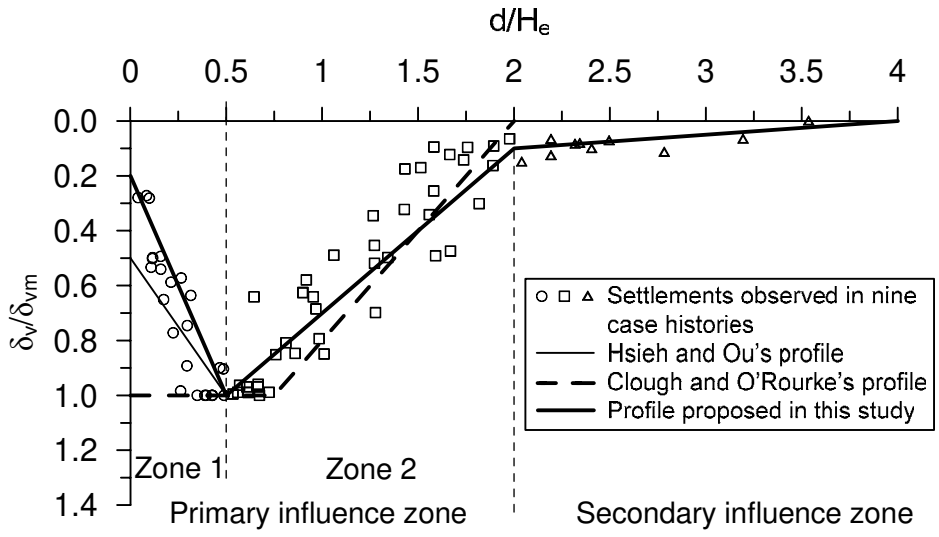

Figure 4.6 The proposed surface settlement profile (trough) and other data

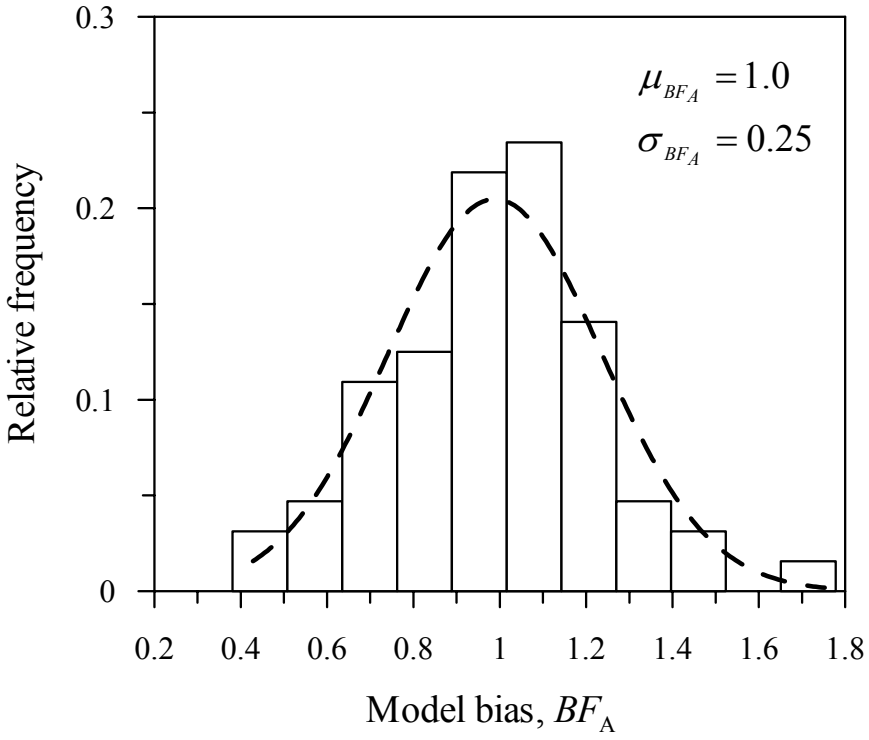

Figure 4.7 Histograms of model bias for Model A

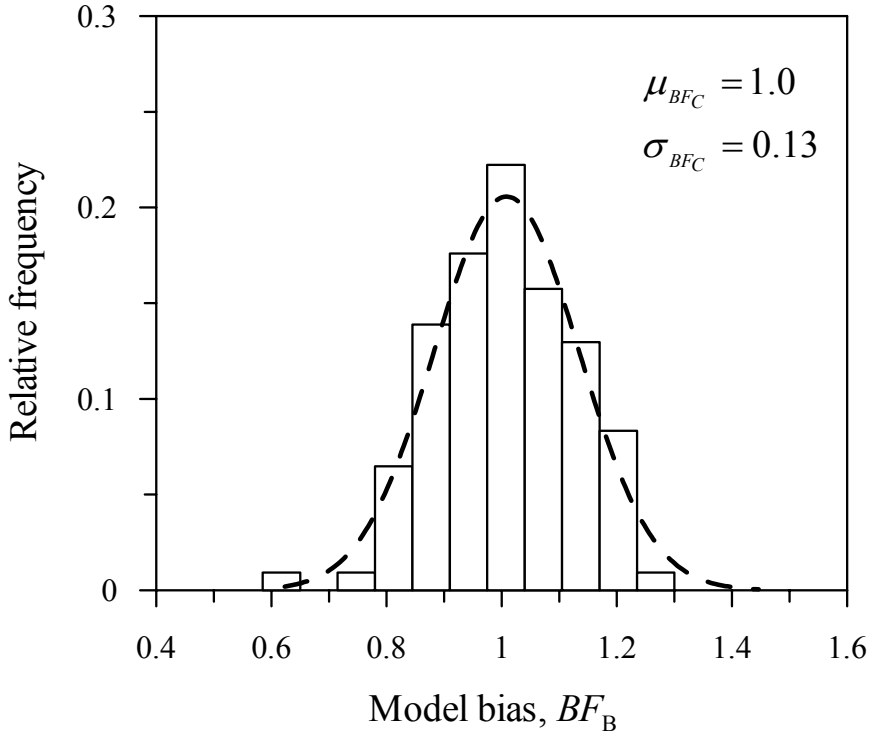

Figure 4.8 Histograms of model bias for Model B

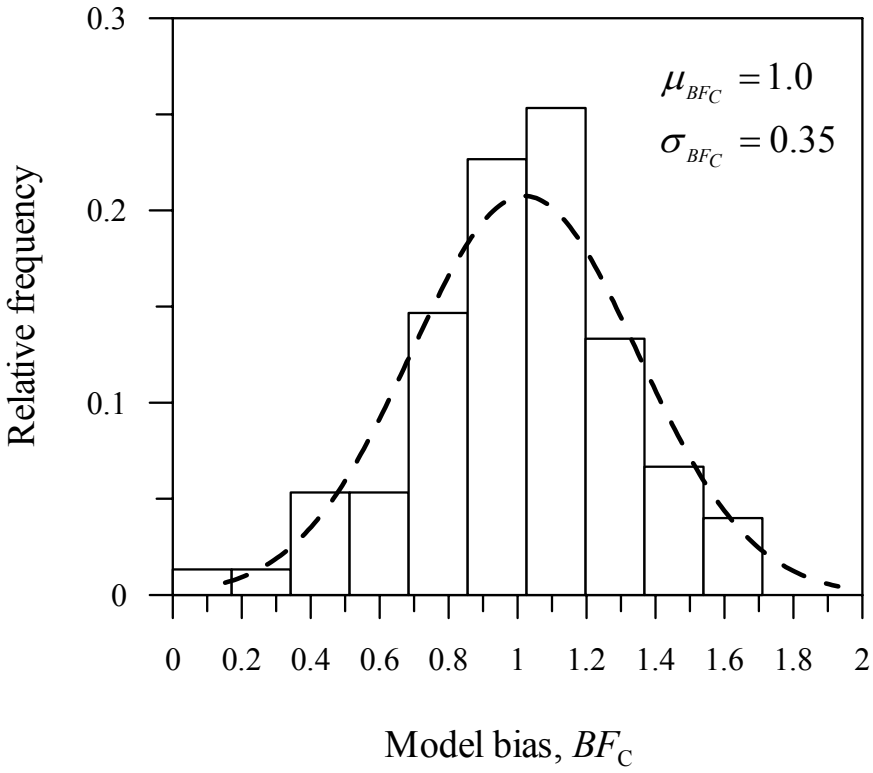

Figure 4.9 Histograms of model bias for Model C

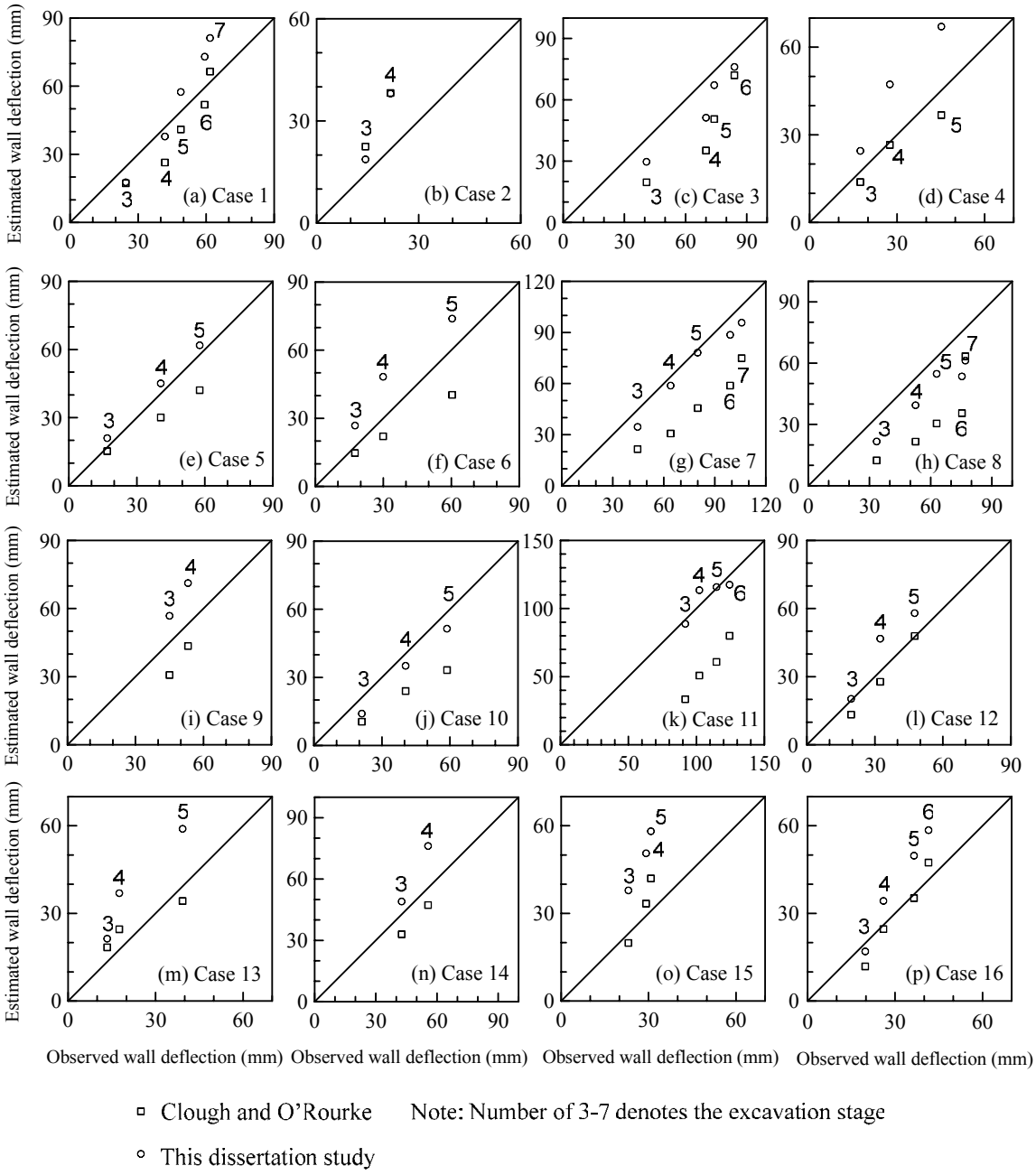

Figure 4.10(a) Comparison of wall deflections predicted by the least-sqaure regression and the Clough and O'Rourke method at stages 3 through 7 in each of the twenty-eight cases: Cases 1 to 16

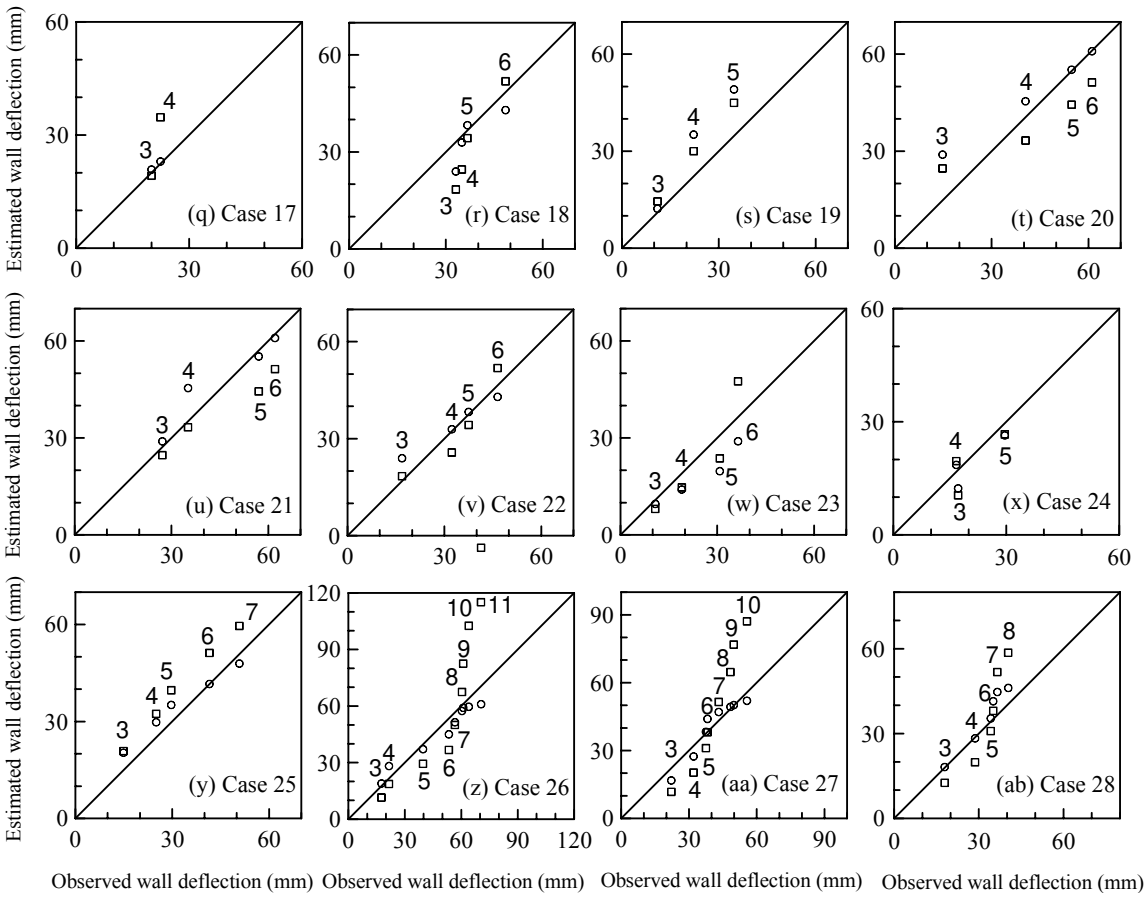

Figure 4.10(b) Comparison of wall deflections predicted by the least-square regression and the Clough and O'Rourke method at stages 3 through 7 in each of the twenty-eight cases: Cases 17 to 26

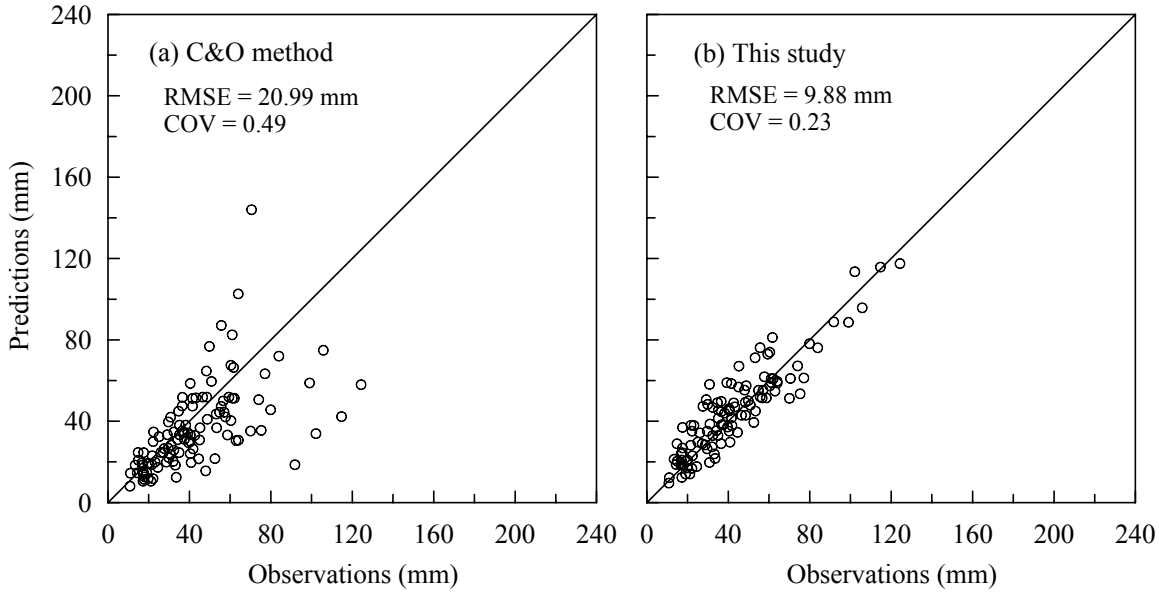

Figure 4.11 Comparison of wall deflection predictions between the proposed KJHH model and the C&O method (Cases 1 to 30)

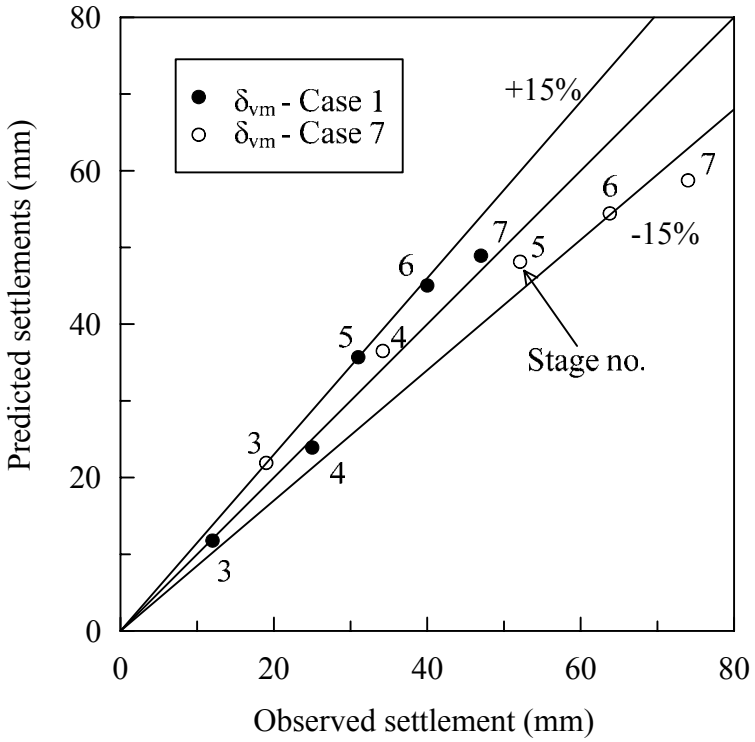

Figure 4.12 Performance of the proposed model for predicting maximum surface settlement at various stages of excavation in Cases 1 and 7

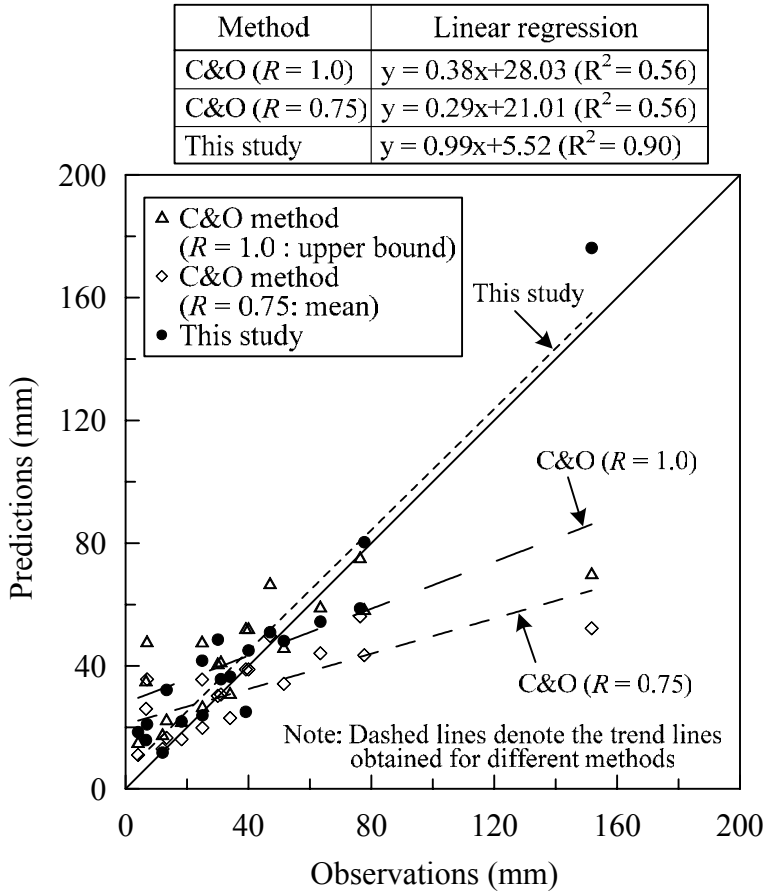

Figure 4.13 Comparison of maximum surface settlement predictions at various excavation stages between the proposed model and the C&O method

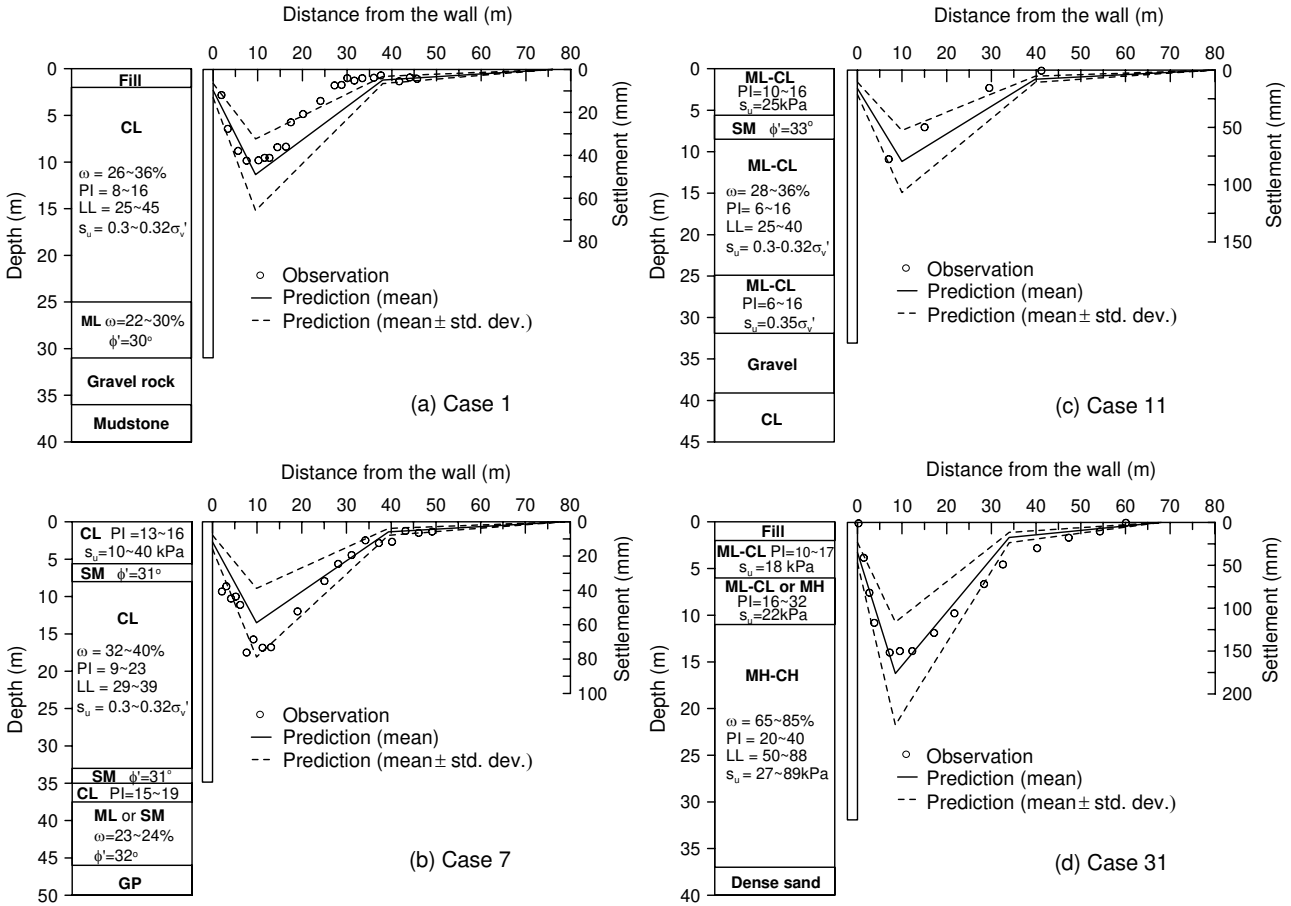

Figure 4.14 Predictions of surface settlement profiles in four cases using the proposed model (Soil profiles adapted from Hsieh and Ou 1998)

CHAPTER V

RELIABILITY ANALYSIS OF EXCAVATION-INDUCED GROUND SETTLEMENT and BUILDING SERVICEABILITY PROBLEM*

Introduction

Construction of a braced excavation system inevitably causes wall deflections and ground movements, which can have detrimental effects on adjacent buildings. In practice, the excavation-induced maximum ground surface settlement (δ_{vm}) and angular distortion (ω) are often used as performance indicators for estimating the damage potential of buildings adjacent to an excavation. In the context of this dissertation study, the term "damage" is synonymous of the state of a building where the violation of serviceability requirements occurs. The serviceability requirements are usually expressed in terms of some threshold values (or tolerable limits) of ground surface settlement or angular distortion. In a deterministic approach, serviceability of a building adjacent to a braced excavation can be assured if the predicted δ_{vm} and/or ω are less than the specified tolerable limits. In reality, such tolerable limits and predicted δ_{vm} and ω are random variables in light of the presence of uncertainty. Therefore, the development of a reliability-based approach for estimating the serviceability of a building adjacent to a braced excavation is desirable.

---

*A similar form of this chapter has been submitted for consideration for publication at the time of writing; Hsiao, E.C.L., Schuster, M, Juang C.H., and Kung, G.T.C., "Reliability analysis and updating of excavation-induced ground surface settlement for building serviceability evaluation."

In this study, a newly developed KJHH model (Chapter 4) for the excavation-induced wall deflection and ground movements is adopted for developing the reliability-based approach. Specifically, the δ_{vm} predicted by the KJHH model is used as an indicator to assess the damage potential of buildings adjacent to an excavation, and the tolerable limits such as those proposed by Skempton and MacDonald (1956), Wahls (1994), and Zhang and Ng (2005) are used as the evaluation criterion. In the context of serviceability reliability of the buildings adjacent to an excavation, the calculated δ_{vm} is the *load* and the tolerable limit of δ_{vm} is the *resistance*. In a real-world problem, either or both the load and the resistance can be a random variable.

In the reliability-based approach, the observed settlements at various stages of excavation may be used to update the KJHH model for the predictions of settlement at the subsequent stages. Updating model parameters, such as parameters of a soil model in a finite element solution, based on the field observations is often adopted during the construction phase of a deep excavation project (Ou and Tang 1994, Calvello and Finno 2004, Hashash et al. 2004, Finno and Calvello 2005). This approach of combining the numerical capability of the finite element method with the observational method has been used successfully in many excavation projects. In this study, however, the updating of the KJHH model during the construction is carried out with a different approach. Here, the KJHH model is updated through the change in its *model bias factor* based on the recognition that the observed ground responses reflect the effect of all factors in the field, not just soil parameters in the model.

The reliability of the building against damage at each stage of excavation is first evaluated prior to excavation. With the proceeding of excavation, the bias factor of the KJHH model is re-calibrated at the end of each stage and prior to next stage of excavation based on the observed settlements from the current stage. The serviceability reliability of the building in subsequent stages can then be re-evaluated with the updated bias factor of the KJHH model.

Reliability Analysis of Serviceability of Adjacent Buildings

Analysis Steps

In this study, reliability analysis of excavation-induced ground surface settlement for building serviceability evaluation is evaluated through the following steps:

(a) Estimate the mean values and coefficients of variation (*COVs*) for all input variables of the KJHH model.

(b) Calculate the excavation-induced maximum ground settlement δ_{vm} using the KJHH model.

(c) Define the performance function as $g(\ ) = \delta_{\text{lim}} - \delta_{vm}$, where δ_{lim} is the limiting tolerable settlement (or tolerable settlement for short) and δ_{lim} can be treated as the resistance, and δ_{vm} is treated as the load. Thus, $g(\ ) \geq 0$ defines a satisfactory performance region, while $g(\ ) < 0$ defines an unsatisfactory performance region.

(d) Perform reliability analysis to obtain the reliability index and the probability of exceedance (i.e., the probability of exceeding a tolerable settlement) in each stage of excavation.

It is noted that the excavation-induced maximum settlement δ_{vm} can be obtained by multiplying δ_{hm} with R. In Chapter 4, the uncertainty of the entire model for δ_{vm} was previously characterized with a model bias factor that follows a normal distribution with a mean of 1.0 and a standard deviation of 0.34. Including the bias factor, this model for maximum ground settlement δ_{vm} can be expressed as:

$$\delta_{vm} = BF \cdot R \cdot \delta_{hm} \tag{5.1}$$

Where BF is the model bias factor. Because of the variation in the input variables, the calculated δ_{vm} is a random variable.

Example Application

The Taipei National Enterprise Center (TNEC) case (case 7 in Table 3.1) is used as an example to illustrate the reliability assessment of serviceability of an adjacent building. The mean values and *COV*s of input variables of the KJHH model in the TNEC case as shown in Table 5.1. For the convenience of illustration, all input variables in the KJHH model are assumed to follow a normal distribution. A normal distribution requires the knowledge of the mean and standard deviation. For the TNEC case history, the mean values of s_u / σ'_v and E_i / s_u are found to be 0.31 and 2135, respectively. The coefficients of variation

(*COV*) of both s_u / σ'_v and E_i / s_u are found to be 0.16 based on the statistical analysis of the data obtained from Kung (2003). The *COV* of the model bias factor (*BF*) is 0.34 as indicated in Chapter 4. The *COV*s of other non-soil variables in the KJHH model are generally small and assumed herein to be 0.05. This assumption is considered appropriate for the TNEC case history.

Correlations among variables in the KJHH model are considered in the reliability analysis. Based on statistical analysis of the data presented in Kung (2003), the correlation coefficient between s_u / σ'_v and E_i / σ'_v is estimated to be 0.3. As shown in Figure 5.1, the effect of the degree of correlation between s_u / σ'_v and E_i / σ'_v on the calculated probability of exceedance is not significant. Other variable pairs are assumed uncorrelated, as there is no evidence to suggest otherwise. The random variable which represents model bias factor, *BF*, is assumed to be uncorrelated with input variables in the model. In a recent study by Phoon and Kulhawy (2005), the model bias factor is found to be weakly or moderately correlated with individual input variables. Further, the assumption of no correlation between input variables and the model bias factor yields an "upper bound" in the calculated probability of exceedance, when compared to those analyses with various degrees of correlation. Thus, the assumption of no correlation is deemed acceptable in this study.

As an example to illustrate the analysis procedure, the tolerable settlement is set to be 75 mm as suggested by Skempton and MacDonald (1956). Other criteria may be used, including the *random variable* tolerable settlement criteria by Zhang and Ng (2005). With the knowledge of the statistical distributions of

input variables and the tolerable settlement, the reliability analyses can be conducted using the first-order reliability method (FORM). It is noted that the FORM analysis can be easily implemented in a spreadsheet (e.g., Low and Tang 1997; Phoon 2004) as shown in Figures 5.2 through 5.4. In these analyses, the adjacent building is assumed to be located where the maximum excavation-induced settlement occurred. As shown in Figure 5.5, the reliability index (calculated based on the performance function, $g(\ ) = \delta_{\text{lim}} - \delta_{vm}$) decreases as the excavation proceeds (i.e., the excavation depth increases), indicating that adjacent buildings are more likely to undergo settlement greater than the tolerable settlement at the later stage of excavation.

Sensitivity Analysis

A series of sensitivity analyses are performed to study the effect of a number of assumptions made during the reliability analysis. Particularly, the tolerable settlement, the *COV* of s_u / σ'_v and E_i / σ'_v, and the assumed distribution of the input variables are studied. Results of these analyses are presented herein.

Effect of the Magnitude and Variation of Limiting Tolerable Settlement

To determine the effect of the tolerable settlement on the results of reliability analysis, a number of cases are studied that have the same excavation dimensions and soil parameters, but different fixed values of tolerable settlement ranging from 60 mm to 160 mm. As shown in Figure 5.6, the reliability index

increases and the probability of exceedance decreases for the same loading as the tolerable settlement increases. The results indicate that the calculated probability of exceedance depends on the choice of tolerable settlement.

Since settlement is most likely an uncertain variable, a subsequent analysis is performed to examine the effect of this uncertainty on the results of the reliability analysis. The same cases are employed in this analysis as those used previously except the tolerable settlement is assumed to have a standard deviation of 73 mm as suggested by Zhang and Ng (2005). Similar to the results when the tolerable settlement was a fixed value, the reliability index increases and the probability of exceedance decreases as the tolerable settlement increases as shown in Figure 5.6. However, Figure 5.6 also illustrates that for the range of tolerable settlements studied, the reliability index is generally lower and the probability of exceedance is generally higher when the tolerable settlement is assumed to be a random variable. This result demonstrates that the uncertainty in the tolerable settlement has a significant effect and needs to be properly characterized.

Relative Importance of Input Variables to the Calculated Reliability Index

The sensitivity of the reliability index to a given input variable is also studied for the two scenarios where the tolerable settlement is assumed to be a fixed and an uncertain (random) variable. This sensitivity may be expressed in terms of the "variation rate index" defined as follows:

$$\gamma_i = \frac{\left| \frac{\mu_{x_i} - X_i}{\mu_{x_i}} \right|}{\sum \left| \frac{\mu_{x_i} - X_i}{\mu_{x_i}} \right|} \tag{5.2}$$

where γ_i is the variation rate index for input variable x_i in the KJHH model ($x_1 = H_e$, $x_2 = EI/\gamma_w h_{avg}^4$, $x_3 = B/2$, $x_4 = s_u/\sigma'_v$, $x_5 = E_i/\sigma'_v$, $x_6 = \sum H_{clay}/H_{wall}$, and $x_7 = BF$), μ_{x_i} is the mean value of input variables, and X_i is the value at the design point searched for input variable x_i in the FORM analysis.

The variation rate index can be calculated for each input variable with Eq. 5.2 after the reliability index and probability of exceedance are calculated with FORM analysis. It should be noted that the variation rate index measures the relative contribution of each input variable to the calculated probability of exceedance. Therefore, the calculated probability of exceedance is most sensitive to the input variables with the highest variation rate indices.

Figure 5.7(a) displays the variation rate indices for different input variables when tolerable settlement is assumed to be fixed. Figure 5.7(b), on the other hand, illustrates the variation rate indices for different input variables when the tolerable settlement is assumed to be uncertain. Additionally, a number of other analyses were performed with different values of tolerable settlement and uncertainty. In all cases, similar results were observed. The analyses indicate the importance of the model bias factor (*BF*) as the calculated probability of exceedance is most sensitive to this input. Furthermore, the calculated probability

of exceedance is also shown to be sensitive, to a lesser degree, to the normalized shear strength (s_u/σ'_v) and normalized Young's modulus (E_i/σ'_v), and to be insensitive to excavation depth (H_e), excavation width (*B/2)*, system stiffness ($EI/\gamma_w h_{avg}^4$), and $\sum H_{clay}/H_{wall}$. These findings are consistent with the assumptions made previously based on different sensitivity analyses that the variations in excavation depth (H_e), excavation width (*B/2)*, system stiffness ($EI/\gamma_w h_{avg}^4$), and $\sum H_{clay}/H_{wall}$ have little effect on the reliability analysis.

Effect of Variation in Soil Properties

Since the probability of exceedance is found to be sensitive to soil strength (s_u/σ'_v) and stiffness (E_i/σ'_v), it is important to study the effect of the variation (expressed as *COV*) in s_u/σ'_v and E_i/σ'_v on the probability of exceedance. Thus, a subsequent study is performed to determine the effect that the *COV* of s_u/σ'_v and E_i/σ'_v has on the probability of exceedance. Figure 5.8 demonstrate that the variation rate index for s_u/σ'_v increases significantly as the *COV* of s_u/σ'_v increases. Similarly, Figure 5.9 shows that the variation rate index for E_i/σ'_v increases significantly as the *COV* of E_i/σ'_v increases. This indicates that the probability of exceedance becomes increasingly sensitive to s_u/σ'_v and E_i/σ'_v as the *COV* of s_u/σ'_v and E_i/σ'_v increase. As shown in Figure 5.8, when the *COV* of s_u/σ'_v (or E_i/σ'_v in the case of Figure 5.9) exceeds a certain value (≈30%), the probability of exceedance becomes more sensitive to s_u/σ'_v and

E_i / σ'_v than it is to the model bias factor. Therefore, it is important to accurately characterize the *COV* of s_u / σ'_v and E_i / σ'_v.

Figures 5.10 and 5.11 illustrate the effect that the *COV* of s_u / σ'_v and E_i / σ'_v has on the probability of exceedance. Generally, at a prescribed tolerable settlement, the probability of exceedance increases as the *COV* of s_u / σ'_v or E_i / σ'_v increases. However, the difference is less significant in the case of lower prescribed tolerable settlement than in the case of higher prescribed tolerable settlement. At a given *COV* level, the probability of exceedance decreases as the tolerable settlement increases, and this trend is more profound at lower *COV* levels than at higher *COV* levels.

Effect of Assumed Distribution of Input Random Variables

Figure 5.12 shows the effect of the assumed distribution (normal vs. lognormal) of input variables, mainly those of the soil strength and stiffness (s_u / σ'_v and E_i / σ'_v), on the probability of exceedance. When the *COVs* of these variables are relatively low (<20%), the effect of the assumed distribution is negligible. When the *COVs* of these variables become greater (say at the level of 40 to 60%), the difference in the resulting probability of exceedance becomes noticeable but not very significant. Overall, the effect of the assumed distribution is quite modest.

Updating Settlement Predictions and Serviceability Reliability

As an excavation proceeds, the settlement may be observed at various stages of excavation, and thus, these observed settlements at various stages of excavation may be used to update the KJHH model for the predictions of settlement at the subsequent stages using the Bayesian updating approach (e.g., Ang and Tang 2006). Accordingly, the reliability analysis may be repeated or updated using the updated settlement prediction.

As mentioned previously, engineers often adopt the approach of combining the numerical capability of the finite element method with the observational method in excavation projects. This is usually carried out by updating soil parameters based on field observations during the construction. The soil parameters are updated or back-calculated through the back analysis using the finite element method so that the responses of the wall and soil match the field observations. In this study, however, the updating of the KJHH model during the construction is carried out with a different approach. Here, the KJHH model is updated through the change in its *model bias factor* based on the recognition that the observed ground responses reflect the effect of all factors in the field, not just soil parameters in the model. Thus, for the same excavation case, the variable R and δ_{hm} in Eq. 5.1 won't be updated but the variable BF will be updated.

Since the KJHH model is developed on the basis of the extensive artificial cases and real-world case histories, the model may be treated as a global empirical correlation. Thus, the standard deviation of the model bias factor (BF) may be attributable to the combined effects of the "within-site" variability and the "cross-

site" variability (e.g. Zhang and Tang, 2002). The sources of the within-site variability (σ_w) of the predicted excavation-induced settlement may include: inherent variability of soil properties and the uncertainty associated with construction effects such as dewatering activity and over excavation prior to support installation. Furthermore, the sources of the cross-site variability (σ_o) may be generated from the differences in soil and construction details, and other factors at the different sites. Therefore, the variance of the predicted settlement using the KJHH model at a particular site becomes: $\sigma_{BF}^2 = \sigma_0^2 + \sigma_w^2$.

Bayesian Updating of Serviceability Reliability

In the reliability analysis, it is essential to incorporate the uncertainty not only in the input variables, but also in the predictive model expressed in terms of a model bias factor. To increase the confidence in the reliability assessment of the serviceability of adjacent buildings, a more precise and accurate model is desirable. With the proceeding of the excavation, the site-specific observed settlements become available. Using the observed settlements, the uncertainty in the predictions could be reduced with a Bayesian approach. Use of the Bayesian updating techniques in geotechnical engineering is of course not new (e.g., Kay 1976, Baecher and Rackwitz 1982, Lacasse et al. 1990, Tang et al. 1999, Zhang and Tang 2002, and Zhang et al. 2004). In particular, Zhang et al. (2004) formalized procedures for three levels of uncertainty reduction associated with the use of the empirical predictive model based on regional data and site-specific observations. In this study, the procedures for level 3 (Bayesian updating for a

specific site using limited observations) are employed for updating the model bias factor (or model factor) of the KJHH model. In principle, the model factor represents the uncertainty of a predictive model and thus should not depend on the observations. However, in this paper, the updating of settlement is performed through an updated model factor, as the model factor back-calculated from the observed settlement reflects the overall effect of all changes in the ground conditions during the excavation. For this reason, the model factor is referred to hereinafter as the *apparent* model factor.

The TNEC case history is again used here for the illustration of this procedure. With the proceeding of excavation, observed maximum settlements at various stages of excavation are used to update the model bias factor (*BF*) of the KJHH model using the Bayesian approach. As noted previously, most site-specific uncertainty such as the variation of soil properties and construction effects shall be reflected in the field observations. Therefore, the model bias factor *BF* of the KJHH model at a particular stage of excavation of TNEC can be re-calibrated by comparing the observed settlement with the predicted settlement. In addition, in order to carry out Bayesian updating analysis, the knowledge of prior distribution (empirical distribution) of the mean of the model bias factor of the KJHH model needs to be first obtained. As discussed earlier in Chapter 4, the model bias factor (*BF*) of the KJHH model is found to be normally distributed with a mean of 1.0 ($\mu_{BF} = 1.0$) and a standard deviation of 0.34 ($\sigma_{BF} = 0.34$). This means that prior to excavation, the prior distribution parameters (Zhang and Tang, 2000) are:

$$\mu' = \mu_{BF} \tag{5.3}$$

$$\sigma' = \sqrt{\sigma_{BF}^2 - \sigma_w^2} \tag{5.4}$$

Suppose that at the end of the third stage of excavation, the *observed* mean of the apparent model factor is $\overline{BF}$. Assuming the within-site variability of *BF* (σ_w) is 0.20 (estimated based on observed settlements in the TNEC case history), and according to the Bayesian sampling theory (e.g. Ang and Tang 2006), the updated mean of apparent model factor (μ'') and the updated standard deviation of the apparent model factor (σ'') at the end of the third stage can be computed as follows:

$$\mu'' = \frac{\mu'\sigma_w^2 + \overline{BF}\,\sigma'^2}{\sigma_w^2 + \sigma'^2} \tag{5.5}$$

$$\sigma'' = \frac{\sigma_w^2\sigma'^2}{\sigma_w^2 + \sigma'^2} \tag{5.6}$$

As noted previously, within the site, the observed settlements are also subject to the within-site variability, in terms of σ_w. As a result, the updated distribution of apparent model factor *BF* based on the observation at the end of the third stage is used for the prediction of settlements at the subsequent stages. With the proceeding of excavation, as additional observed settlements are obtained, the distribution of the apparent model factor (*BF*) is updated by treating

the posterior result of the previous updating as the prior result for the next updating until the completion of excavation.

Table 5.2 shows the mean and standard deviation of the updated apparent model factors that are used in the subsequent settlement predictions. Table 5.3 shows the observed maximum ground settlements and the predicted maximum settlements at various stages of excavation using the updated apparent model factors. It should be noted that under normal construction conditions, the damage caused by the excavation-induced ground settlement in the first two stages of excavation is generally negligible and thus, no settlement prediction in the first two stages of excavation is made.

The predictions made after the 3rd stage and prior to the 4th stage of excavation are those based on the updated apparent model factor that has incorporated the observed data from the 3rd stage of excavation. In other words, the maximum settlement is still calculated from Eq. 5.1 but with an updated apparent model actor *BF*. The predictions made at the end of subsequent stages are interpreted in the same way. To see if the updated settlement predictions offer any improvement over the predictions made prior to excavation, the updated settlement predictions and their variations prior to each excavation stage are plotted.

Figure 5.13 shows the settlement predictions at various excavation stages, Stages 4, 5, 6, and 7 (or their corresponding target depths, 11.8 m, 15.2 m, 17.3 m, and 19.7 m). Prior to the 4th stage of excavation, the observed data from stage 3 is available, and based on this data, the apparent model factor is updated, and the

settlements at various target depths (11.8 m, 15.2 m, 17.3 m, and 19.7 m) are updated or recalculated. These results (i.e. settlements predicted at four target depths) are represented with a "triangle" symbol as shown in Figure 5.13. As the excavation proceeds beyond stage 4, there is no need to "predict" the settlement at the depth of 11.8 m, the target depth of stage 4. Thus, in Figure 5.13, only one settlement prediction is made at the depth of 11.8 m. Similarly, prior to stage 5 of excavation, with the observed data from stage 4, the settlements at the depths of 15.2 m, 17.3 m, and 19.7 m (the target depths at stages 5, 6, and 7) are recalculated based on the updated apparent model factor. The settlement predictions at these three target depths are also shown in Figure 5.13. In a similar manner, two settlements predictions are made at the target depths of 17.3 m and 19.7 m prior to stage 6 of excavation, and one settlement prediction is made at the target depth of 19.7 m prior to stage 7 of excavation. Also shown in Figure 5.13 is the observed settlement at the final stage (Stage 7) of excavation, which is at the depth of 19.7 m. The results shown in Figure 5.13 indicate that as the excavation proceeds, and with more and more observed data, the settlement prediction becomes more *accurate* compared to the final observed settlement at the depth of 19.7 m. Finally, it should be mentioned that the settlement predictions shown in Figure 5.13 are the "mean" settlements, and the variations of these predictions are discussed next.

Figure 5.14 shows the *COV* of the updated settlement predictions at various stages of excavation. As the excavation proceeds, the settlement prediction becomes more *precise* as reflected by the decrease in the *COV* of the

predicted settlement prior to each stage of excavation. It is noted that the *COV* of the predicted settlement is the same as the *COV* of the updated apparent model factor, as the updated settlement is calculated based *solely* on the updated apparent model factor, as described previously. At the final stage of excavation, the *COV* of the predicted settlement is approximately equal to 22%. Taking the mean prediction plus and minus one standard deviation, the updated predicted settlement would be approximately in the range of 48 to 74 mm, where the observed settlement after this final stage of excavation is 74.2 mm.

Figure 5.15 shows the probability of exceedance (exceeding the limiting tolerable settlement of 75 mm) predicted at various target depths. Similar to the updated settlement prediction, the probability of exceedance is updated prior to stages 4, 5, 6, and 7 of excavations (using the observed data at the end of stages 3, 4, 5, and 6, respectively). As the excavation proceeds and the apparent model factor is updated, the mean model factor increases, which causes the predicted settlement to increase in this TNEC case, as shown previously in Figure 5.13. Consequently, the increase in the mean settlement causes the probability of exceedance to increase. It should be noted that the *COV* of the apparent model factor decreases as the apparent model factor is updated, as shown previously in Figure 5.14, which results in less variation in the predicted settlement and a decreased probability of exceedance. However, the change in the *COV* of the predicted settlement has a lesser effect on the probability of exceedance, compared to the effect caused by the change in the mean settlement prediction.

The overall effect of updating the settlement prediction on the probability of exceedance in this TNEC case is thus shown in Figure 5.15.

Summary and Conclusions

The KJHH model is a simplified empirical method used for the estimation of excavation-induced ground settlements in soft to medium clay. Since the uncertainty of the KJHH model has been quite well characterized, it is ideal for use as the deterministic model for the intended reliability analysis. In this paper, the reliability analysis of the serviceability of buildings adjacent to an excavation is demonstrated using a limiting tolerable settlement, and the probability of exceedance (i.e., exceeding a prescribed tolerable settlement) is calculated for each stage of the excavation. The procedure for such analysis is outlined and demonstrated with an example.

Sensitivity analyses are performed to determine the effects of a number of assumptions, including the magnitude and variation of the limiting tolerable settlement, the apparent model factor, *COV* of soil properties, and assumed distribution of input variables. The results indicate that the calculated probability of exceedance depends on the choice of tolerable settlement, as expected. The results also showed that the uncertainty in the limiting tolerable settlement has a significant effect and thus, the limiting tolerable settlement, which is considered as a resistance in the reliability analysis, needs to be properly characterized.

The calculated probability of exceedance is shown to be most sensitive to the model bias factor, which indicates the importance of the accuracy and

precision of the deterministic settlement model adopted for reliability analysis. Furthermore, the calculated probability of exceedance is also shown to be sensitive, albeit to a lesser degree, to the normalized shear strength (s_u/σ'_v) and normalized Young's modulus (E_i/σ'_v), and to be insensitive to excavation depth (H_e), excavation width (*B/2)*, system stiffness ($EI/\gamma_w h_{avg}^4$), and $\sum H_{clay}/H_{wall}$. However, the probability of exceedance becomes increasingly sensitive to s_u/σ'_v and E_i/σ'_v as the *COV* of s_u/σ'_v and E_i/σ'_v increase. Therefore, it is important to accurately characterize the *COV* of s_u/σ'_v and E_i/σ'_v.

Generally, at a prescribed tolerable settlement, the probability of exceedance increases as the *COV* of s_u/σ'_v or E_i/σ'_v increases. However, the difference is less significant at a lower prescribed tolerable settlement than at a higher prescribed tolerable settlement. At a given *COV* level, the probability of exceedance decreases as the limiting tolerable settlement increases, and this trend is more profound at lower *COV* levels than at higher *COV* levels.

The effect of the assumed distribution of input variables on the probability of exceedance is found to be insignificant, particularly when the *COVs* of these variables are relatively low (<20%). Even at higher *COV* levels, the effect is still quite modest.

Finally, a method to update the apparent model factor is presented. As the excavation proceeds, the observed settlement from a prior stage can be used to update the apparent model factor of the KJHH model, which, in turn, can be used to improve the prediction of settlement at various target depths in future stages. The probability of exceedance is then recalculated based on the updated

settlement predictions. As reflected in the example application presented, the model factor is shown to be more accurately and precisely characterized as more observations are used for updating, which in turn leads to a more *accurate* and *precise* estimation of ground surface settlement and probability of exceedance.

Table 5.1 Mean values of excavation depths and system stiffness of TNEC case history

Factor	Excavation sequence (Stage No.)				
	3	4	5	6	7
Depth, H_e (m)	8.6	11.8	15.2	17.3	19.7
System stiffness, $EI/\gamma_w h_{avg}^4$	1023	966	1109	1115	1294

- Mean of other factors required for determining maximum ground surface settlement using KJHH model: $B/2$ = 20.6 m, s_u/σ'_v = 0.31 and E_i/σ'_v = 650, $\sum H_{clay}/H_{wall}$ = 0.87, model bias factor (*BF*) = 1.0, and tolerable settlement (δ_{lim}) = 75 mm.
- *COV*s of H_e, $EI/\gamma_w h_{avg}^4$, $B/2$, and $\sum H_{clay}/H_{wall}$ = 0.05
- *COV*s of s_u/σ'_v and E_i/σ'_v = 0.16
- *COV* of *BF* = 0.34
- *COV* of δ_{lim} = 0.0
- Correlation of s_u/σ'_v and E_i/σ'_v = 0.3

Table 5.2 Apparent model factors used in the prediction of TNEC case history

	Excavation sequence				
	Prior to Excavation	End of 3rd stage	End of 4th stage	End of 5th stage	End of 6th stage
Mean	1.000	0.889	0.952	1.001	1.037
Standard deviation	0.340	0.257	0.236	0.227	0.221

Table 5.3 Observed and predicted maximum settlements of TNEC case history

Excavation		Maximum settlement (mm)					
			Prediction				
Stage	Depth (m)	Observation	Prior to Excavation	End of 3rd stage	End of 4th stage	End of 5th stage	End of 6th stage
3	8.6	18.2	21.9	-	-	-	-
4	11.8	34.0	36.5	32.4	-	-	-
5	15.2	51.5	48.1	42.8	45.8	-	-
6	17.3	63.4	54.4	48.4	51.8	54.5	-
7	19.7	74.2	58.7	52.2	55.9	58.8	60.9

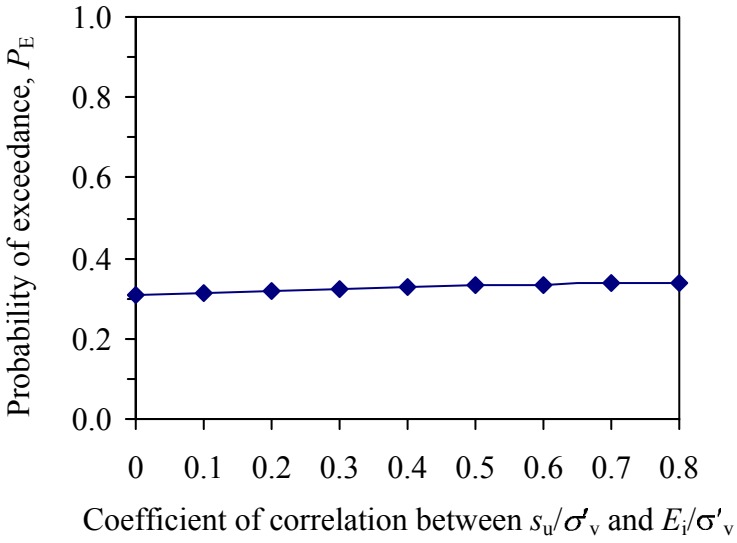

Figure 5.1 Probabilities of exceedance for various degree of correlation between s_u/σ'_v and E_i/σ'_v

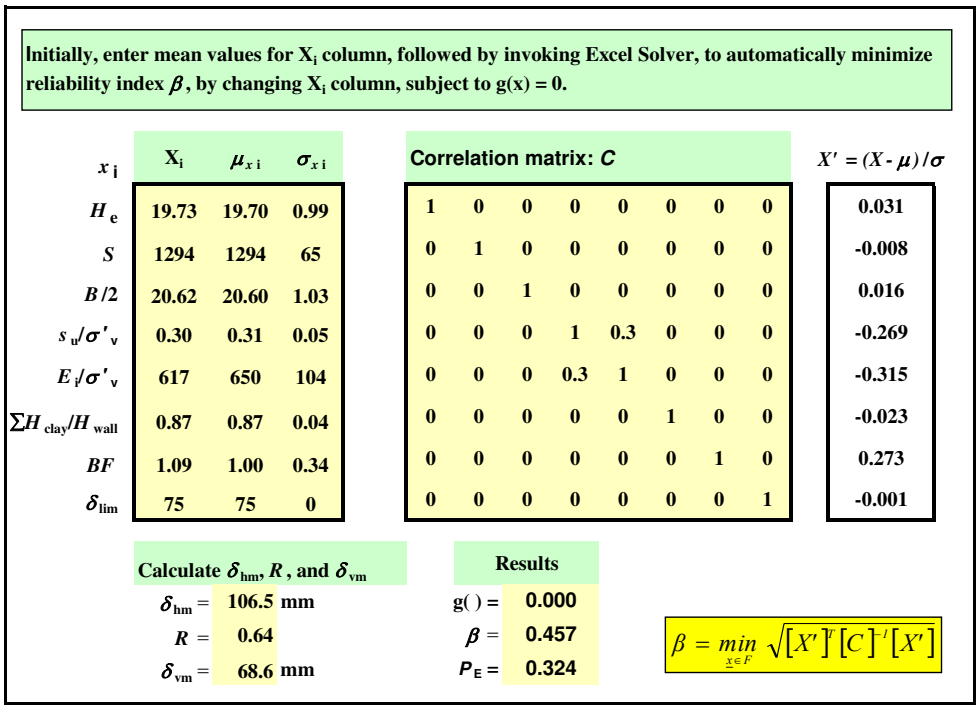

Figure 5.2 An example of reliability analysis of excavation-induced ground settlement and building serviceability using Microsoft Excel assuming input variables follow normal distribution (after Low and Tang, 1997)

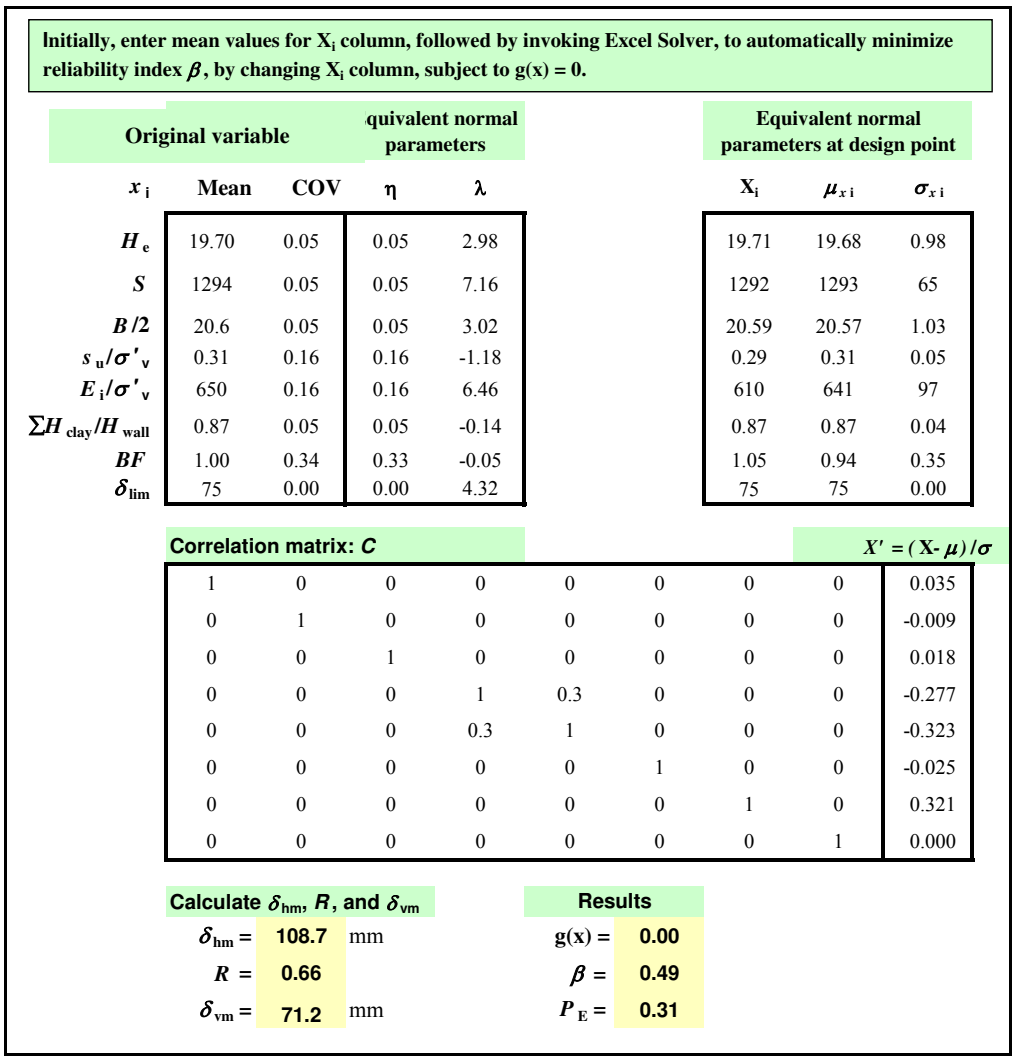

Initially, enter mean values for X_i column, followed by invoking Excel Solver, to automatically minimize reliability index β, by changing X_i column, subject to g(x) = 0.

	Original variable		Equivalent normal parameters		Equivalent normal parameters at design point		
x_i	Mean	COV	η	λ	X_i	$\mu_{x\,i}$	$\sigma_{x\,i}$
H_e	19.70	0.05	0.05	2.98	19.71	19.68	0.98
S	1294	0.05	0.05	7.16	1292	1293	65
$B/2$	20.6	0.05	0.05	3.02	20.59	20.57	1.03
s_u/σ'_v	0.31	0.16	0.16	-1.18	0.29	0.31	0.05
E_i/σ'_v	650	0.16	0.16	6.46	610	641	97
$\sum H_{clay}/H_{wall}$	0.87	0.05	0.05	-0.14	0.87	0.87	0.04
BF	1.00	0.34	0.33	-0.05	1.05	0.94	0.35
δ_{lim}	75	0.00	0.00	4.32	75	75	0.00

Correlation matrix: C

								$X' = (X - \mu)/\sigma$
1	0	0	0	0	0	0	0	0.035
0	1	0	0	0	0	0	0	-0.009
0	0	1	0	0	0	0	0	0.018
0	0	0	1	0.3	0	0	0	-0.277
0	0	0	0.3	1	0	0	0	-0.323
0	0	0	0	0	1	0	0	-0.025
0	0	0	0	0	0	1	0	0.321
0	0	0	0	0	0	0	1	0.000

Calculate δ_{hm}, R, and δ_{vm}

δ_{hm} = **108.7** mm

R = **0.66**

δ_{vm} = **71.2** mm

Results

g(x) = **0.00**

β = **0.49**

P_E = **0.31**

Figure 5.3 An example of reliability analysis of excavation-induced ground settlement and building serviceability using Microsoft Excel assuming input variables follow lognormal distribution (after Low and Tang, 1997)

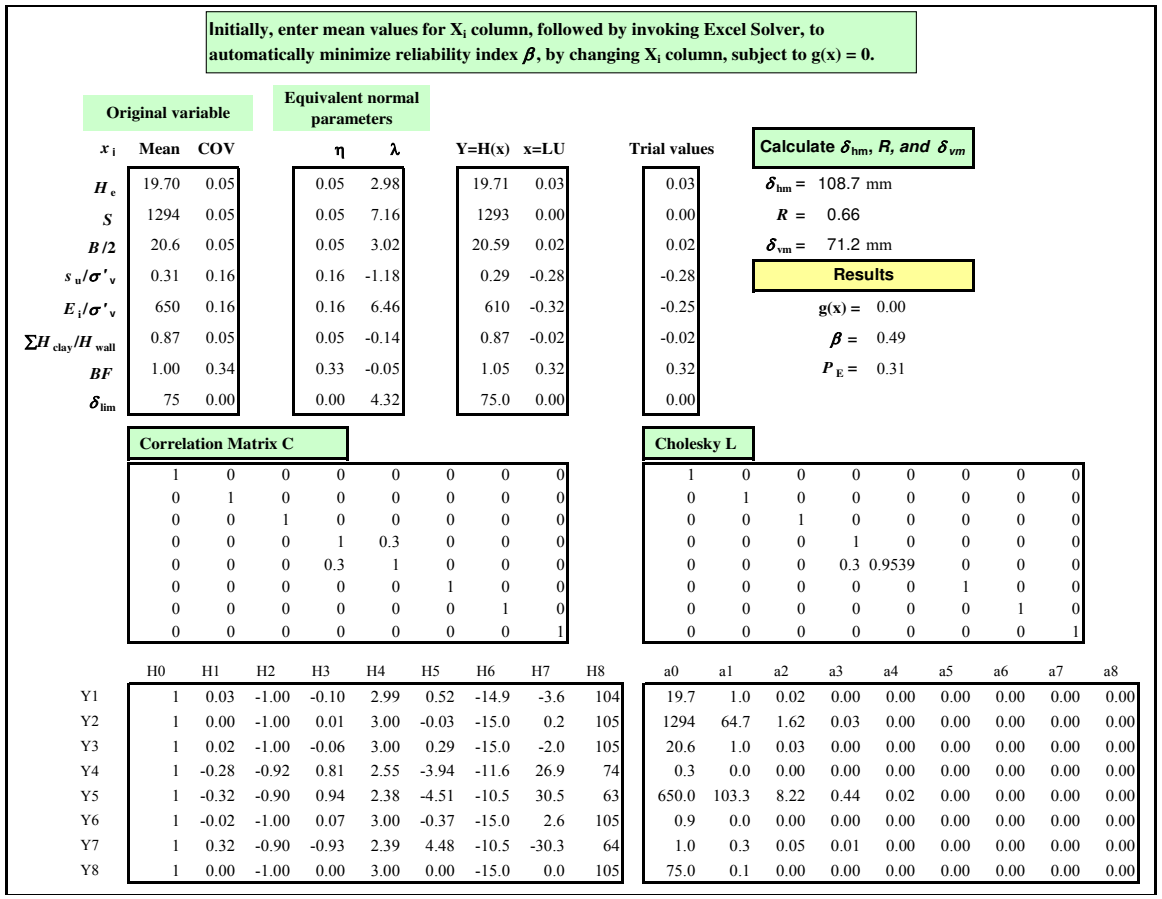

Figure 5.4 An example of reliability analysis of excavation-induced ground settlement and building serviceability using Microsoft Excel assuming input variables follow lognormal distribution (after Phoon, 2004)

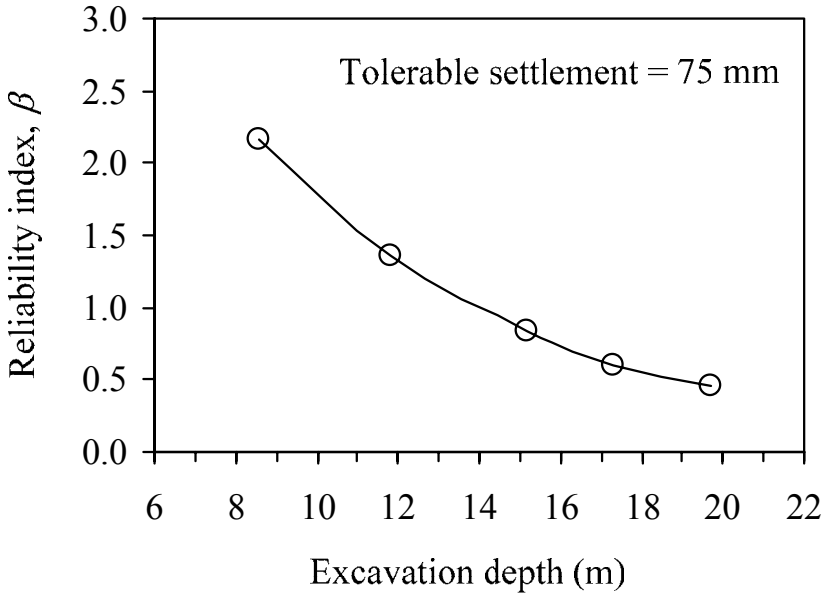

Figure 5.5 Computed reliability indices at various excavation depths

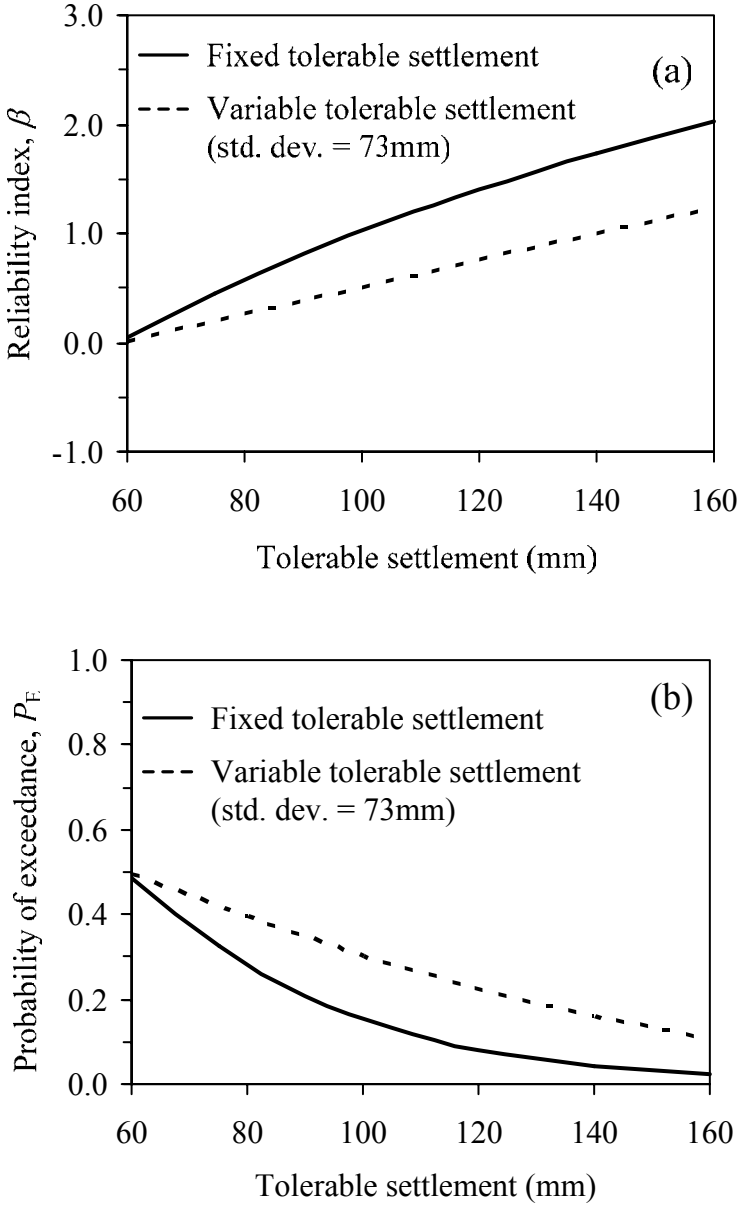

Figure 5.6 Effect of various tolerable settlements at the final depth of excavation on (a) reliability index and (b) probability of exceedance

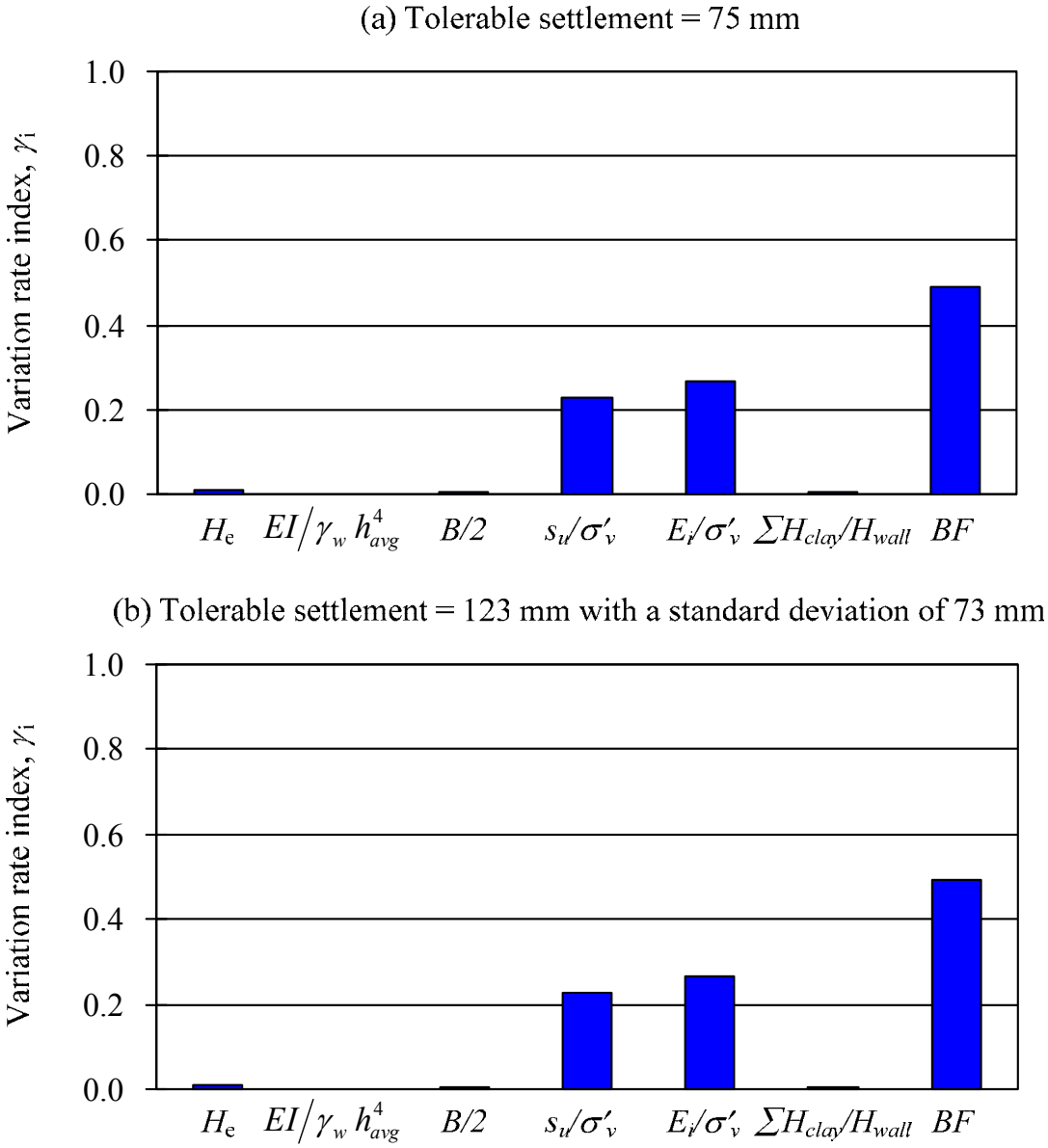

Figure 5.7 Relative importance of input variables, in terms of variation rate index under the assumption of (a) a fixed tolerable settlement, and (b) a variable tolerable settlement

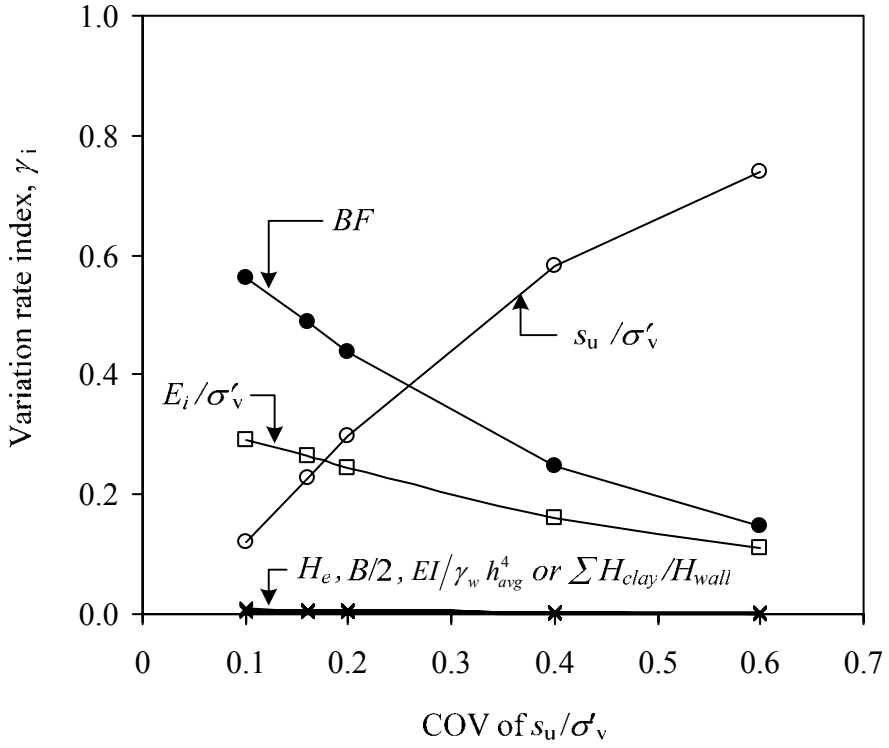

Figure 5.8 Variation rate index at various COVs of $s_u / \sigma_v^{'}$
(tolerable settlement = 75mm)

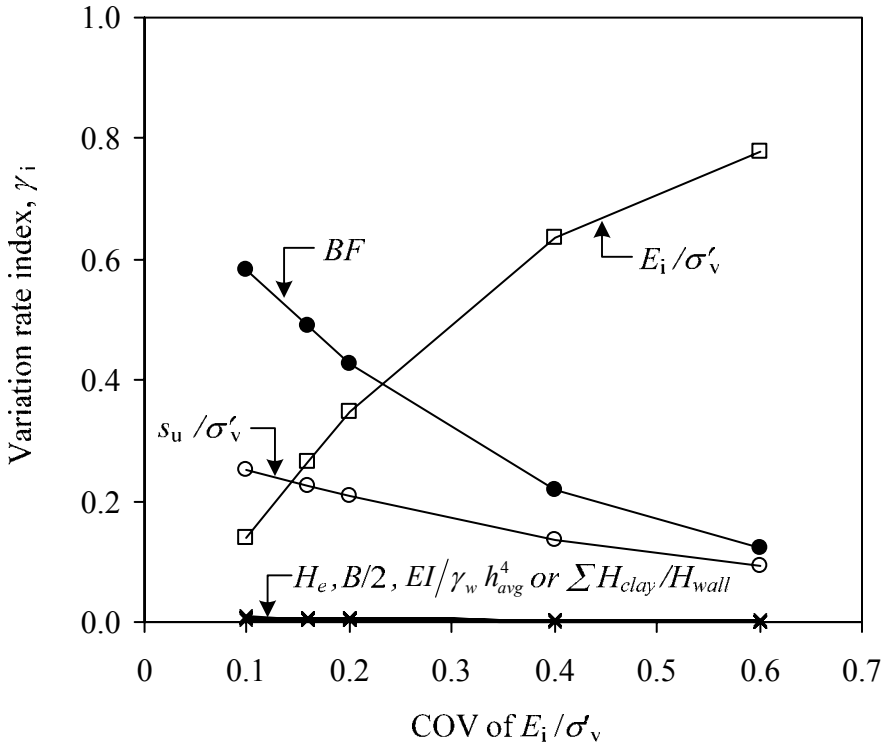

Figure 5.9 Variation rate index at various COVs of E_i/σ'_v
(tolerable settlement = 75mm)

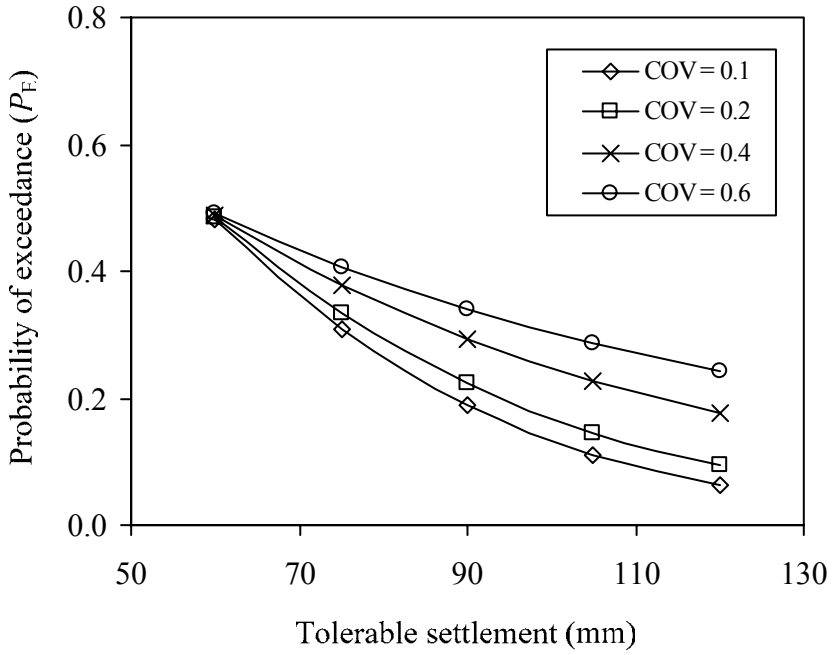

Figure 5.10 Probability of exceedance at various COVs of s_u / σ_v'

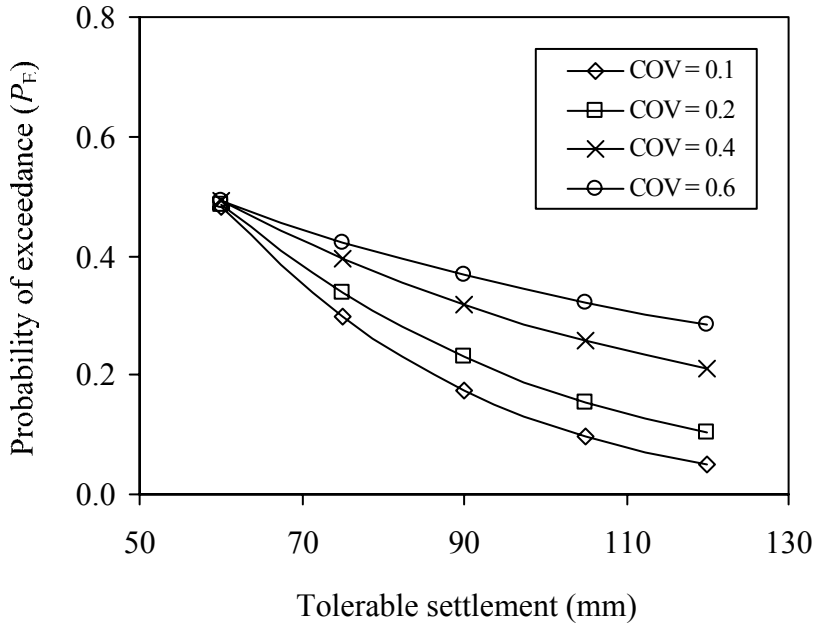

Figure 5.11 Probability of exceedance at various COVs of E_i/σ'_v

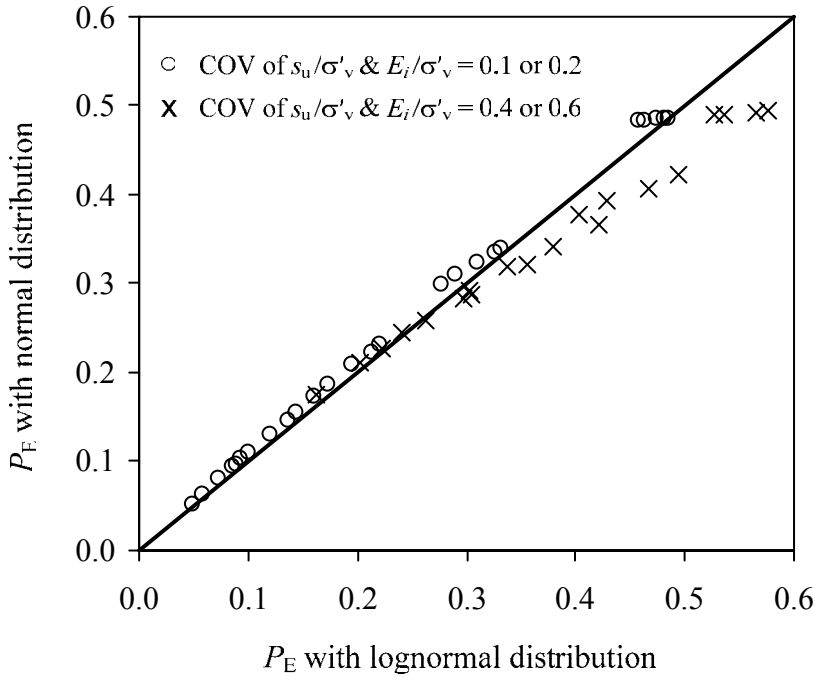

Figure 5.12 Probabilities of exceedance for various distributions under the assumption of a fixed tolerable settlement

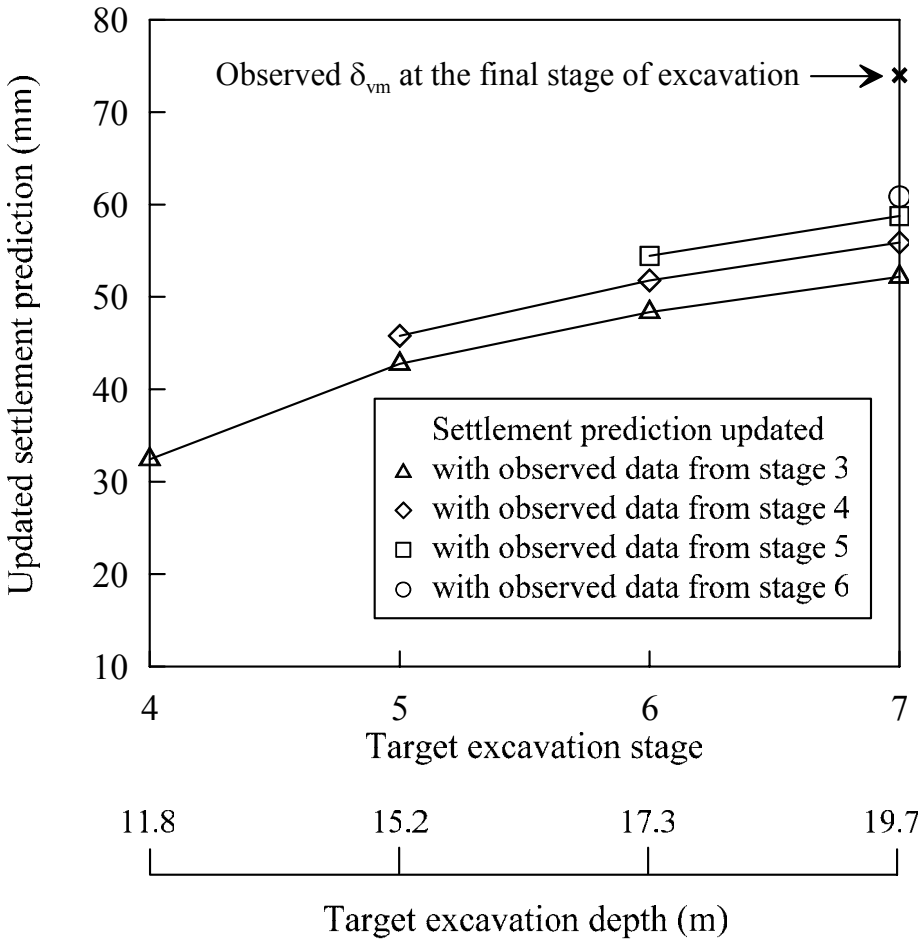

Figure 5.13 Bayesian updating of settlement predictions

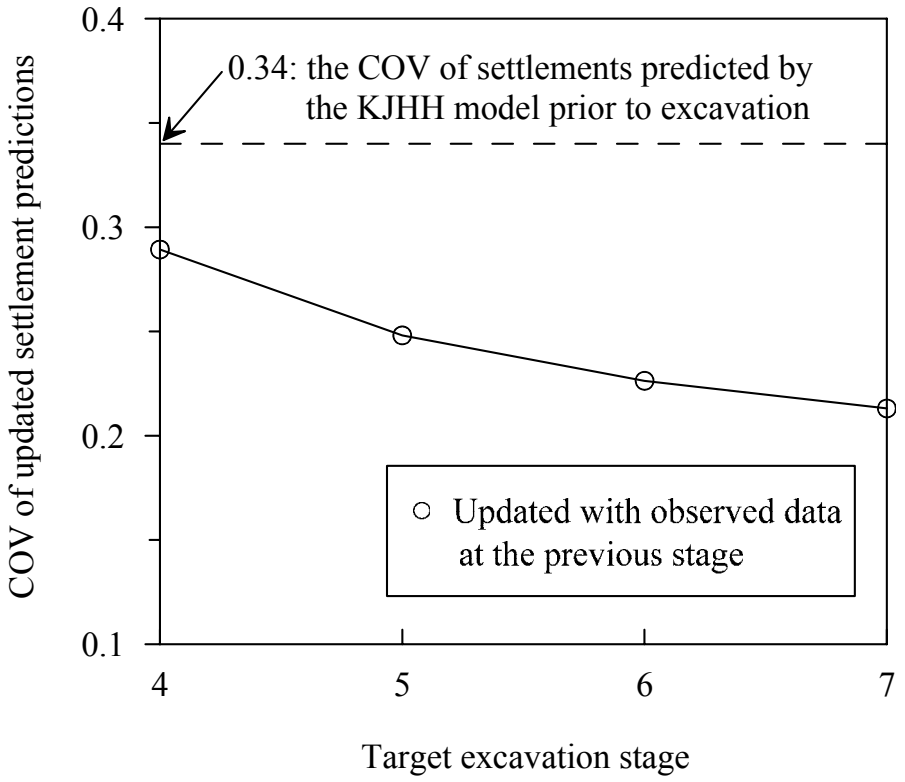

Figure 5.14 Bayesian updating of *COV* of settlement predictions

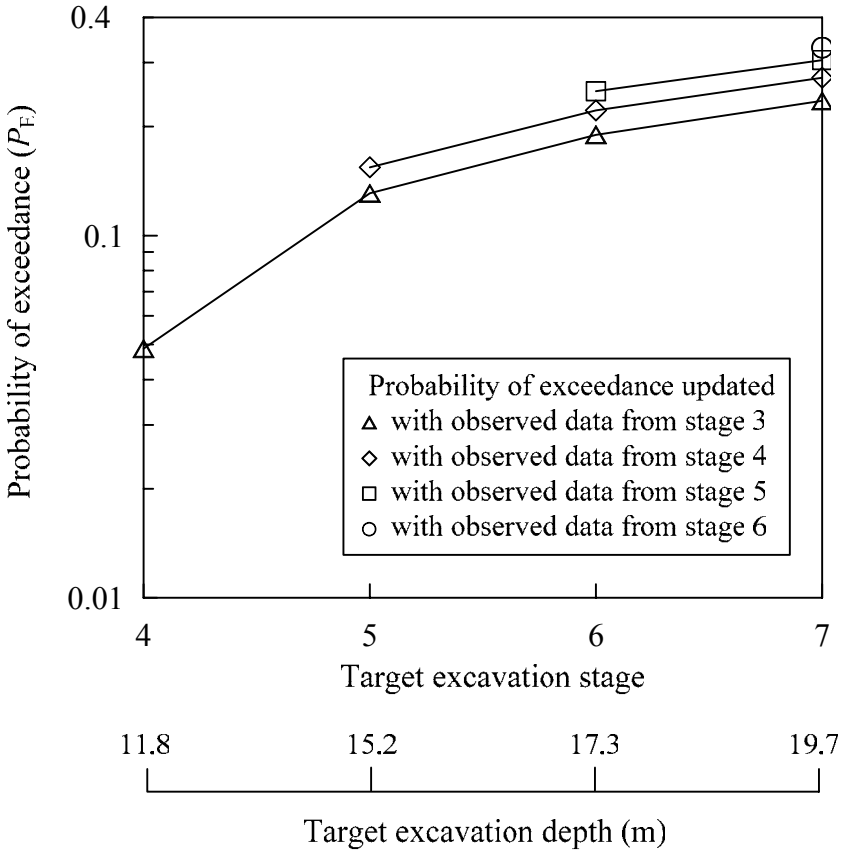

Figure 5.15 Probabilities of exceedance updated with observed data

CHAPTER VI

CONCLUSIONS

Conclusions

The following conclusions are drawn from the results of the evaluation of a simplified small-strain soil model for analysis of excavation-induced movements presented in Chapter II:

- The Modified Pseudo-Plasticity (MPP) model improves upon the hyperbolic model in three aspects: (1) the anisotropic undrained shear strength can be accounted for to differentiate the states of primary loading and unloading-reloading; (2) the stress-strain equation of soil is modified to account for soil behaviors at small strain, and (3) the tangential Young's modulus is determined based on the unloading-reloading stiffness.
- The results of FEM analyses of the two well-documented case histories showed that the predicted wall deflection profile generally agreed well with the observations. The predictions of the maximum wall deflection and its location are generally satisfactory. For ground surface settlement, the predicted settlement profile generally resembles the observed profile. The trend of the measured concave settlement adjacent to the wall can be correctly predicted by the MPP model. The maximum surface settlement can also be fairly accurately predicted. For lateral soil deformation behind the wall at relatively shorter distance, the predictions of the maximum lateral soil deformation agreed well with the observations. However, at

greater distance from the wall, the predicted deformation profile exhibited deep inward movement, which did not agree well with the observed cantilever movement behavior. In view of the general difficulty of obtaining satisfactory predictions for various aspects of the excavation responses (wall deflection, surface settlement, and lateral soil deformation) *simultaneously* with a finite element analysis, however, the results obtained in this study using the MPP soil model are considered satisfactory.

The following conclusions are drawn from the results of the study on the compilation of excavation case histories and generation of artificial data of wall deflection and ground settlement presented in Chapter III:

- In this dissertation study, thirty-three (33) case histories of braced excavations in soft to medium clays are obtained from Taipei, Singapore, Oslo, Tokyo, and Chicago. However, the total number of collected case histories is less than ideal for the purpose of developing empirical models for estimating the wall deflection and ground surface settlement. Thus, in this study, secondary data were artificially generated from numerical experimentation using FEM solutions with the previously-validated MPP soil model.
- Literature review and parametric study using FEM show that six factors are considered essential for predicting the wall deflection ; they are excavation depth (H_e), system stiffness ($EI/\gamma_w h_{avg}^4$), excavation width

(B), ratio of the average shear strength over the vertical effective stress (s_u/σ'_v), ratio of the average initial Young's modulus over the vertical effective stress (E_i/σ'_v), and ratio of the depth to hard stratum measured from the current excavation level over the excavation width (T/B). Literature review and parametric study using FEM also indicate that the deformation ratio is believed to be strongly influenced by three parameters; they are ratio of the average shear strength over the vertical effective stress (s_u/σ'_v), ratio of the average initial Young's modulus over the vertical effective stress (E_i/σ'_v), and the normalized clay layer thickness with respect to the wall length ($\sum H_{clay}/H_{wall}$). These influential factors are then included in the FEM numerical experimentation for generating hypothetical cases for the development of the intended model.

The following conclusions are drawn from the results of the simplified models for wall deflection and ground surface settlement caused by braced excavation in clays presented in Chapter IV:

- The effect of the presence of hard stratum on the excavation-induced maximum wall deflection is investigated through an extensive series of FEM experimentation. The effect is expressed as a reduction factor K that is related to the ratio of the depth to hard stratum, measured from the current excavation level, over the excavation width (T/B). At smaller T/B ratios ($T/B < 0.4$), the presence of the hard stratum is seen to have a great influence on the magnitude of the calculated maximum wall

deflection, and at $T/B > 0.4$ and beyond, the influence of the hard stratum is negligible. For the cases with $T/B < 0.4$, the modified maximum wall deflections ($\delta_{hm,m}$), rather than δ_{hm}, should be reported.

- Consistent with FEM numerical experiments, six factors, H_e, $B/2$, $EI/\gamma_w h_{avg}^4$, s_u/σ'_v, E_i/σ'_v, and T/B are considered essential for predicting the excavation-induced maximum wall deflection. These factors are the required variables in Model A, the first component of the proposed KJHH model. Two steps are needed for estimation of the maximum wall deflection using Model A. First, the first five factors are used to estimate δ_{hm} using Eqs. 4.1 and 4.2, and then the estimated δ_{hm} is modified into $\delta_{hm,m}$ considering the effect of hard stratum (Eqs. 4.3 and 4.4). Model A (Eqs. 4.1 through 4.4) is validated with 30 excavation case histories, and the results show that $\delta_{hm,m}$ (or δ_{hm} if the hard stratum is not present) can be accurately predicted using this model.
- The deformation ratio R in a braced excavation in clay-dominant sites is found to be influenced by three normalized parameters, $\sum H_{clay}/H_{wall}$, s_u/σ'_v, and $E_i/1000\sigma'_v$. These three normalized parameters are the required input variables of Model B, the second component of the KJHH model. Satisfactory performance of Model B for predicting the deformation ratio R is evidenced by high R^2 and low COV obtained in the regression analysis. Validation of Model B using quality case histories is performed and satisfactory results are also obtained.

- The proposed KJHH model is able to predict reasonably well the maximum wall deflection, the maximum ground surface settlement, and the ground surface settlement profile caused by braced excavations in soft to medium clays. It has improved upon the important contributions of earlier investigators.
- The model bias of the KJHH model is assessed at the component level as well as the entire model as a whole. The KJHH model is judged to be accurate (with all mean bias factors approximately equal to 1.0), and the precision of the model is quite high for this type of soil-structure interaction problem, as the variation of the model prediction is generally small (COVs of 25%, 13%, and 35% for predictions of the maximum wall deflection, the deformation ratio, and the ground surface settlement, respectively).
- The proposed KJHH model assumes normal workmanship and no basal failure in the braced excavation. Possible uncertainty caused by the soil variability at the excavation site and construction-related issues such as dewatering activity and over excavation prior to support installation, are not explicitly addressed in this paper. Engineering judgment is required and must be carefully exercised to adjust the model bias of the developed KJHH model, as necessary, to account for these factors. They are, however, beyond the scope of this dissertation study.
- Although it has been shown to be effective in estimating the excavation-induced maximum wall deflection, maximum surface settlement and

surface settlement profile, the developed KJHH model should be regarded as the "first-order" approximation and more advanced numerical solutions should be pursued as appropriate.

The following conclusions are drawn from the results of reliability analysis and updating of excavation-induced ground surface settlement for building evaluation presented in Chapter V:

- The KJHH model is a simplified empirical method used for the estimation of excavation-induced ground settlements in soft to medium clay. Since the uncertainty of the KJHH model has been quite well characterized, it is ideal for use as the deterministic model for the intended reliability analysis.
- Sensitivity analyses are performed to determine the effects of a number of assumptions in the reliability analysis, including the magnitude and variation of the limiting tolerable settlement, the apparent model factor, *COV* of soil properties, and assumed distribution of input variables. The results indicate that the calculated probability of exceedance depends on the choice of tolerable settlement, as expected. The results also showed that the uncertainty in the limiting tolerable settlement has a significant effect and thus, the limiting tolerable settlement, which is considered as a resistance in the reliability analysis, needs to be properly characterized.
- The calculated probability of exceedance is shown to be most sensitive to the model bias factor, which indicates the importance of the accuracy and precision of the deterministic settlement model adopted for reliability

analysis. Furthermore, the calculated probability of exceedance is also shown to be sensitive, albeit to a lesser degree, to the normalized shear strength (s_u/σ'_v) and normalized Young's modulus (E_i/σ'_v), and to be insensitive to excavation depth (H_e), excavation width (*B/2)*, system stiffness ($EI/\gamma_w h_{avg}^4$), and $\sum H_{clay}/H_{wall}$. However, the probability of exceedance becomes increasingly sensitive to s_u/σ'_v and E_i/σ'_v as the *COV* of s_u/σ'_v and E_i/σ'_v increase. Therefore, it is important to accurately characterize the *COV* of s_u/σ'_v and E_i/σ'_v.

- Generally, at a prescribed tolerable settlement, the probability of exceedance increases as the *COV* of s_u/σ'_v or E_i/σ'_v increases. However, the difference is less significant at a lower prescribed tolerable settlement than at a higher prescribed tolerable settlement. At a given *COV* level, the probability of exceedance decreases as the limiting tolerable settlement increases, and this trend is more profound at lower *COV* levels than at higher *COV* levels.
- The effect of the assumed distribution of input variables on the probability of exceedance is found to be insignificant, particularly when the *COVs* of these variables are relatively low (<20%). Even at higher *COV* levels, the effect is still quite modest.
- Finally, a method to update the apparent model factor is presented. As the excavation proceeds, the observed settlement from a prior stage can be used to update the apparent model factor of the KJHH model, which, in turn, can be used to improve the prediction of settlement at various target

depths in future stages. The probability of exceedance is then recalculated based on the updated settlement predictions. As reflected in the example application presented, the model factor is shown to be more accurately and precisely characterized as more observations are used for updating, which in turn leads to a more *accurate* and *precise* estimation of ground surface settlement and probability of exceedance.

BIBLIOGRAPHY

ACI Committee 318 (1995), *Building code requirements for structural concrete (ACI 318-95) and commentary (ACI 318R-95)*.

Ang, A.H. and Tang, W.H. (2006), *Probability concepts in engineering: Emphasis on applications to civil and environmental engineering*, 2nd Edition, John Wiley & Sons, New York, N.Y.

Addenbrooke, T.I., Potts, D.M., and Dabee, B. (2000), "Displacement flexibility number for multipropped retaining wall design," *Journal of Geotechnical and Geoenvironmental Engineering*, ASCE, Vol. 126, No. 8, pp. 718-726.

Atkinson, J.H. (1993), "An introduction to the mechanics of soils and foundations: through critical state soil mechanics," McGraw-Hill, London, pp. 158-167.

Baecher, G.B., and Rackwitz, R. (1982), ''Factors of safety and pile load tests,'' *Int. J. Numer. Analyt. Meth. Geomech.*, Vol. 6, No. 4, pp. 409–424.

Bowles, J.E. (1988), *Foundation analysis and design*, 4th edtion, McGraw-Hill Book Company, New York, N.Y.

Burland, J.B. (1989), "Ninth Laurits Bjerrum memorial lecture: Small is beautiful-the stiffness of soils at small strain," *Canadian Geotechnical Journal*, Vol. 26, No. 4, pp. 499-516.

Calvello, M., and Finno, R.J. (2004). "Selecting parameters to optimize in model calibration by inverse analysis," *Computers and Geotechnics*, Vol. 31, No. 5, pp. 411-425.

Carter, J.P., and Balaam, N.P. (1990), *A Finite Element Numerical Algorithm*, Users' manual, Centre for Geotechnical Research, University of Sydney, Sydney.

Clough, G.W., and O'Rourke, T.D. (1990), "Construction-induced movements of in-situ walls," *Proc.*, *ASCE Conference on Design and Performance of Earth Retaining Structure*, *Geotechnical Special Publication No. 25*, New York, pp. 439-470.

Day, R.A., and Potts, D.M. (1993), " Modeling sheet pile retaining walls," *Computers and Geotechnics*, Vol. 15, No. 3, pp. 125-143.

Duncan, J.M., and Chang, C.Y. (1970), "Nonlinear analysis of stress and strain in soils," *Journal of the Soil Mechanics and Foundations Division*, ASCE, Vol. 96, No. 5, pp. 637-659.

Finno, R.J. and Calvello, M. (2005), "Supported excavations: observational method and inverse modeling," *Journal of Geotechnical Geoenvironmental Engineering*, ASCE, Vol. 131, No. 7, pp. 826-836.

Finno, R.J., and Chung, C.K. (1992), "Stress-strain-strength responses of compressible Chicago glacial clays," *Journal of Geotechnical Engineering*, Vol. 118, No. 10, pp. 1607-1625.

Finno, R.J., and Harahap, I.S. (1991), "Finite element analyses of HDR-4 excavation," *Journal of Geotechnical and Geoenvironmental Engineering*, Vol. 117, No. 10, pp. 1590-1609.

Finno, R.J., and Roboski, J.F. (2005), "Three-dimensional response of a tied-back excavation through clay," *Journal of Geotechnical and Geoenvironmental Engineering*, Vol. 131, No. 3, pp. 273-282.

Harr, M.E. (1987), *Reliability-based design in civil engineering*, McGraw-Hill Book Company, New York, N.Y.

Hashash, Y.M.A., and Whittle, A.J. (1996), "Ground movement prediction for deep excavations in soft clay," *Journal of Geotechnical Engineering*, Vol. 122, No. 6, pp. 474-486.

Hashash, Y.M.A., Jung, S., and Ghaboussi, J. (2004), "Numerical implementation of a neural network based material model in finite element analysis," *International Journal for Numerical Methods in Engineering*, Vol. 59, No. 8, pp. 989-1005.

Hight, D.W., and Higgins, K.G. (1995), "An approach to the prediction of ground movements in engineering practice: Background and Application," *Proc., Pre-failure Deformation Characteristics of Geomaterials*, pp. 909-945.

Holman, T.P. (2005), "*Small strain behavior of compressible Chicago glacial clay*," Ph.D Dissertation, Northwestern University, Evanston, Illinois, USA.

Hsiao, E.C.L., Kung, G.T.C., Juang, C.H., and Schuster, M. (2006), "Estimation of wall deflection in braced excavation in clays using artificial neural networks," *GeoCongress 2006 (CD-ROM)*, Atlanta, ASCE.

Hsieh, P.G. (1999), "*Prediction of ground movements caused by deep excavation in clay*," Ph.D. Dissertation, National Taiwan University of Science and Technology, Taipei, Taiwan.

Hsieh, P.G., and Ou, C.Y. (1997), "Use of the modified hyperbolic model in excavation analysis under undrained condition," *Geotechnical Engineering Journal*, SEAGS, Vol. 28, No. 2, pp. 123-150.

Hsieh, P.G., and Ou, C.Y. (1998), "Shape of ground surface settlement profiles caused by excavation," *Canadian Geotechnical Journal*, Vol. 35, No. 6, pp. 1004-1017.

Hsieh, P.G., Kung, T.C., Ou, C.Y., and Tang, Y.G. (2003), "Deep excavation analysis with consideration of small strain modulus and its degradation behavior of clay," *Proc., 12th Asian Regional Conference on Soil Mechanics and Geotechnical Engineering*, Singapore, Vol. 1, pp. 785-788.

Huang, C.T., Lin Y.K., Kao, T.C., and Zoh, Z.C. (1987), "Geotechnical engineering mapping of the Taipei city," *Proc*., *9th Southeast Asia Geotechnical Society Conference,* Bangkok, Vol. 1, pp. 3.109-3.120.

Jardine, R.J., Potts, D.M., Fourie, A.B., and Burland, J.B. (1986), "Studies of the influence of non-linear stress-strain characteristics in soil-structure interaction," *Geotechnique*, Vol. 36, No. 2, pp. 377-396.

Jardine, R.J., St John, H.D., Hight, D.W., and Potts, D.M. (1991), "Some practical applications of a non-linear ground model," *Proc*., *10th European Conference on Soil Mechanics and Foundation Engineering*, Florence, Vol. 1, pp. 223-228.

Juang, C.H., Fang, S.Y., and Khor, E.H. (2006), "First order reliability method for probabilistic liquefaction triggering analysis using CPT," *Journal of Geotechnical and Geoenvironmental Engineering*, ASCE, Vol. 132, No. 3, pp. 337-350.

Kay, J.N. (1976), ''Safety factor evaluation for single piles in sand,'' *J. Geotech. Eng. Div.,* ASCE, Vol. 102, No. 10, pp. 1093–1108.

Kung, T.C. (2003), "*Surface settlement induced by excavation with consideration of small strain behavior of Taipei silty clay*," Ph.D. Dissertation, Department of Construction Engineering, National Taiwan University of Science and Technology, Taipei, Taiwan.

Kung, G.T.C., Hsiao, E.C.L., Schuster, M., and Juang, C.H. (2007a), "A neural network approach to estimating excavation induced wall deflection in soft clays," *Computers and Geotechnics*, (accepted).

Kung, G.T.C., Hsiao, E.C.L. and Juang, C.H. (2007b), "Evaluation of a simplified small strain soil model for predicting excavation-induced wall deflection and ground movement," *Canadian Geotechnical Journal*, (accepted).

Kung, G.T.C., Juang, C.H., Hsiao, E.C.L., and Hashash, Y.M.A. (2007), "A simplified model for wall deflection and ground surface settlement caused by braced excavation in clays," *Journal of Geotechnical and Geoenvironmental Engineering*, *ASCE*, Vol. 133, No. 6, pp. 1-17 (in press).

Lacasse, S., Guttormsen, T.R., and Goulois, A. (1990), ''Bayesian updating of axial capacity of single pile,'' *Proc., 5th Int. Conf. on Structural Safety and Reliability*, H.-S. Ang, M. Shinozuka, and G. I. Schuller, eds., ASCE, New York, pp. 287–290.

Lim, K.W., Wong, K.S., Orihara, K., and Ng, P.B. (2003), "Comparison of results of excavation analysis using WALLUP, SAGE CRISP and EXCAV97," *Proc*., *Singapore Underground 2003*, Singapore, pp. 83-94.

Low, B.K., and Tang, W.H. (1997), "Efficient reliability evaluation using spreadsheet," *Journal of Engineering Mechanics, ASCE*, Vol. 123, No. 7, pp. 749-752

Mana, A.I., and Clough, G.W. (1981), "Prediction of movements for braced cuts in clay," *Journal of Geotechnical Engineering*, Vol. 107, No. 6, pp. 759-777.

Miyoshi, M. (1977), "Mechanical behavior of temporary braced wall," *Proceeding, 9th International Conference on Soil Mechanics and Foundation Engineering*, Tokyo, Vol. 2, pp. 655-658.

Norwegian Geotechnical Institute (1962), "Measurements at a strutted excavation, Oslo Subway, Vaterland 1." Norwegian Geotechnical Institute, Technical Report 6.

Ou, C.Y., and Chang, T.Y. (2002), "Undrained elasto-plastic behavior of the remolded Taipei silty clay," *Journal of the Chinese Institute of Civil and Hydraulic Engineering*, Vol. 14, No. 3, pp. 531-540 (in Chinese).

Ou, C.Y., Chiou, D.C., and Wu, T.S. (1996), "Three-dimensional finite element analysis of deep excavations," *Journal of Geotechnical Engineering*, Vol. 122, No. 5, pp. 337-345.

Ou, C.Y., Hsieh, P.G., and Chiou, D.C. (1993), "Characteristics of ground surface settlement during excavation." *Canadian Geotechenical Journal*, Vol. 30, No. 5, pp. 758-767.

Ou, C.Y., Liao, J.T., and Lin, H.D. (1998), "Performance of diaphragm wall using Top-down method," *Journal of Geotechnical and Geoenvironmental Engineering*, Vol. 124, No. 9, pp. 798-808.

Ou, C.Y., Liao, J.T., and Cheng, W.L. (2000), "Building respond and ground movements induced by a deep excavation," *Geotechnique*, Vol. 50, No. 3, pp. 209-220.

Ou, C.Y., and Tang, Y.G. (1994), "Soil parameter determination for deep excavation analysis by optimization," *Journal of the Chinese Institute of Engineers*, Vol. 17, No. 5, pp. 671-688.

Peck, R.B. (1969), "Deep excavation and tunneling in soft ground," *Proc*., *7th International Conference on Soil Mechanics and Foundation Engineering*, State-of-the Art Volume, Mexico City, pp. 225-290.

Phoon, K.K. (2004), General Non-Gaussian Probability Models for First Order Reliability Method (FORM): A State-of-the Art Report. *ICG Report 2004-2-4 (NGI Report 20031091-4)*, International Center for Geohazards, Oslo, Norway.

Phoon, K.K., and Kulhawy, F.H. (2005), "Characterization of model uncertainties for laterally loaded rigid drilled shafts," *Geotechnique*, Vol. 55, No. 1, pp. 45–54.

Prevost, J.H. (1979), "Undrained shear tests on clay," *Journal of the Geotechnical Engineering Division*, ASCE, Vol. 105, No. 1, pp. 49-64.

Simpson, B. (1993), "Development and application of a new soil model for prediction of ground movements," *In Predictive soil mechanics, Proc. Wroth Memorial Symp.*, G.T. Houlsby and A.N. Schofield, eds., Oxford, London, Thomas Telford, pp. 628-643.

Skempton, A.W., and MacDonald, D.H. (1956), "The allowable settlement of buildings," *Proc. Instn Civ. Engrs*, Vol. 3, No. 5, pp. 727–768.

Stallebrass, S.E., and Taylor, R.N. (1997), "The development and evaluation of a constitutive model for the prediction of ground movements in overconsolidation clay," *Geotechnique*, Vol. 47, No. 2, pp. 235-253.

Tang, W.H., Stark, T., and Angulo, M. (1999), ''Reliability in back analysis of slope failures,'' *Soils Foundations*, Vol. 39, No. 5, pp. 73–80.

Terzaghi, C. (1943), *Theoretical soil mechanics*, John Wiley & Sons, New York, N.Y.

Wahls, H.E. (1994), "Tolerable deformations," *Geotechnical Special Publication No. 40*, ASCE, New York, pp. 1611–1628.

Whittle, A.J. (1990), "*A constitutive model for overconsolidated clay*," MIT Sea Grant Report MITSG90-15, Massachusetts Institute of Technology, Cambridge, Massachusetts.

Whittle, A.J., and Hashash, Y.M.A. (1994), "Soil modeling and prediction of deep excavation behavior." *Proc*., *Pre-failure Deformation of Geomaterials*, Hokkaido, pp. 589-594.

Whittle, A.J., Hashash, Y.M.A., and Whitman, R.V. (1993), "Analysis of deep excavation in Boston," *Journal of Geotechnical Engineering*, Vol. 119, No. 1, pp. 69-90.

Wong, K.S., and Broms, B.B. (1989), "Lateral wall deflections of braced excavations in clay," *Journal of Geotechnical Engineering*, Vol. 115, No. 6, pp. 853-870.

Wood, D.M. (1990), *Soil Behavior and Critical State Soil Mechanics*, Cambridge University Press, Cambridge.

Zhang, L.M., and Tang, W.H. (2002), ''Use of load tests for reducing pile length,'' *Deep foundations 2002*, *Geotechnical Special Publication No. 116*, ASCE, Reston, Va., pp. 993–1005.

Zhang, L.M., Tang, W.H., Zhang, L.L., and Zheng, J.G. (2004), "Reducing uncertainty of prediction from empirical correlations," *Journal of Geotechnical and Geoenvironmental Engineering, ASCE*, Vol. 130, No. 5, pp. 526-534.

Zhang, L. M., and Ng, A. M. Y. (2005), "Probabilistic limiting tolerable displacement for serviceability limit state design of foundations," *Géotechnique*, Vol. 55, No. 2, pp. 151-161.

Zienkiewicz, O.C. (1979), *The Finite Element Method*. 3rd edition, McGraw Hill, London.